Volume

I

EDITOR-
IN-CHIEF
Sayigh

COMPREHENSIVE
RENEWABLE ENERGY

TJ 807
.4
.C66
2012
v. 1
Copy 1

ELSEVIER

ELSEVIER

EDITOR-IN-CHIEF
Ali Sayigh

COMPREHENSIVE RENEWABLE ENERGY

Volume

I

Photovoltaic Solar Energy

VOLUME EDITOR
Wilfried G.J.H.M. van Sark

HANWHA 1043

LC COPYRIGHT
0 030 998 701 9

COMPREHENSIVE RENEWABLE ENERGY

Volume 1 Photovoltaic Solar Energy
Volume 2 Wind Energy
Volume 3 Solar Thermal Systems: Components and Applications
Volume 4 Fuel Cells and Hydrogen Technology
Volume 5 Biomass and Biofuel Production
Volume 6 Hydro Power
Volume 7 Geothermal Energy
Volume 8 Ocean Energy

ELSEVIER store.elsevier.com

9 780080 971605
Volume I
ISBN: 978-0-08-097160-5

9 780080 878720
Set
ISBN: 978-0-08-087872-0

Cover image courtesy of Stockphoto © Pedro Castellano

Volume I

EDITOR-IN-CHIEF
Sayigh

COMPREHENSIVE RENEWABLE ENERGY

TJ 807
.4
.C66
2012
v. 1
Copy 1

ELSEVIER

COMPREHENSIVE RENEWABLE ENERGY

EDITOR-IN-CHIEF

Ali Sayigh

Chairman of WREC, Director General of WREN, and
Chairman of IEI, Brighton, UK

VOLUME 1

PHOTOVOLTAIC SOLAR ENERGY

VOLUME EDITOR

Wilfried G.J.H.M. van Sark

Utrecht University, Copernicus Institute, Utrecht, The Netherlands

ELSEVIER

AMSTERDAM BOSTON HEIDELBERG LONDON NEW YORK OXFORD
PARIS SAN DIEGO SAN FRANCISCO SINGAPORE SYDNEY TOKYO

Elsevier
Radarweg 29, PO Box 211, 1000 AE Amsterdam, The Netherlands
The Boulevard, Langford Lane, Kidlington, Oxford OX5 1GB, UK
225 Wyman Street, Waltham, MA 02451, USA

Copyright © 2012 Elsevier Ltd. All rights reserved.

4.04 Hydrogen Safety Engineering: The State-of-the-Art and Future Progress
Copyright © 2012 V Molkov

5.16 Renewable Fuels: An Automotive Perspective
Copyright © 2012 Lotus Cars Limited

The following articles are US Government works in the public domain and not subject to copyright:
1.19 Cadmium Telluride Photovoltaic Thin Film: CdTe
1.37 Solar Power Satellites
4.02 Current Perspective on Hydrogen and Fuel Cells
5.02 Historical Perspectives on Biofuels

No part of this publication may be reproduced, stored in a retrieval system or transmitted in any form or by any means electronic, mechanical, photocopying, recording or otherwise without the prior written permission of the publisher

Permissions may be sought directly from Elsevier's Science & Technology Rights Department in Oxford, UK: phone (+44) (0) 1865 843830; fax (+44) (0) 1865 853333; email: permissions@elsevier.com. Alternatively you can submit your request online by visiting the Elsevier web site at http://elsevier.com/locate/permissions, and selecting *Obtaining permission to use Elsevier material*

Notice
No responsibility is assumed by the publisher for any injury and/or damage to persons or property as a matter of products liability, negligence or otherwise, or from any use or operation of any methods, products, instructions or ideas contained in the material herein. Because of rapid advances in the medical sciences, in particular, independent verfication of diagnoses and drug dosages should be made.

British Library Cataloguing in Publication Data
A catalogue record for this book is available from the British Library

The Library of Congress Control Number: 2012934547

ISBN: 978-0-08-087872-0

For information on all Elsevier publications
visit our website at books.elsevier.com

Printed and bound in Italy

11 12 13 14 10 9 8 7 6 5 4 3 2 1

Working together to grow
libraries in developing countries
www.elsevier.com | www.bookaid.org | www.sabre.org
ELSEVIER BOOK AID International Sabre Foundation

Editorial: Gemma Mattingley, Joanne Williams
Production: Edward Taylor, Maggie Johnson

CONTENTS

Editor-in-Chief v

Volume Editors vii

Contributors for All Volumes xi

Preface xix

Volume 1 Photovoltaic Solar Energy

Renewable Energy

1.01 Renewable Energy Policy and Incentives 1
D Porter

Photovoltaic Solar Energy

1.02 Introduction to Photovoltaic Technology 5
WGJHM van Sark

1.03 Solar Photovoltaics Technology: No Longer an Outlier 13
LL Kazmerski

1.04 History of Photovoltaics 31
LA Lamont

Economics and Environment

1.05 Historical and Future Cost Dynamics of Photovoltaic Technology 47
GF Nemet and D Husmann

1.06 Feed-In Tariffs and Other Support Mechanisms for Solar PV Promotion 73
D Jacobs and BK Sovacool

1.07 Finance Mechanisms and Incentives for Photovoltaic Technologies in Developing Countries 111
M Moner-Girona, S Szabo, and S Rolland

1.08 Environmental Impacts of Photovoltaic Life Cycles 143
VM Fthenakis and HC Kim

1.09 Overview of the Global PV Industry 161
A Jäger-Waldau

1.10 Vision for Photovoltaics in the Future 179
E Despotou

1.11 Storage Options for Photovoltaics 199
VM Fthenakis and T Nikolakakis

Resource and Potential

1.12 Solar Radiation Resource Assessment for Renewable Energy Conversion 213
DR Myers

1.13 Prediction of Solar Irradiance and Photovoltaic Power 239
E Lorenz and D Heinemann

Basics

1.14 Principles of Solar Energy Conversion 293
LC Hirst

1.15 Thermodynamics of Photovoltaics 315
V Badescu

Technology

1.16 Crystalline Silicon Solar Cells: State-of-the-Art and Future Developments 353
SW Glunz, R Preu, and D Biro

1.17 Thin-Film Silicon PV Technology 389
M Zeman and REI Schropp

1.18 Chalcopyrite Thin-Film Materials and Solar Cells 399
T Unold and CA Kaufmann

1.19 Cadmium Telluride Photovoltaic Thin Film: CdTe 423
TA Gessert

1.20 Plastic Solar Cells 439
L Sims, H-J Egelhaaf, JA Hauch, FR Kogler, and R Steim

1.21 Mesoporous Dye-Sensitized Solar Cells 481
A Hagfeldt, UB Cappel, G Boschloo, L Sun, L Kloo, H Pettersson, and EA Gibson

1.22 Multiple Junction Solar Cells 497
M Yamaguchi

1.23 Application of Micro- and Nanotechnology in Photovoltaics 515
L Tsakalakos

1.24 Upconversion 533
TW Schmidt and MJY Tayebjee

1.25 Downconversion 549
MJY Tayebjee, TW Schmidt, and G Conibeer

1.26 Down-Shifting of the Incident Light for Photovoltaic Applications 563
Y Jestin

1.27 Luminescent Solar Concentrators 587
JC Goldschmidt

1.28 Thermophotovoltaics 603
J van der Heide

1.29 Intermediate Band Solar Cells 619
E Antolín, A Martí, and A Luque

1.30 Plasmonics for Photovoltaics 641
S Pillai and MA Green

1.31 Artificial Leaves: Towards Bio-Inspired Solar Energy Converters 657
A Pandit and RN Frese

Applications

1.32 Design and Components of Photovoltaic Systems 679
WGJHM van Sark

1.33 BIPV in Architecture and Urban Planning 697
TH Reijenga and HF Kaan

1.34 Product-Integrated Photovoltaics 709
AHME Reinders and WGJHM van Sark

1.35 Very Large-Scale Photovoltaic Systems 733
T Ehara, K Komoto, and P van der Vleuten

1.36 Concentration Photovoltaics 745
M Martinez, O de la Rubia, F Rubio, and P Banda

1.37 Solar Power Satellites 767
GA Landis

1.38 Performance Monitoring 775
N Pearsall and R Gottschalg

1.39 Standards in Photovoltaic Technology 787
H Ossenbrink, H Müllejans, R Kenny, and E Dunlop

Volume 2 Wind Energy

2.01 Wind Energy – Introduction 1
JK Kaldellis

2.02 Wind Energy Contribution in the Planet Energy Balance and Future Prospects 11
JK Kaldellis and M Kapsali

2.03 History of Wind Power 41
DT Swift-Hook

2.04 Wind Energy Potential 73
H Nfaoui

2.05 Wind Turbines: Evolution, Basic Principles, and Classifications 93
S Mathew and GS Philip

2.06 Energy Yield of Contemporary Wind Turbines 113
DP Zafirakis, AG Paliatsos, and JK Kaldellis

2.07 Wind Parks Design, Including Representative Case Studies 169
D Al Katsaprakakis and DG Christakis

2.08 Aerodynamic Analysis of Wind Turbines 225
JN Sørensen

2.09 Mechanical-Dynamic Loads 243
M Karimirad

2.10 Electrical Parts of Wind Turbines 269
GS Stavrakakis

2.11 Wind Turbine Control Systems and Power Electronics 329
A Pouliezos

2.12 Testing, Standardization, Certification in Wind Energy 371
F Van Hulle

2.13 Design and Implementation of a Wind Power Project 391
T Wizelius

2.14 Offshore Wind Power Basics 431
M Kapsali and JK Kaldellis

2.15 Wind Energy Economics 469
D Milborrow

2.16 Environmental-Social Benefits/Impacts of Wind Power 503
E Kondili and JK Kaldellis

2.17 Wind Energy Policy 541
GC van Kooten

2.18 Wind Power Integration 569
JA Carta

2.19 Stand-Alone, Hybrid Systems 623
KA Kavadias

2.20 Wind Power Industry and Markets 657
PE Morthorst

2.21 Trends, Prospects, and R&D Directions in Wind Turbine Technology 671
JK Kaldellis and DP Zafirakis

2.22 Special Wind Power Applications 725
E Kondili

Volume 3 Solar Thermal Systems: Components and Applications

Solar Thermal Systems

3.01 Solar Thermal Systems: Components and Applications – Introduction 1
SA Kalogirou

3.02 Solar Resource 27
HD Kambezidis

3.03 History of Solar Energy 85
VG Belessiotis and E Papanicolaou

Components

3.04 Low Temperature Stationary Collectors 103
YG Caouris

3.05 Low Concentration Ratio Solar Collectors 149
SA Kalogirou

3.06 High Concentration Solar Collectors 165
B Hoffschmidt, S Alexopoulos, J Göttsche, M Sauerborn, and O Kaufhold

3.07 Thermal Energy Storage 211
LF Cabeza

3.08 Photovoltaic/Thermal Solar Collectors 255
Y Tripanagnostopoulos

3.09 Solar Selective Coatings 301
P Yianoulis, M Giannouli, and SA Kalogirou

3.10 Glazings and Coatings 313
G Leftheriotis and P Yianoulis

3.11 Modeling and Simulation of Passive and Active Solar Thermal Systems 357
A Athienitis, SA Kalogirou, and L Candanedo

Applications

3.12 Solar Hot Water Heating Systems 419
G Faninger

3.13 Solar Space Heating and Cooling Systems 449
SA Kalogirou and GA Florides

3.14 Solar Cooling and Refrigeration Systems 481
GG Maidment and A Paurine

3.15 Solar-Assisted Heat Pumps 495
DA Chwieduk

3.16 Solar Desalination 529
E Tzen, G Zaragoza, and D-C Alarcón Padilla

3.17 Industrial and Agricultural Applications of Solar Heat 567
B Norton

3.18 Concentrating Solar Power 595
B Hoffschmidt, S Alexopoulos, C Rau, J Sattler, A Anthrakidis, C Boura, B O'Connor, and P Hilger

3.19 Passive Solar Architecture 637
D Kolokotsa, M Santamouris, A Synnefa, and T Karlessi

Volume 4 Fuel Cells and Hydrogen Technology

4.01 Fuel Cells and Hydrogen Technology – Introduction 1
AJ Cruden

4.02 Current Perspective on Hydrogen and Fuel Cells 13
K Burke

4.03 Hydrogen Economics and Policy 45
N Hughes and P Agnolucci

4.04 Hydrogen Safety Engineering: The State-of-the-Art and Future Progress 77
V Molkov

4.05 Hydrogen Storage: Compressed Gas 111
D Nash, D Aklil, E Johnson, R Gazey, and V Ortisi

4.06 Hydrogen Storage: Liquid and Chemical 137
P Chen

4.07 Alkaline Fuel Cells: Theory and Application 159
F Bidault and PH Middleton

4.08 PEM Fuel Cells: Applications 183
AL Dicks

4.09 Molten Carbonate Fuel Cells: Theory and Application 227
T Leo

4.10 Solid Oxide Fuel Cells: Theory and Materials 241
A Tesfai and JTS Irvine

4.11 Biological and Microbial Fuel Cells 257
K Scott, EH Yu, MM Ghangrekar, B Erable, and NM Duteanu

4.12 Hydrogen and Fuel Cells in Transport 281
K Kendall and BG Pollet

4.13 H_2 and Fuel Cells as Controlled Renewables: FC Power Electronics 295
N Schofield

4.14 Future Perspective on Hydrogen and Fuel Cells 331
K Hall

Volume 5 Biomass and Biofuel Production

Biomass and Biofuels

5.01 Biomass and Biofuels – Introduction 1
DJ Roddy

5.02 Historical Perspectives on Biofuels 11
G Knothe

Case Studies

5.03 Bioethanol Development in Brazil 15
A Altieri

5.04 Biomass Power Generation 27
A Malmgren and G Riley

5.05 Biomass Co-Firing 55
A Nuamah, A Malmgren, G Riley, and E Lester

Issues, Constraints & Limitations

5.06 A Global Bioenergy Market 75
O Olsson and B Hillring

5.07 Biomass CHP Energy Systems: A Critical Assessment 87
M Börjesson and EO Ahlgren

5.08 Ethics of Biofuel Production 99
I Waller

5.09 Life Cycle Analysis Perspective on Greenhouse Gas Savings 109
N Mortimer

Technology Solutions – New Processes

5.10 Biomass Gasification and Pyrolysis 133
DJ Roddy and C Manson-Whitton

5.11 Biomass to Liquids Technology 155
G Evans and C Smith

5.12 Intensification of Biofuel Production 205
AP Harvey and JGM Lee

5.13 Biofuels from Waste Materials 217
AA Refaat

Technology Solutions – Novel Feedstocks

5.14 Woody Biomass 263
LL Wright, LM Eaton, RD Perlack, and BJ Stokes

5.15 Potential for Yield Improvement 293
J Spink, E Mullins, and P Berry

Technology Solutions – Novel End Uses

5.16 Renewable Fuels: An Automotive Perspective 305
RJ Pearson and JWG Turner

5.17 Use of Biofuels in a Range of Engine Configurations 343
A Roskilly, Y Wang, R Mikalsen, and H Yu

Expanding the Envelope

5.18 Biochar 357
CE Brewer and RC Brown

5.19 Extracting Additional Value from Biomass 385
MF Askew

5.20 Biomass to Chemicals 395
A Kazmi and J Clark

5.21 Bioenergy Policy Development 411
P Thornley

Volume 6 Hydro Power

Hydro Power

6.01 Hydro Power – Introduction 1
A Lejeune

Constraints of Hydropower Development

6.02 Hydro Power: A Multi Benefit Solution for Renewable Energy 15
A Lejeune and SL Hui

6.03 Management of Hydropower Impacts through Construction and Operation 49
H Horlacher, T Heyer, CM Ramos, and MC da Silva

Hydropower Schemes Around the World

6.04 Large Hydropower Plants of Brazil 93
BP Machado

6.05 Overview of Institutional Structure Reform of the Cameroon Power Sector and Assessments 129
J Kenfack and O Hamandjoda

6.06 Recent Hydropower Solutions in Canada 153
M Fuamba and TF Mahdi

6.07 The Three Gorges Project in China 179
L Suo, X Niu, and H Xie

6.08 The Recent Trend in Development of Hydro Plants in India 227
SP Sen

6.09 Hydropower Development in Iran: Vision and Strategy 253
E Bozorgzadeh

6.10 Hydropower Development in Japan 265
T Hino

6.11 Evolution of Hydropower in Spain 309
A Gil and F Bueno

6.12 Hydropower in Switzerland 343
B Hagin

Design Concepts

6.13 Long-Term Sediment Management for Sustainable Hydropower 355
F Rulot, BJ Dewals, S Erpicum, P Archambeau, and M Pirotton

6.14 Durability Design of Concrete Hydropower Structures 377
S Jianxia

6.15 Pumped Storage Hydropower Developments 405
T Hino and A Lejeune

6.16 Simplified Generic Axial-Flow Microhydro Turbines 435
A Fuller and K Alexander

6.17 Development of a Small Hydroelectric Scheme at Horseshoe Bend, Teviot River, Central Otago, New Zealand 467
P Mulvihill and I Walsh

6.18 Recent Achievements in Hydraulic Research in China 485
J Guo

Volume 7 Geothermal Energy

7.01 Geothermal Energy – Introduction 1
TI Sigfusson

7.02 The Physics of Geothermal Energy 3
G Axelsson

7.03 Geothermal Energy Exploration Techniques 51
ÓG Flóvenz, GP Hersir, K Sæmundsson, H Ármannsson, and Þ Friðriksson

7.04 Geochemical Aspects of Geothermal Utilization 95
H Ármannsson

7.05 Direct Heat Utilization of Geothermal Energy 169
JW Lund

7.06 Shallow Systems: Geothermal Heat Pumps 187
L Rybach

7.07 Geothermal Power Plants 207
R DiPippo

7.08 Corrosion, Scaling, and Material Selection in Geothermal Power Production 239
SN Karlsdóttir

7.09 Geothermal Cost and Investment Factors 259
H Kristjánsdóttir and Á Margeirsson

7.10 Sustainable Energy Development: The Role of Geothermal Power 271
B Davidsdottir

Volume 8 Ocean Energy

8.01 Generating Electrical Power from Ocean Resources 1
AS Bahaj

8.02 Historical Aspects of Wave Energy Conversion 7
AFO Falcão

8.03 Resource Assessment for Wave Energy 11
EBL Mackay

8.04 Development of Wave Devices from Initial Conception to Commercial Demonstration 79
V Heller

8.05 Air Turbines 111
AFO Falcão and LMC Gato

8.06 Economics of Ocean Energy 151
T Stallard

Index 171

This material may be protected by Copyright law (Title 17 U.S. Code)

1.16 Crystalline Silicon Solar Cells: State-of-the-Art and Future Developments

SW Glunz, R Preu, and D Biro, Fraunhofer Institute for Solar Energy Systems, Freiburg, Germany

© 2012 Elsevier Ltd. All rights reserved.

1.16.1	**General Introduction**	353
1.16.1.1	Photovoltaic Market	353
1.16.1.2	Historical Development of Cell Efficiency	354
1.16.1.3	Maximum Achievable Efficiency	354
1.16.2	**Current Status of Silicon Solar Cell Technology**	355
1.16.2.1	Basic Structure of a Silicon Solar Cell	355
1.16.2.2	Physical Structure of an Industrial Silicon Solar Cell	355
1.16.2.3	Process Sequence	358
1.16.3	**Influence of Basic Parameters**	363
1.16.4	**Strategies for Improvement**	364
1.16.4.1	Dielectric Surface Passivation	364
1.16.4.1.1	Influence of surface passivation	364
1.16.4.1.2	Passivation mechanisms of dielectric layers	365
1.16.4.1.3	Layers and processes for surface passivation	365
1.16.4.2	Metallization	366
1.16.4.2.1	Front contacts	366
1.16.4.2.2	Back contacts	368
1.16.4.3	Bulk Properties	368
1.16.5	**High-Efficiency Cell Structures on p-type Silicon**	371
1.16.5.1	Main Approaches for High Efficiencies in p-type Devices	371
1.16.5.2	Passivated Emitter and Rear Cell	371
1.16.5.3	Metal Wrap-Through Solar Cells	372
1.16.5.4	MWT-PERC	373
1.16.5.5	Emitter Wrap-Through Solar Cells	374
1.16.6	**High-Efficiency Structures on n-type Silicon**	375
1.16.6.1	Aluminum-Alloyed Back Junction	375
1.16.6.2	n-Type Cells with Boron-Diffused Front Emitter	376
1.16.6.3	Back-Contact Solar Cells with Boron-Diffused Back Junction	377
1.16.6.4	Heterojunction Solar Cells	379
1.16.6.5	Alternative Emitters	380
1.16.6.5.1	Polysilicon emitters	380
1.16.6.5.2	Implanted emitters	381
1.16.7	**Conclusion**	381
References		381

1.16.1 General Introduction

1.16.1.1 Photovoltaic Market

Crystalline silicon photovoltaic (PV) is the working horse of the PV energy market from its invention in the 1950s up to today. In the last decade, the market share of crystalline silicon PV has always been in the range between 80% and 90% (see blue sections in **Figure 1**).

Crystalline silicon PV can be subdivided into cells made of multicrystalline, monocrystalline, and ribbon silicon, with multicrystalline silicon (mc-Si) playing the most important role closely followed by monocrystalline silicon (mono-Si). The dominance of crystalline silicon PV has historical reasons: the early invention of this solar cell type and the parallel development of the microelectronic industry; in addition, the superior properties of silicon and silicon solar cells have also contributed to the dominance of crystalline silicon PV:

- Silicon is an *abundant* material (about 25% of the earth's crust is comprised of silicon).
- Silicon is *nontoxic*. This is especially important for a green technology.
- PV modules with crystalline silicon solar cells are *long-term stable* outdoors (>20 years). This is decisive for the cost competitiveness of PV because currently investment starts to pay back around the 10th year after the initial installation of the PV system.
- *High energy conversion efficiency*. A high efficiency reduces system costs and enables installation of high-power systems at sites with limited available space like rooftops. The best commercial silicon solar cells available today exceed 20% efficiency [1].

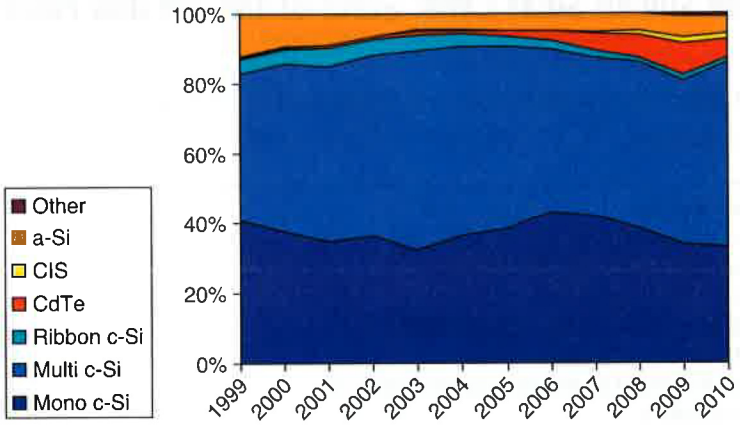

Figure 1 Market shares of different photovoltaic technologies. Data based on the yearly market surveys published in *Photon International*. Aachen, Germany: Photon Europe.

- *Considerable potential for further cost reductions.* Although there have been returning predictions that silicon PV has reached its cost minimum, the costs went down following a learning curve with a learning rate of 20% [2] (20% cost reduction for doubling the cumulated installed power) which will quite probably be extended in the future.

1.16.1.2 Historical Development of Cell Efficiency

In 1941, the first silicon solar cell was reported by Ohl [3]. It featured a melt-grown pn-junction and an energy conversion efficiency of less than 1%. A great progress was made in the early 1950s when Pearson, Fuller, and Chapin at the Bell Laboratories prepared silicon solar cells with a diffused pn-junction. The first cells were fabricated on p-type silicon and reached an efficiency of up to around 4.5% [4]. Then they switched to arsenic-doped n-type silicon with a boron-doped emitter [5]. This increased efficiency to a value of more than 6%. The first application of these 'solar batteries' was as power source for satellites. They won the competition against other power supplies such as chemical batteries [6]. The space race was of national interest for Americans and Soviets during the cold war and solar cells played an important technical role. In fact, today, PV panels are still the dominant power source for satellites and other space applications. Up to the end of the 1950s, the cells were mainly fabricated on n-type silicon, leading to superior efficiencies of up to around 14%. However, it was found that space radiation hardness was less detrimental for cells with a p-type base [7]. This became more clear when a high-atmosphere nuclear bomb was ignited by the Americans, leading to failure of the solar panels of satellites [8]. Thus, in the early 1960s, there was a switch to cells on p-type silicon with a phosphorus-doped emitter [9]. These cells had a higher radiation hardness but started with a lower efficiency. It took up to 1973 to achieve higher efficiencies with cells on p-type silicon than those reached in the early 1960s with cells on n-type base.

A second strong phase of cell development started in the 1980s with the passivated emitter solar cell (PESC) clearing the important 20% hurdle in 1985 [10]. The PESC and also its successors the passivated emitter and rear cell (PERC) [11] and the passivated emitter, rear locally diffused cell (PERL) [12] have a very important feature in common: surface passivation in order to reduce recombination of charge carriers at the surfaces. Indeed this is a crucial prerequisite for all high-efficiency silicon solar cells particularly for interdigitated back-contact cells [13, 14] where the collecting junction is at the rear side and most carriers have to diffuse a long way. Back-contact cells have always played an important role in the race for record efficiencies and are the base structure for today's best commercial solar cells with efficiencies greater than 22%. The best efficiency for a mono-Si solar cell is 25% [4, 15] getting quite close to the 'practical' limit of around 26% [16].

Although cell efficiencies on mono-Si are significantly higher, it is very important to keep an eye on cells on mc-Si since 5 out of 10 solar cells today are made of this material type. Mc-Si is cheaper than mono-Si but unfortunately also has a lower material quality due to a higher amount of crystal defects and metal impurities. Since this difference in material quality is especially relevant for record solar cells where hyper-pure floating-zone (FZ) silicon is used for monocrystalline cells, it is fair to report record efficiencies for multicrystalline cells separately. The major interest in mc-Si started in the mid-1970s with record efficiencies of around 15%. In this case, the historical increase in efficiency was mainly influenced by the improvement in material quality either during the crystallization process or during the cell process utilizing gettering and internal hydrogen passivation of crystal defects (see Section 1.16.4.3). An effective way to reduce the influence of material quality is the reduction of cell thickness and usage of effective surface passivation. This path led to today's record solar cell on mc-Si with an efficiency of 20.4% and a thickness of only 99 μm [17, 18].

1.16.1.3 Maximum Achievable Efficiency

A major question related to efficiencies of solar cells is of course how far one can get. The answer to this question was given in a very elegant way by Shockley and Queisser in the 1960s [19]. Based on a detailed balance calculation for the ideal case that the only

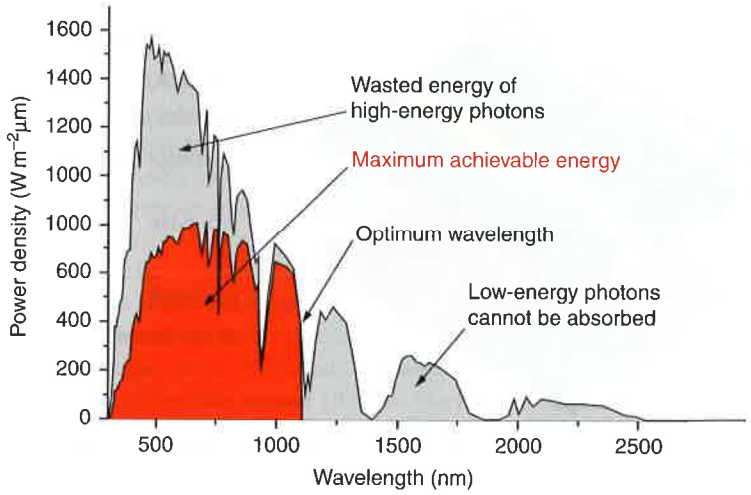

Figure 2 Spectral losses in a solar cell. The figure shows the maximum achievable energy of a silicon solar cell in relation to the sun spectrum (AM1.5).

recombination channel is radiative recombination, they calculated the maximum achievable efficiency, which is around 30% for a band gap of 1.1 eV (sic!).

Figure 2 visualizes the main loss mechanism in a silicon solar cell: spectral losses. It shows the maximum achievable energy of a silicon solar cell in relation to the sun spectrum. Photons carrying a specific energy can generate only one electron–hole pair even if their energy is higher. The energy greater than the band-gap energy is lost in thermalization of the hot carriers, that is, as heat (see the upper gray part in **Figure 2**). Photons with energies lower than the band-gap energy cannot generate an electron–hole pair (nonabsorption; see the right gray part in **Figure 2**). These two losses account for about 50% of the power carried in the sun spectrum.

In contrast to the calculation of Shockley and Queisser, in a realistic crystalline silicon solar cell radiative recombination does not play a dominant role due to the indirect band structure of silicon. Instead of this, Auger recombination plays a dominant role. Recent accurate determination of the Auger coefficients in silicon has led to the calculation of the maximum achievable efficiency of a silicon solar cell as being 29% [20]. However, such an idealized device without contacts is only of theoretical interest and cannot be realized. For a realistic but optimized silicon solar cell, an efficiency limit of 26% was predicted [16].

1.16.2 Current Status of Silicon Solar Cell Technology

1.16.2.1 Basic Structure of a Silicon Solar Cell

This section will give an overview of the technology currently used in industry to produce a silicon solar cell. A solar cell technology is defined by two features:

- the physical structure of the solar cell, which consists of a geometrical order of structure elements, and
- the production technology, that is, equipment, materials, and processes applied to realize such a product.

For a working solar cell, at least three structure elements are needed:

- An absorber that absorbs incoming photons and translates their energy to an excited state of a charge carrier. Typically, a semiconductor like silicon is used as the absorber and the absorption process generates an electron in the conduction band, that is, an electron from the valence band is transferred to the conduction band leaving behind a 'hole' in the valence band.
- A membrane that prevents the reverse process in which the excited carrier recombines with its ground state. Such a recombination may transfer the excitation energy of the electron into the excitation of a photon, transfer the energy of the electron to another already excited electron, or lead to lattice vibration. In the current technology, a junction formed by adjacent areas of p- and n-conducting semiconductor layers called the pn-junction is used.
- Contacts that allow for collection of carriers and interconnection with other solar cells or an outer load.

In principle, these elements would be sufficient, but an industrial solar cell is more complex as described in the following section.

1.16.2.2 Physical Structure of an Industrial Silicon Solar Cell

The currently dominating physical structure of mono-Si and mc-Si solar cells is mostly denoted as a co-fired screen-printed aluminum back surface field (Al-BSF) cell.

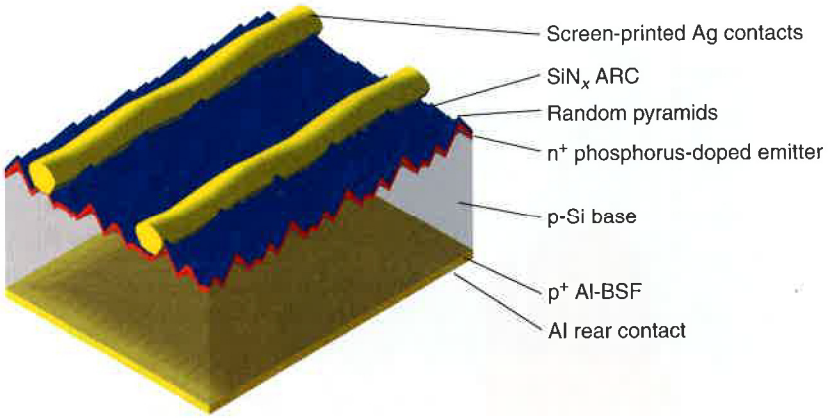

Figure 3 Structure of aluminum back surface field (Al-BSF) solar cell. ARC, Antireflection coating.

Although there are a number of variations within the family of Al-BSF cells, all have several distinct structure elements in common, making up around 80% of the world market share. In the following, these common characteristics are described (compare **Figure 3**):

1. The cell is most probably made from a $156 \times 156 \times 0.2\ mm^3$ sized boron-doped crystalline silicon wafer with an acceptor density N_A of around $10^{16}\ cm^{-3}$, which corresponds to a base resistivity of around $1\ \Omega\,cm$ (p-type substrate). The wafers are from either mono-Si or mc-Si. Mono-Si is typically grown and cut with the (100) plain parallel to the large surface of the wafer. Furthermore, these wafers are typically not full-square, but rather pseudo-square, that is, the diagonal measures about 5–20 mm shorter than a matching full-square and are with radial geometry at the corners. Mc-Si wafers are full-square with only slightly beveled corners. Multicrystalline means that the crystal area size is typically in the range of mm^2 to cm^2; thus, the number of crystals per wafer is in the range of several 10^3. The wafers are typically extremely pure, with metallic impurity levels below 1 ppm. In mono-Si wafers, oxygen is the dominant impurity with concentrations typically in the range of several $10^{17}\ cm^{-3}$. Mc-Si wafers show comparatively higher concentrations of metals and carbon, which accumulate in the grain boundaries. The oxygen concentration is rather in the range of $10^{17}\ cm^{-3}$ or below [21]. The main functions of a p-type substrate are to efficiently absorb incoming photons on a large surface, to enable diffusion of minority carriers (electrons), and to behave as a good conductor to enable efficient transport of majority carriers (holes) to the contacts.
2. The front side (within this text, front side refers to the side of a solar cell that faces the sun) of the solar cell is textured with a texture depth of typically a few micrometers. While mono-Si features upstanding randomly distributed pyramids, the surface of mc-Si solar cells mostly features a randomly distributed order of round-shaped valleys (compare **Figure 4**). The main functions of the texture are to increase the transmission of incoming photons into the silicon absorber and to increase the path length of the photons inside the absorber (oblique direction of the photon propagation relative to the surface and high internal reflection at the surfaces).
3. The top layer at the front side of the cell is doped with phosphorus. The donor concentration N_D falls steeply from more than $10^{20}\ cm^{-3}$ at the silicon surface to values below N_A in a depth of less than 1 µm forming a net n-type layer with a sheet resistivity of around $75\ \Omega\,sq^{-1}$ and a pn-junction of several hundreds of nanometers. The main functions are to allow the formation of this pn-junction with reasonable thickness to separate charge carriers, to enable a sufficient diffusion length of minority carriers

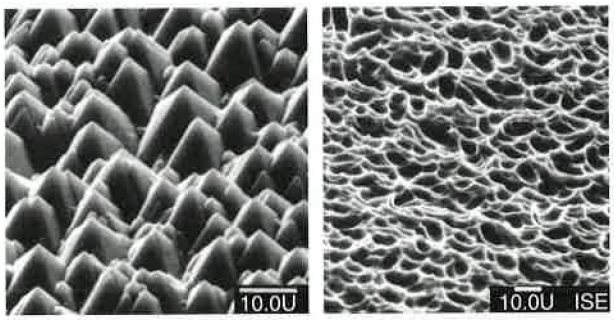

Figure 4 Texture on the front side of monocrystalline (left) and multicrystalline (right) silicon solar cells.

(holes) within the layer, and to allow for effective conduction to enable efficient transport of majority carriers (electrons) to the contacts.

4. The front side is further coated with an approximately 75 nm thin layer of amorphous hydrogenated silicon nitride. The layer is slightly silicon-rich leading to a refractive index of approximately 2.1 [22] for an effective reduction of front reflection. The amorphous structure allows for the incorporation of hydrogen concentration of typically more than 10 at.%. The main functions are to provide antireflection coating based on refractive index matching and quarter-wavelength thickness and passivation (the term passivation is used in order to indicate reduction of carrier recombination rates, typically by technical means; passivation can take place at the surface or within the volume and is denoted accordingly) of the n-type surface as well as the volume based on the incorporated hydrogen [23, 24].
5. At the front surface an H-like pattern of sintered silver paste is formed [25], which punches through the silicon nitride layer [26, 27]. The H-like pattern is continuous and makes up approximately 8% of the front surface. Below the sintered paste, pure silver crystallites are penetrating through the silicon nitride into the silicon along the (111) planes with a depth of up to around 100 nm and a surface area fraction of typically around 10–30%. The bulk of the sintered silver paste is densely formed from round- and flake-shaped silver particles, which are interconnected to each other by sinter necks (compare **Figure 5**). The volume in between the silver particles is filled with glass frit. The main function of the H-like pattern is efficient carrier transport and transparency for the incoming light, that is, low shading. It can be subdivided into two device elements, which are denoted contact busbars and contact fingers, which fulfill specific functions:
   - Mostly three busbars are used, which are approximately 1.5 mm wide and 20 µm high, equally spaced in parallel to the wafers edge. Their main functions are collection of current from the contact fingers and allow for a soldering interconnection to a coated copper ribbon with good electrical and mechanical contact (minimum adhesion force 1 N).
   - Contact fingers are approximately 100 µm wide and 20 µm high and are situated perpendicular to the busbars with a pitch of typically 2 mm. At the outer edges of the wafer which are parallel to the busbars, the fingers are frequently interconnected to each other. At all edges there is a range of typically 1.5 mm which is not covered by contacts at all. The main functions of the contact fingers are to provide low contact resistance to the underlying n-type silicon surface and an excellent lateral conductivity for efficient carrier transport. The interconnection of fingers at the edge enables good carrier collection from the edge of the solar cell and tolerance to individual finger interruptions at the outer side of the cells. Analysis of the microstructure of the contact area between screen-printed finger and silicon has revealed that the silver bulk is typically separated by a thin glass from the silicon surface. Different current transport paths have been discussed and found including grown-in silver crystals in close contact with the silver bulk as well as enhanced carrier transport due to metallic particles in the glass layer allowing for multistep tunneling (compare **Figure 5**) [28, 30–32].
6. The rear side is fully metallized. The main function is efficient carrier transport. Again the rear side metallization can be subdivided into two areas.
   - Around 5% of the rear side area is used as contact pads, which are situated on the opposite side of the front busbar. They form either a continuous or an interrupted line. These contact pads are typically 4 mm wide and consist of approximately 20 µm thick silver paste. Frequently, a low fraction of aluminum is also incorporated. The vertical structure at the rear silver contact pads is similar to the one at the front contacts. The aluminum allows for a slight doping underneath the silver contact pads [33]. The main functions of these contact pads are to collect the current from the metallized area and to enable a high-conducting electrode for later soldering to the interconnector ribbon with good mechanical contact (minimum adhesion force 1 N).
   - The remaining area of the rear side consists of a multilayer area which is surrounded by a nonmetallized 1.5 mm wide area all around the wafer edge. The silicon surface at the metallized rear area is doped with aluminum of approximately 5 µm deep to a

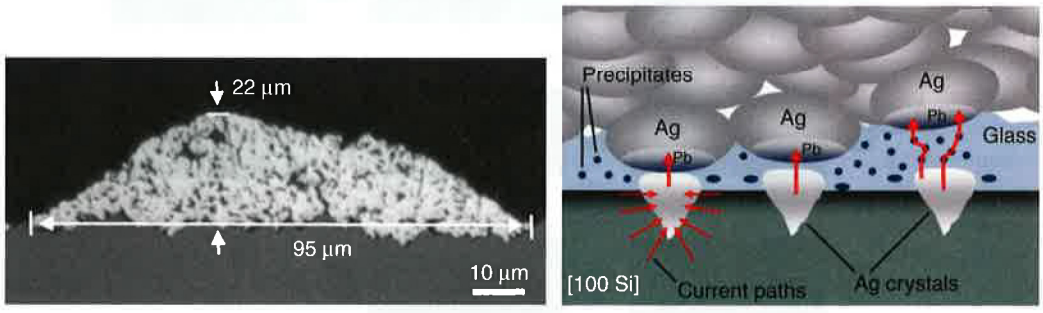

Figure 5 (Left) Picture of a current screen-printed contact. (Right) Model for the current transport at the screen-printed silver contact. Three different current transport routes between silver crystals and silver bulk are proposed: direct contact, tunneling through the glass, and multitunneling via metal precipitates in the glass. Reproduced with permission from Kontermann S, Hörteis M, Kasemann M, *et al.* (2009) Physical understanding of the behavior of silver thick-film contacts on n-type silicon under annealing conditions. *Solar Energy Materials and Solar Cells* 2009(93): 1630–1635 [28] (copyright 2009 Elsevier) after Schubert G (2006) Thick Film Metallisation of Crystalline Silicon Solar Cells. Dissertation, Universität Konstanz [29].

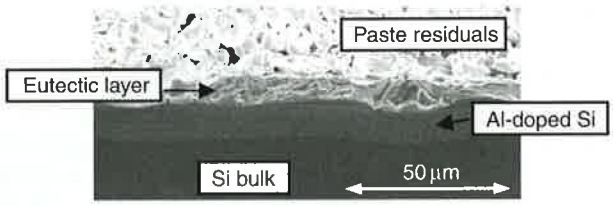

Figure 6 Scanning electron microscopy (SEM) image of the cross section of the rear Al contact and the underlying doped area (aluminum back surface field (Al-BSF)). Reproduced with permission from Krause J, Woehl R, and Biro D (2010) Analysis of local Al-p^+-layers for solar cells processed by small screen-printed structures. In: *Proceedings of the 25th European Photovoltaic Solar Energy Conference and Exhibition*, pp. 1899–1904. Valencia, Spain [36]. Copyright 2010, WIP, Munich.

maximum concentration of around $3–4 \times 10^{18}\,cm^{-3}$, which slowly decreases toward the surface [34, 35]. On top of the doped silicon surface, there is a eutectic layer, also approximately 10 µm (see **Figure 6**). On top of the eutectic layer, there is a layer of sintered aluminum paste with substantial in-diffusion of silicon [36]. The main functions of these areas are to provide a low contact and lateral resistance as well as a passivation of the rear side by implementing a high–low junction or back surface field (BSF).

7. The edge of the solar cell consists of an interruption of the highly n-doped layer on the front and the p-doped layer on the rear side of the solar cell. This interruption is at least a few micrometers wide. The main function of this area is to interrupt an unwanted carrier transport from the n-type emitter at the front to the rear p-layer in order to prevent parasitic shunting.

Typical efficiencies for this cell structure in current production lines are 17.5–18.0% for mono-Si and 16.5–17.0% for mc-Si.

The main drivers for the enormous success of this cell structure are as follows:

- The simplicity of the production technologies related to realize the structure in comparison to the efficiency which can be obtained.
- The tolerance of structure and process against variations of wafer quality, that is, variations in the concentration of base material doping, metallic and other impurities as well as grain boundaries.
- One of the most important points for the success of this cell structure is the availability of the associated production technology. None of the vital structure elements or process sequences is severely protected by patents or other legal issues. This allowed many equipment and material manufacturers to join the competition for best and lowest cost products.

Due to the enormous demand for production technology on the market, these drivers were keys to a very rapid increase in production capacity.

1.16.2.3 Process Sequence

In the following, the individual process steps are discussed in detail. The corresponding process flow is shown in **Figure 7**.

1. Incoming inspection and sorting into carriers

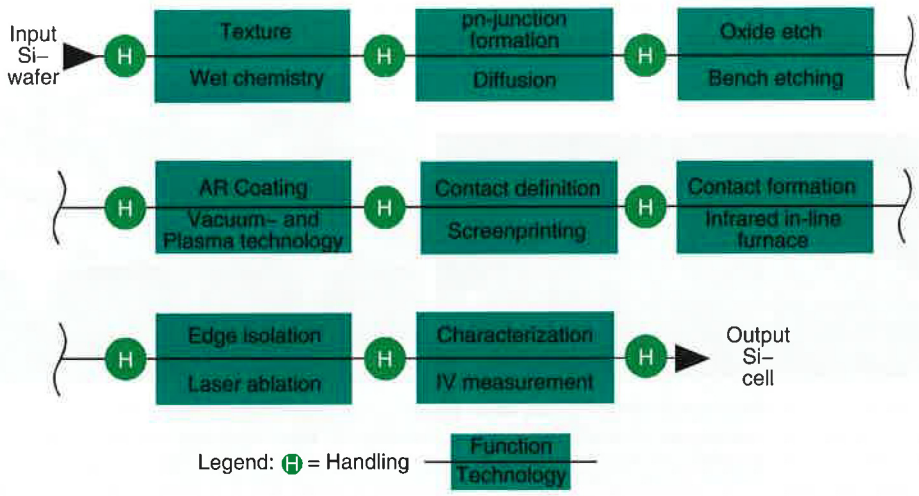

Figure 7 Schematic process flow for an industrial crystalline silicon solar cell line.

The entrance interface is the wafer in a stack. As a first step the wafers are typically inspected for microcracks using infrared transmission. Then they are either sorted into wet chemical carriers or directly put onto a belt for further processing depending on whether further processing is batch or in-line processing, respectively.

2. Saw damage removal, texturing, and cleaning

Differences in the texturing process used depend mostly on the crystallinity of the wafer. Mono-Si wafers are etched in 70–80 °C hot aqueous sodium hydroxide with organic additives (typically isopropanol) for approximately 20–30 min to attain the random pyramidal structure. The main reaction can be summarized as

$$2KOH + Si + H_2O \rightarrow K_2SiO_3 + 2H_2\uparrow \quad [1]$$

Care has to be taken with the released molecular hydrogen and eventually evaporated organic additives. Due to the long etching time and high temperature, batch-type wet benches are the standard for this process in order to achieve high capacity and throughput. The etching is typically stopped using a short dip in an acidic solution. Specific cleaning is partially applied at this point to remove metal ions and other impurities from the surface. Then rinsing is performed and the wafers are dried.

Mc-Si is textured by treating with acidic agents that are simultaneously oxidizing and oxide etching like mixtures of deionized water, HNO_3, and HF for approximately 1–2 min. The process temperature is typically reduced to values of 10–15 °C for better control and reduced etching since the process is strongly exothermic. The main reaction that takes place is

$$3Si + 4HNO_3 + 12HF \rightarrow 3SiF_4 + 4NO + 8H_2O \quad [2]$$

Care has to be taken with the nitrous oxide released during the process. After the texturing, a thin porous surface layer (stain), which remains after the etching process, is removed in aqueous potassium hydroxide. The low temperature and short process times enable the use of in-line wet bench systems, which offer improved material flow compared to the carrier-based wet bench processing. The wafers are rinsed in cascade benches and dried.

3. Phosphorus diffusion

The textured and cleaned wafers are then transferred into quartz carriers for phosphorus diffusion. Narrow wafer distance in the carrier and back-to-back processing allow for up to 500 wafers being processed simultaneously in one tube. The quartz carrier is then transferred into a hot tube and the furnace is closed. For phosphorus diffusion, pure nitrogen is used as a carrier gas, which is guided through a container of liquid phosphorus oxychloride ($POCl_3$) and released to the chamber together with oxygen to perform the following reaction on the wafer surface:

$$4POCl_3 + 3O_2 \rightarrow 2P_2O_5 + 6Cl_2 \quad [3]$$

The production of chlorine is beneficial in terms of the removal of metallic impurities like sodium. This part of the process is typically denoted predeposition. A second reaction takes place from the phosphorus oxide, which can be described as

$$2\,P_2O_5 + 5\,Si \rightarrow 5\,SiO_2 + 4\,P \quad [4]$$

This phosphorus silicate glass (PSG) is grown to a thickness of a few tens of nanometers and then the flow of $POCl_3$ is turned off to keep the phosphorus content at a finite level. This allows a deeper diffusion for a given surface concentration during the subsequent drive-in. The temperature is typically increased for this part of the process to plateau temperatures in the range of 820–850 °C. At the end of the process, the furnace is purged and the carrier is taken out of the furnace. A typical cycle time is around 1 h [37].

In-line diffusion has been used for many years instead of tube furnace diffusion. Here the phosphorus dopant is applied outside the furnace, for example, by ultrasonic spraying. In-line diffusion has clearly lost market share due to several reasons even though low contamination furnaces based on ceramic rolls or strings have proven to enable clean processing [38].

4. Phosphorus glass removal

The PSG is removed in a further wet chemical etching processing. Hydrofluoric acid is used due to its excellent etch selectivity with the ratio of etching rate of phosphorus glass to silicon around 400:1 for standard processing conditions. Nevertheless, since the phosphorus surface concentration is very high after the diffusion, a controlled etch back of a few nanometers of the highly doped surface area is desirable and is used in many production lines. Again rinsing and drying is applied after processing. The full process cycle takes just a few minutes and can be applied in either batch- or in-line-type wet benches.

5. Deposition of antireflection coating

As a next step, the hydrogenated amorphous silicon nitride layer is deposited. The dominating technology is plasma-enhanced chemical vapor deposition (PECVD) based on silane and ammonia. There are a number of different PECVD approaches in the field, two most important being a low-frequency direct plasma or a microwave plasma based on linear antennas for in-line processing (compare **Figure 8**). The plasma partially dissociates the silane and ammonia and the deposition takes place via different mechanisms [40].

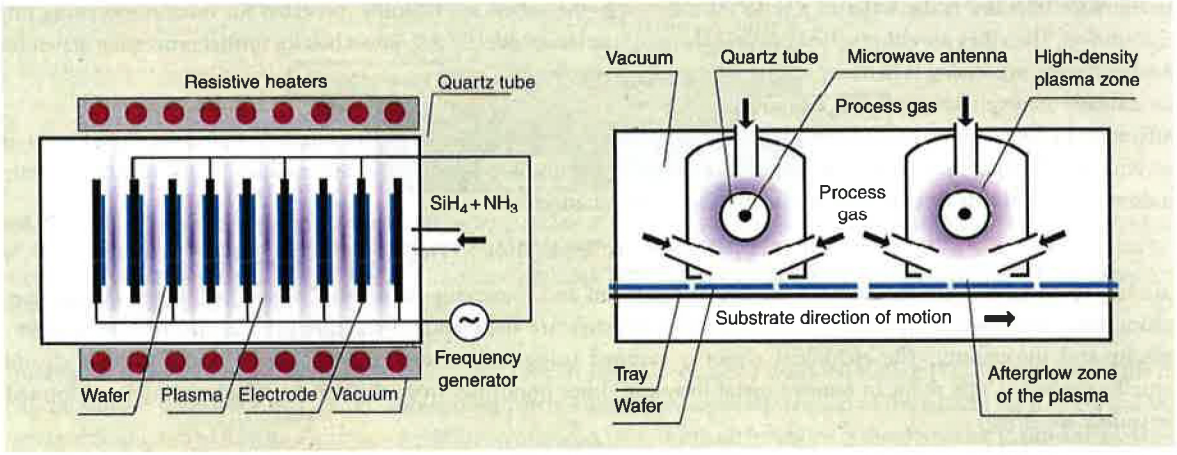

Figure 8 Schematic drawing of the two dominating plasma-enhanced chemical vapor deposition (PECVD) techniques. (Left) Direct low-frequency plasma and (right) microwave antenna. Reprinted with permission from Photon International, March 2003 [39]. Copyright 2003 Photon Holding GmbH.

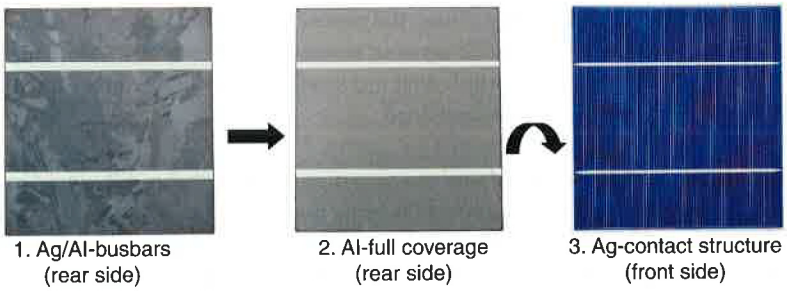

Figure 9 The three print steps for contact formation.

Reactive sputtering based on silicon-containing targets and nitrogen and ammonia as reactive gases was introduced as an alternative with excellent lateral homogeneity and optical performance, but has not succeeded in substituting the dominating PECVD approach [41].

6. Screen printing of contacts

   The contact definition is performed via subsequent printing of three different pastes – rear Ag, rear Al, and front Ag paste – and subsequent drying. During the printing process, the paste is distributed by the fast moving squeegee. The paste makes contact with the wafer substrate through the openings of the screen. A typical procedure is shown in **Figure 9**, but the printing can also be applied in a different order, for example, printing the front H-like pattern first. The pastes typically contain particles of metal and glass frits with maximum size in the range of 10 µm to prevent clogging of the screen and efficient formation of sinter necks in the following high-temperature steps. Further constituents are solvents and other organic compounds that are added in order to improve the printability and give the pastes their thixotropic behavior, that is, reduced viscosity under the application of shear stress during printing. Substantial developments have taken place in the formulation of the pastes, which enabled a large part of the efficiency development within the last 10 years. Consequently, the emitter sheet resistance could be increased from 40 to nearly 80 $\Omega\,sq^{-1}$. Also the formulation of the rear paste has been improved substantially, which allows the formation of a more homogeneous and highly doped BSF and reduced mechanical stress which appears due to the quite different expansion coefficients of silicon and aluminum. Drying at 200 °C is important to remove the solvents from the paste to prevent spreading. The last drying step can be included in the final firing step.

7. Contact firing

   After the last printing step, the wafers undergo a further thermal treatment in a conveyor belt furnace. During temperature ramp-up, the organic compounds with low boiling temperature that have been added by the last printing step are removed. In the second phase, the remaining organic compounds are burned in an oxygen-containing atmosphere at around 400 °C. Then the wafers are heated to temperatures around 800 °C within a few seconds and cooled directly thereafter. The front and rear contact formation takes place during this part of the process. The most widely used models for the contact formation are shown in schematic graphs in **Figures 10** and **11**.

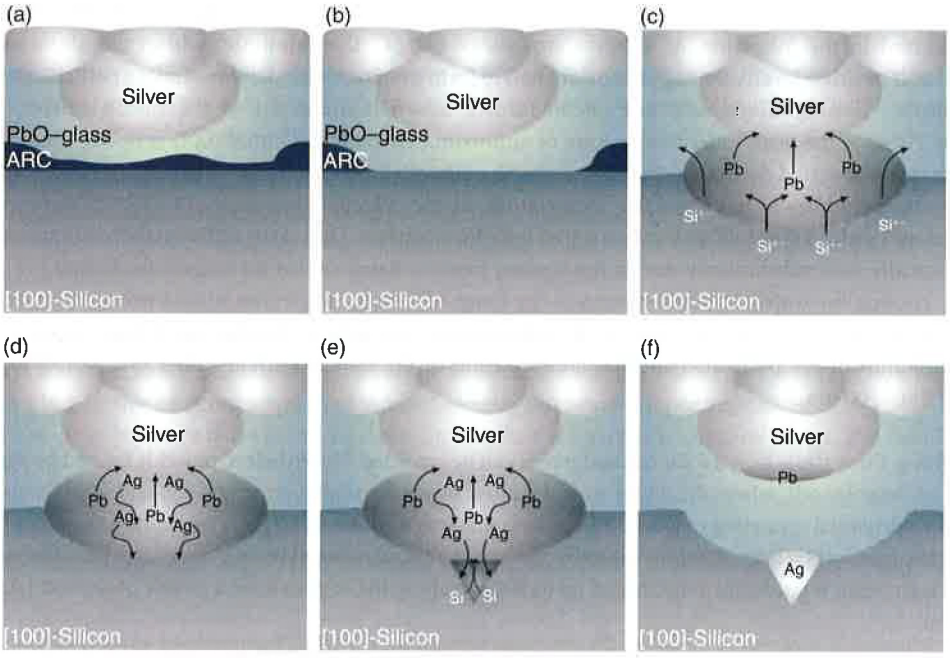

Figure 10 Simplified model of contact formation. (a) Schematic cross section of Ag thick film paste on <100> Si after combustion of organics. (b) Glass etches through SiN*x* layer. (c) Redox reaction between Si and glass. Pb is formed. (d) Liquid Pb starts to melt Ag. (e) Ag–Pb melt reacts with Si. Inverted pyramids are formed. (f) On cooling down, Ag recrystallizes on (111)-Si planes. Reproduced with permission from Schubert G (2006) Thick Film Metallisation of Crystalline Silicon Solar Cells. Dissertation, Universität Konstanz [29].

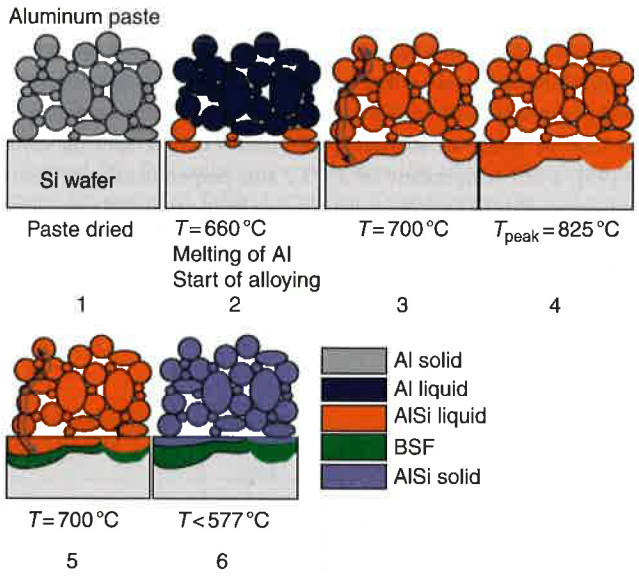

Figure 11 Formation of the aluminum back surface field and rear contact from a screen-printed aluminum paste: (1) paste after drying; (2) at 660 °C, melting of aluminum occurs and silicon dissolves in a mixed phase; (3) around 700 °C, all the aluminum is completely molten and substantial incorporation of silicon occurs; (4) at the peak temperature, the liquid phase has its maximum thickness; (5) during cooling down, the silicon recrystallizes with incorporation of aluminum, while the silicon content in the mixed liquid phase reduces, (6) at the eutectic temperature, the mixed phase of aluminum and silicon solidifies. Reproduced with permission from Huster F (2005) Investigation of the alloying process of screen printed aluminium pastes for the BSF formation on silicon solar cells. In: *Proceedings of the 20th European Photovoltaic Solar Energy Conference*, pp. 1466–1469. Barcelona, Spain [42]. Copyright 2005 WIP, Munich.

The front contact formation process is described in the model of Schubert [29]. Within the firing process, the glass contained in the paste etches the dielectric layer and gets into direct contact with the underlying silicon. Then, the liquid glass promotes dissolution of silver from the silver particles and silicon into this liquid phase as well as of the metallic glass particles into the silver particles. The dissolution of the silicon appears preferentially along the strongly bound (111) planes within the silicon forming the special shape of the crystallites [28].

The formation of the p-doped rear layer can be subdivided into several steps according to the model of Huster [42], and is briefly summarized in the following. At temperatures above 660 °C, the aluminum within the aluminum oxide-coated particles melts and punches locally through the oxide shell to form a contact with the surrounding particles and the underlying silicon. On further heating, aluminum and silicon form a mixed liquid phase at the silicon surface, with a ratio of approximately 70/30 at the peak wafer temperature of approximately 825 °C. During cooling down, the process is reversed, but aluminum is incorporated during the epitaxial regrowth of the silicon at the surface. The concentration of the aluminum is determined by the solubility at the respective temperature. At the eutectic temperature ($T = 577$ °C), the remaining mixed phase solidifies and yields a continuous layer on top of the silicon surface. Due to the different thermal expansion coefficients, the wafer is typically bent substantially during the cooling process. Based on his investigations, Huster [43] proposed stress relief cooling: cooling the wafers to temperatures in the range of −40 °C accelerates plastic reformation of the rear contact layer, which can be used to completely eliminate the otherwise occurring bow. This has partly been used in the industry, but adapted formulations of the paste also allowed minimization of the bow to current values of 1–2 mm for standard wafer thicknesses of 180–200 µm.

8. Edge isolation

   After contact firing, the wafer is now a solar cell and power can be extracted. Nevertheless, power is limited by a severe shunt path over the edge of the solar cell, where the highly doped emitter meets the highly doped Al-BSF and yields high–high junctions, which allow for substantial tunneling or worse. The process that was introduced 10 years ago is the removal of the n-conducting layer in the near-edge areas by laser ablation. Typically, the area is ablated using a UV solid-state laser featuring nanosecond pulse duration. The laser beam is guided in a distance of up to 200 µm along the edge to form a groove of around 10 µm in depth and 30 µm in width.

   There is one important deviation of this sequence which is based on a different separation of the front and rear junction. Recently, the separation using single-sided wet chemical etch back of the rear phosphorus-doped layer has become a favorable technology for junction isolation. It is performed in combination with the PSG glass removal, which keeps equipment and consumable costs low. Compared to laser edge isolation from the front side, it saves a small amount of active cell area and typically delivers a slight efficiency gain.

9. *I–V* measurement and sorting

   After processing of the cell is finished, the cells are measured for their electrical and optical characteristics. The current–voltage characteristic is determined using illumination via a flash with an intensity plateau of a few tens of milliseconds. The whole measurement from $V = 0$ to $V = V_{oc}$ takes about 20 ms (compare **Figure 12**). The measurement is performed as close to standard testing conditions as possible, that is, using an irradiance of 1000 W m^{-2}, a spectral distribution in accordance with the normalized AM1.5g spectrum [45], a cell temperature of 25 °C, and perpendicular incidence of the light. The deviations of the irradiance from standard testing conditions are taken into account by the signal of a monitor cell placed adjacent to the tested cell. Furthermore, the cell is tested under a reduced light level and in the dark in order to extract further information on the electrical performance of the cell. Further visual measurements are performed, especially to control the visual appearance of the cell. Finally, the cells are sorted into performance bins.

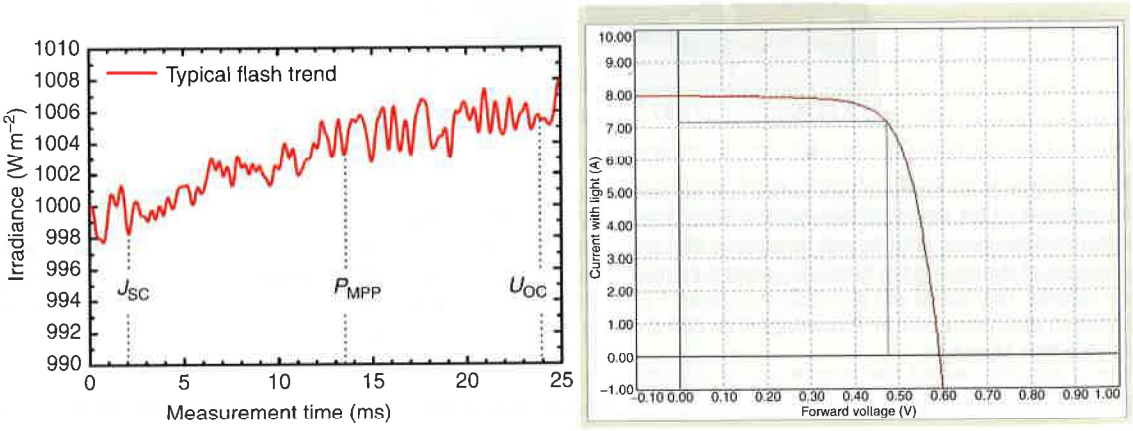

Figure 12 (Left) Typical irradiance within the plateau of a flash tester. The dotted lines indicate typical incidence with the electrical measurement of short-circuit current density (J_{sc}), maximum power point (P_{MPP}), and open-circuit voltage (V_{oc}). (Right) *I–V* curve taken by a flash tester. Reproduced from Krieg A (2007) Inbetriebnahme und Weiterentwicklung eines automatisierten IV-Kennlinienmessplatzes und Entwicklung eines Verfahrens zur Materialverfolgung in der Solarzellenproduktion. Masterarbeit, Fachhochschule für Technik und Wirtschaft Berlin [44].

1.16.3 Influence of Basic Parameters

To optimize the efficiency, that is, to reduce the power losses of silicon solar cells, it is important to understand the influence of different cell and material parameters such as bulk lifetime and cell thickness. In general, the influence of basic parameters can be classified based on the associated loss mechanisms:

1. The ratio of electrons that are not excited to the conduction band per incoming photon, often referred to as optical losses. Here further differentiation can be applied based on whether
   - the loss occurs since the photon does not enter the solar cell. This might be due to reflection from the metallized areas of the active surface of the cell.
   - the photon enters the cell but leaves it again without absorption within the cell. This is mainly controlled by the internal reflectance at front and rear and takes place for near-band-gap photons.
   - the photon is absorbed in the cell but no excitation of an electron from the valence to the conduction band occurs, which mainly takes place by free carrier absorption of infrared radiation in heavily doped regions.
2. Electrons that are excited but not delivered to an outer circuit, often referred to as electrical losses. The electrical losses can be subdivided into
   - Losses due to recombination of electrons with holes. The recombination takes place in every structure element of the wafer (excluding deposited layers and contacts).
   - Losses due to scattering of the (majority) charge carriers, which leads to ohmic heat. This takes place in all structure elements of the solar cells.

The physics of the solar cell can be described well by a number of basic equations, partially being of differential type in time and space. Thus, exact calculations of the performance of a solar cell can be obtained by only one- to three-dimensional numerical simulators. Since sound multidimensional calculations are time consuming in both the description of the problem and the computer-based numerical calculation, a one-dimensional approach using the program PC1D is probably the most widely used approach to simulate solar cells [46]. A number of lumped parameters are used due to the one-dimensional characteristic of the simulator. **Table 1** gives an overview of a standard set of parameters that can be used to describe and simulate a screen-printed mono-Si solar cell yielding an efficiency of 18.0%.

It is of specific interest to assess the impact of the variation of relevant parameters on solar cell's efficiency. Three parameters are most relevant to determine recombination in the base of the solar cell: the thickness of the solar cell, the bulk carrier lifetime, and the rear surface recombination velocity. Changing the thickness and the bulk carrier lifetime of the solar cell can only be achieved by changing the wafers used for processing, which is of specific importance since the wafer covers a substantial cost share of the whole solar cell (60–70%). We have performed PC1D simulations to visualize the effect of variation of these parameters for a standard industrial cell based on the parameter set shown in **Table 1** applying a variation of the rear surface recombination velocity in the range of $S_{rear} = 1250\,cm\,s^{-1}$ (bad Al-BSF), $500\,cm\,s^{-1}$ (standard Al-BSF), and $200\,cm\,s^{-1}$ (excellent Al-BSF). A value as low as $80\,cm\,s^{-1}$ has so far been demonstrated only for dielectric passivation with localized Al-BSFs, which also changes the internal reflectivity at the rear side to values of up to 95% [50, 51].

Table 1 Cell and material parameters used for model calculation of a equation monocrystalline silicon solar cell yielding an efficiency of 18.0% ($V_{oc} = 620\,mV$, $J_{sc} = 36.5\,mA\,cm^{-2}$, FF = 79.5%)

Parameter	*Value*
Base resistivity, ρ_{base}	$\rho_{base} = 2\,\Omega\,cm$, typical value of industrial monocrystalline silicon solar cells
Oxygen concentration, $[O_i]$	$6 \times 10^{17}\,cm^{-3}$
Bulk recombination due to boron–oxygen complex, τ_{CZ}	Fundamental limit given by Bothe *et al.* [48] with a factor of 2 due to improvements by high-temperature steps [48, 49] Using $\rho_{base} = 2\,\Omega\,cm$, which corresponds to $N_{A,base} = 7.2\,cm^{-3}$, $[O_i] = 7 \times 10^{17}\,cm^{-3}$, and yields $\tau_{CZ} = 84\,\mu s$
Shaded area fraction due to front metallization, f_{shaded}	7%
Reflection on active cell area	Measured data with $R_{weighted} = 3\%$
Emitter doping and passivation	$R_{sheet} = 75\,\Omega\,sq^{-1}$, error function profile, $S_{front} = 4 \times 10^4\,cm\,s^{-1}$
Rear recombination and internal reflectance (due to the difficulties in describing an aluminum BSF properly in PC1D)	$S_{rear} = 500\,cm\,s^{-1}$ [50] $R_{int} = 65\%$ [50, 51]
Lumped series resistance	$R_s = 0.6\,\Omega\,cm^2$
Lumped parallel resistance	$R_p = 10\,k\Omega\,cm^2$

The used internal reflectance and surface recombination velocity data are based on accurate internal quantum efficiency analysis of current solar cells [47].

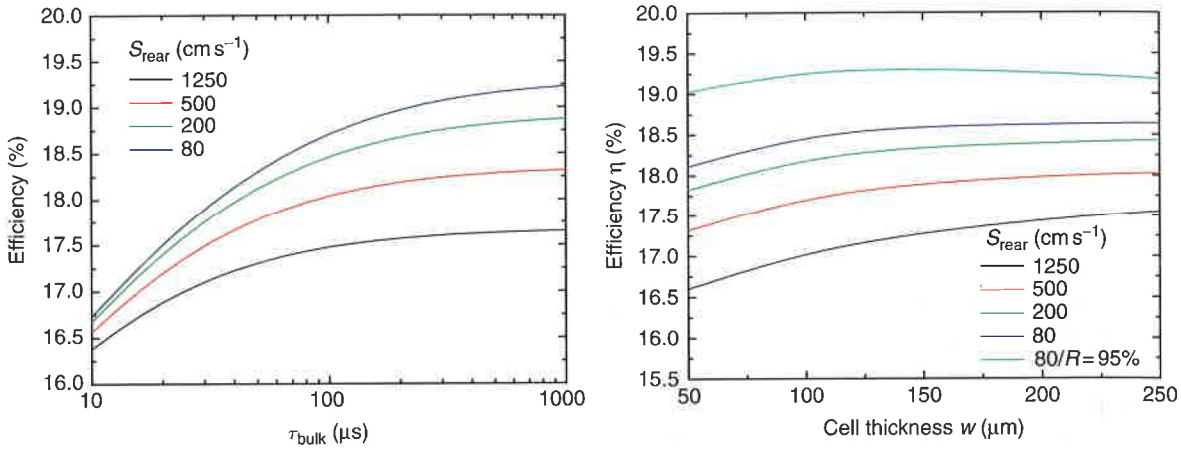

Figure 13 PC1D simulation of cell efficiency for variations of the bulk lifetime τ_{bulk} (left, cell thickness $w = 200\,\mu m$) and cell thickness w (right, $\tau_{bulk} = 84\,\mu s$) for different rear surface recombination velocity S_{rear}. The figure on the right also includes the result for an increased internal rear reflectance (95%). $S_{rear} = 500\,cm\,s^{-1}$ can be taken as state-of-the-art.

In Figure 13, the result of PC1D simulations for variations of bulk lifetime and cell thickness is shown for different rear recombination velocities. The high impact of the bulk lifetime on the efficiency in the range from 10 to 1000 µm is clearly visible. A reduced rear recombination velocity substantially increases the sensitivity due to the more dominant bulk recombination.

The impact of the cell thickness on the efficiency is clearly dependent on the rear recombination velocity. For high S_{rear} of $1250\,cm\,s^{-1}$, a reduction of the thickness will greatly reduce the efficiency of the solar cell. This reduction is only small but still apparent, if S_{rear} is reduced to $80\,cm\,s^{-1}$. But if we further turn on the increased internal reflectivity of a dielectrically passivated rear, then the efficiency actually increases to a thickness of around 100 µm and is just reduced after this.

1.16.4 Strategies for Improvement

1.16.4.1 Dielectric Surface Passivation

1.16.4.1.1 Influence of surface passivation

All cell structures that have shown efficiencies greater than 20% feature an efficient surface passivation with dielectric layers. Especially the rear side is of great importance as shown before. To achieve surface passivation in a cell structure, nearly the full rear surface (around 99%) is covered with a dielectric layer like SiO_2, SiN_x, or Al_2O_3 to greatly reduce the rear surface recombination velocity S_{rear}. Only small point-like or line metal structures on the rear form the base contact (see **Figure 14**).

However, the present state-of-the-art rear surface structure of industrial silicon solar cells is a screen-printed and thermally fired Al-BSF (see Section 1.16.2), which has two major restrictions: (1) the wafer bow due to the firing process and (2) the lower electrical

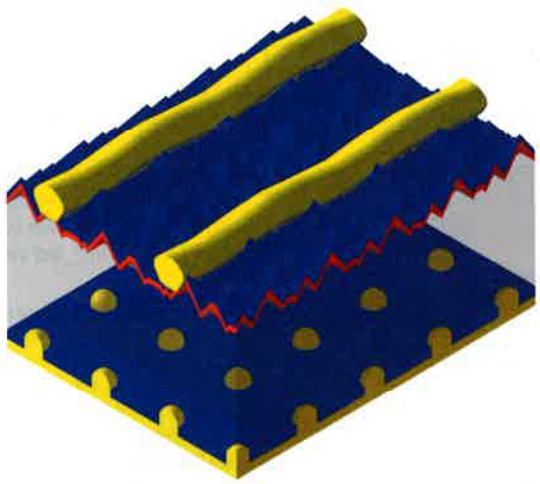

Figure 14 Silicon solar cell with surface passivation (blue) at front and rear surface. Only small point-like metal points (yellow) form the base contact.

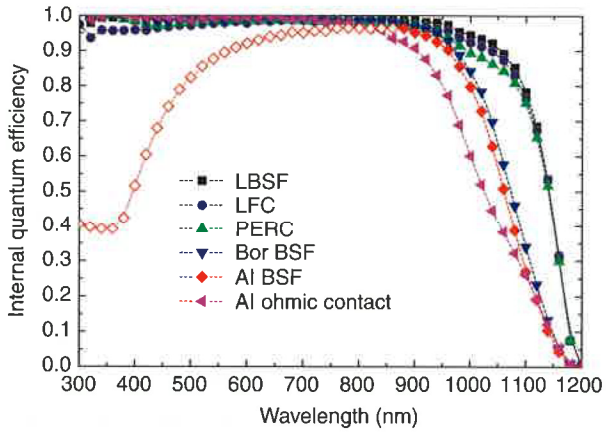

Figure 15 Internal quantum efficiency (IQE) of different rear surface structures on 1 Ω cm 250 µm thick floating-zone (FZ)-Si with a high-efficiency front structure. Note: The low IQE for short wavelengths of the Al-BSF cell (open diamonds) is due to a degradation of front surface passivation during firing. Nevertheless, the IQE starting at 900 nm is identical to the performance of industrial cells. For abbreviations, see **Table 2**.

Table 2 Internal reflectance (R_{int}) and rear surface recombination velocity (S_{rear}) as extracted from the data in **Figure 15**

Structure	R_{int} *(%)*[a]	S_{rear} *(cm s^{-1})*
LBSF (local boron back surface field) [55]	94.5	60
LFC (laser-fired contacts) [56]	95.5	110
PERC (random pyramids, passivated emitter and rear cell) [11]	95.0	200
Bor-BSF (boron-diffused back surface field)	71	430
Al-BSF (screen-printed alloyed Al back surface field)	65	750
Ohmic Al contact (evaporated)	83	10^7

[a] Note that for a proper description, it is necessary to introduce a Phong-like characteristic.
The dielectric passivation layer for the LBSF, LFC, and PERC structure was a thermally grown 105 nm thick oxide.

and optical quality. In particular, the rear surface recombination velocity S_{rear} is a crucial parameter, but exhibits a great range of values found in literature. This makes it difficult to evaluate the potential of Al-BSFs versus dielectric passivation.

Thus, an experimental study of different rear surface structures combined with a high-efficiency front structure which does not limit the cell performance was performed [52]. This makes it possible to determine the surface recombination velocity S_{rear} and the internal reflectance R_{int} quite accurately [53].

Figure 15 shows the measured internal quantum efficiencies (IQEs) of different rear structures starting from a low-quality ohmic Al contact up to a PERL [54]/local back surface field (LBSF) [55] rear surface. The effective S_{rear} and R_{int} have been extracted by fitting a simulation model to the IQE and reflection measurement (see **Table 2**). It should be noted that the quality of the Al-BSF formation has been improved since this investigation. Therefore, in the simulation in Section 1.16.3, S_{rear} values of 500 cm s^{-1} have been used.

1.16.4.1.2 Passivation mechanisms of dielectric layers

There are two different mechanisms leading to good surface passivation (for a comprehensive overview about this topic, see Reference 57): (1) the reduction of interface states D_{it} and (2) field effect passivation, that is, the strong reduction of one carrier type by incorporation of fixed charges Q_f in the passivation layer. Although these mechanisms or the combination of both leads to low surface recombination velocities for different excess carrier densities Δn, the resulting $S(\Delta n)$ curve shows different characteristics (see **Figure 16**). The reduction of interface states is more effectively reached for thermally grown SiO_2 layers, while the field effect passivation together with a moderate reduction of D_{it} is more typical for PECVD-deposited layers like SiN_x. Typical values for SiO_2 are $D_{it} = 10^{10}$ cm^{-2} eV^{-1} and $Q_f = 10^{10}$ cm^{-2}, while values for SiN_x are $D_{it} = 10^{11}$ cm^{-2} eV^{-1} and $Q_f = 10^{11}$ cm^{-2}.

1.16.4.1.3 Layers and processes for surface passivation

Due to the successful implementation of passivation layers for high-efficiency devices in the 1980s, the respective processing technologies have been a field of intense research and development in the past decade. According to their main passivation mechanisms, we can subdivide these layers into four groups:

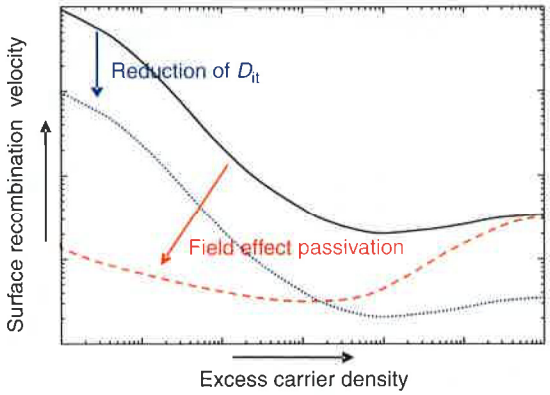

Figure 16 Sketch of the impact of the two passivation schemes, reduction of interface state density D_{it} (dotted) and field effect passivation (dashed).

1. Thermally grown SiO_2 was the passivation layer utilized for the first solar cells with efficiencies greater than 20%. Thermally (800–1000 °C) grown SiO_2 yields excellent passivation on p- and n-type surfaces. The oxidation process is unique as it is not a mere deposition process as all the other layers described in the following, but it actually consumes silicon of a defined thickness of approximately 45% of the total layer thickness during processing [58]. This leads to the fact that the rate of layer formation is linear only for a thickness in the range of a few nanometers and it is limited by diffusion of the reaction species through the already existing oxide layer. The growth rate is thus described by a linear-parabolic model [59, 60]. Under standard conditions, the oxidation takes place at both sides simultaneously. It can be used as a rather thin layer of around 10 nm or rather in the range of 100 nm. The latter thickness is usually used if the layer is meant to also show optical functionality to serve as an antireflection layer on the front or a reflection layer on the rear side. Silicon oxide is not temperature stable when it is covered by aluminum and exposed to temperatures above 500 °C. A capping layer of silicon nitride can be an appropriate choice in such cases. Oxidation was considered to be too expensive, but higher capacity of tube furnaces and in-line oxidation allow for lower cost [61].
2. Excellent passivation on p-type surfaces has been demonstrated with amorphous hydrogenated silicon nitride (a-SiN_x:H) [62], silicon oxide (a-SiO_x:H) [63], and silicon carbide (a-SiC_x:H) [64] layers. These layers have in common that they can provide high densities of positive fixed charges in the range of 10^{12} cm^{-2}, especially for silicon nitride. Deposition of these layers is typically performed using PECVD. Also sputtering has been successfully applied for surface passivation purposes [65]. A substantial practical problem of a-SiN_x:H passivation layers with their high built-in positive charge is that they yield inversion layers for lowly doped p-type silicon, which can lead to shunting of nonoptimum junctions [66]. In principle, they are better suited for n-type silicon passivation where they lead to the accumulation of majority carriers at the surface. In general, the same large variety of plasma excitation systems as for antireflection layers can be used to deposit these layers.
3. Aluminum oxide has been demonstrated with excellent passivation and high negative charge density after thermal treatment based on single-wafer atomic layer deposition (ALD) [67]. Several attempts have been undertaken to convert the ALD approach into an industrially feasible system. Nevertheless, excellent passivation results have also been shown for layers deposited by in-line PECVD or sputtering [68]. For industrial p-type Si passivation, this seems to be an alternative high-quality, low-cost option. Silicon nitride capping layers have proven to improve the thermal stability of aluminum oxide also appropriate for contact firing [69].
4. Intrinsic amorphous silicon (i a-Si) is a semiconductor and yields outstanding passivation [70], but it is thermally unstable at $T > 450$ °C [71]; thus a full low-temperature process is preferably applied like the heterojunction with intrinsic thin-layer (HIT) approach of Sanyo (see Section 1.16.6.4).

1.16.4.2 Metallization

1.16.4.2.1 Front contacts

As the front contacts are facing the sun they have to fulfill various requirements at the same time:

- Low shading losses due to the coverage of the active cell area by metal.
- Low metal/silicon contact resistivity.
- High conductivity in order to allow efficient current transport to collecting structures (e.g., busbars or via holes).
- Solderability and mechanical strength against pull-off forces in the module.

This resulted in screen-printed contacts made of a silver paste that has to be fired after the printing process. Screen printing is a very reliable process and allows for rather small structures especially if they are aligned in parallel such as the front contact fingers of the standard solar cell. Even though very fine lines can be printed at lab scale (~60 μm), currently most production lines fabricate wider fingers to allow for robust production. Very remarkable progress has taken place on the printing equipment side as well as on the materials side where paste vendors are developing paste that is capable of contacting lowly doped high-performance emitters maintaining all the abovementioned requirements at very high yield. In addition to screen printing, stencil printing [72] is also used at lab scale, but it has not found its way into production so far. A special challenge to transfer this well-known technology from printed circuit board (PCB) industry to PV is the shape of the contact grid of the solar cells. The parallel fingers cut through the screens, considerably reducing their stability. Small bridge-like structures increase this stability, but this adds cost to the screens and threatens to interrupt the contacts at these places. Another printing technology to form front contacts is based on extrusion. In this process, the paste is forced through a small orifice and a very high aspect ratio contact line can be deposited on the wafer surface by the relative movement of orifice and wafer. Clogging has to be avoided in this technology and a set of parallel operating orifices should be used to allow high throughput. Recently, very promising results for this noncontact technology have been demonstrated by various authors [73–75].

A very powerful approach to improve the front contact is based on a two-step process [76]. In this process, a seed layer is deposited in a first step. This seed layer is optimized for low contact resistivity and mechanical adhesion to the wafer. Further, it can be deposited in very fine structures as it does not have to feature high aspect ratios. On these fine structures, a second metal is deposited which has electrical contact with the seed. This second layer will carry the current and therefore must have a corresponding cross-sectional area.

There are various options to achieve this structure. Double printing of different pastes is most related to the standard fabrication process. Promising results are already shown by various workers and even production data are already available that show advantages compared to the standard single print [77, 78].

Aerosol printing [79, 80] or inkjet printing [81] of the seed layer allows for very fine structures of the seed layer, and using a plating step this seed layer can be enforced by plating of metal on it. Using a light-induced plating process [82–84] (**Figure 17**), this process can be carried out in a very efficient manner using in-line plating systems. Excellent results have been achieved by this type of contact formation, and various materials and production tools are already tested and used in industrial lines and R&D environments.

Interestingly, this type of plating also allows for plating of copper. Copper could become very important in order to reduce the material cost of the solar cell and to avoid a silver resource issue [85]. Currently, very promising results are achieved by various groups [86–89]; especially the investigation of the impact of copper metallization on solar cell performance is an important subject, as effective copper barriers would allow the use of this cost-effective material [86, 90].

The abovementioned seed layers have in common that they are fired through the antireflection coating. If by a prior process the antireflection coating is already opened (e.g., by laser ablation or local etching), other seed layers can be used [91, 92]. In the early high-efficiency research, metal stack layers have been applied (e.g., Ti/Pd/Ag). The company BP Solar has used plated nickel contacts exploiting the fact that the Ni will deposit on exposed silicon [93]. These Ni layers can be annealed to form nickel silicides, which allow for good mechanical properties. On these seed layers, silver or other metals can be plated (**Figure 18**). Nickel together with copper could become a very cost-effective combination which can also be integrated in high-efficiency concepts [94].

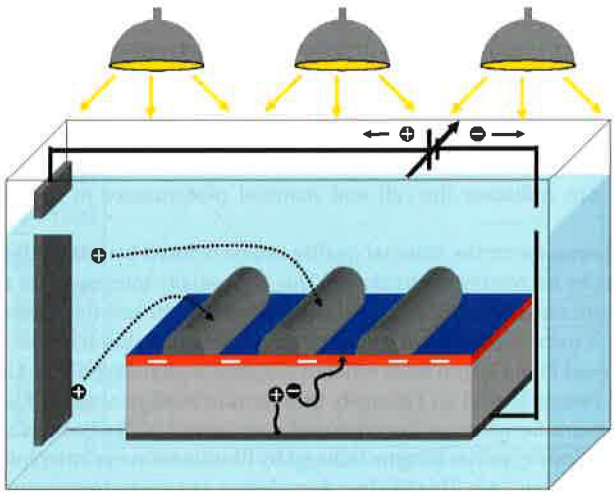

Figure 17 Working principle of light-induced plating of silver. The solar cell is contacted at the rear side. By illuminating the cell, a negative potential at the front contacts is created which attracts the positive silver ions.

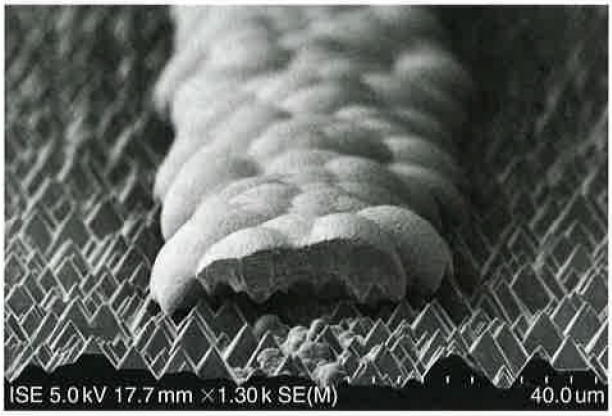

Figure 18 Plated front contact finger consisting of a thin Ni seed layer (see front part) and a thick Ag conductive layer.

1.16.4.2.2 Back contacts

The back contacts of the current solar cells are described in Sections 1.16.2.2 and 1.16.2.3. The applied metal pastes have been optimized in the past in order to allow the usage of thin wafers without too much wafer bow. Furthermore, the surface recombination velocities of the contacts formed have been reduced over the years by various methods. Huster and Schubert [35] describe the effect of added boron to increase the doping level of the back surface field. However, only very limited literature is available that focuses on improving the optical properties of the aluminum contacts [95]. During the transition to a locally contacted rear surface of the solar cell, the role of the aluminum paste changes. It will be in contact with only a small fraction of silicon, whereas the largest share of the aluminum will be placed on a passivating dielectric layer, which also results in high internal reflectance. Therefore, the optimization of pastes for this purpose is still ongoing, but various workers have already reported excellent efficiencies on PERC solar cells with modified conventional aluminum pastes.

A further approach to form the back contact is the usage of physical vapor deposition methods [96, 97]. Here, sputtering or either thermal or e-gun-based evaporation is used. As the formed layers achieve very high conductivities, these methods allow realization of the same performance with considerably lower metal sheet thicknesses.

1.16.4.3 Bulk Properties

Certainly, even the best cell structure will not result in high efficiencies if the material quality is too low. Therefore, the investigation of electrically active defects is of great importance for PV material. Especially for mc-Si with its high amount of metal contaminations [98, 99] and crystal defects, it is very important to understand thermal treatments, gettering [100–102], and hydrogen passivation [103] in order to increase the carrier diffusion length. These measures were extremely important to obtain the record efficiencies on small (20.4% on 1 cm^2) [17] and large area (19.5% on 243 cm^2) [104] multicrystalline substrates.

In a standard cell process, gettering is mainly accomplished by the phosphorus diffusion process. Metal impurities can be removed quite effectively by this step [100]. However, if the main lifetime-limiting effects are crystal defects, it is crucial to apply hydrogen passivation [103] to increase carrier lifetime.

Additional effects caused by defects in mc-Si are shunts and junction breakdowns [105, 106]. This is especially important for the application of these cells in a module where solar cells that are shaded can be driven in reverse by the other illuminated cells.

In order to reduce the material costs, a number of attempts have been made to use other procedures such as the classical Siemens process to clean the metallurgical silicon. The resulting material is called solar-grade or upgraded metallurgical silicon (umg-Si). It seems that the common characteristic of this material type is the unavoidable compensation of boron and phosphorus doping atoms. This can influence the cell and material performance in different ways and is currently under investigation [107–112].

The dependence of the cell performance on the material quality can be reduced by using thinner wafers. Thus, the decisive ratio diffusion length/thickness increases by decreasing the thickness. This is especially interesting for high-efficiency cell structures since the high-quality surface structures are capable of retaining cell performance as the cell thickness decreases. For example, the world record efficiency of 20.4% on mc-Si using a fully surface-passivated cell structure was achieved on 99 µm thick material while an efficiency of 'only' 19.9% was achieved for a 218 µm thick wafer of the same material type [17]. Using high-efficiency cell structures, efficiencies greater than 20% have been achieved on extremely thin monocrystalline wafers of less than 50 µm [113].

Most of the mono-Si solar cell manufacturers use boron-doped Czochralski (Cz) silicon as the starting material. This material type shows a severe degradation of minority carrier lifetime induced by illumination or carrier injection [114, 115] reaching a stable final value after a rather short time of about 24 h. This lifetime degradation can cause degradation of cell efficiency of several tenths to more than $1\%_{absolute}$ depending on the quality of the cell structure. The responsible metastable defect is related clearly to the existence of boron and oxygen [116, 117].

Table 3 Cell and material parameters used for model calculation

Parameter	*Value*
Shadow loss due to front metallization	5%
Recombination in emitter, J_{oe}	100 fA cm^{-2} (–> $V_{oc,max}$ ~ 685 mV)
Maximum achievable FF due to J_{02} and R_p, PFF	~82.5%
Bulk recombination due to boron–oxygen complex, τ_{CZ}	Fundamental limit given by Bothe *et al.* [48] with a factor of 2 due to improvements by high-temperature steps [48, 49]
Residual SRH (Shockley–Read–Hall) bulk recombination due to metal contamination, τ_{metal}	1000 µs
Intrinsic bulk recombination (Auger and direct), τ_{intr}	Doping-dependent parameterization [118]
Base resistivity, ρ_{base}	Variation between 0.1 and 10 Ω cm
Oxygen concentration, [O_i]	0 and 6–9 × 10^{17} cm^{-3}
Surface recombination velocity at the rear dielectric layer, S_{pass}	Doping-dependent parameterization for annealed thermally grown oxide [119]
Surface recombination velocity at laser-fired metal contact points, S_{met}	Doping-dependent parameterization for laser-fired contacts [120]
Effective surface recombination velocity at the rear surface, S_{rear}	Calculation using S_{met} and S_{pass} with Fischer equation [121]
Effective base resistance, R_{base}	Spreading resistance calculation using Cox and Strack's equation [122]
Distance of rear point contacts	Optimum distance calculated for each base doping using PitchMaster software
Additional series resistance due to metallization and emitter, $R_{s,residual}$	0.3 Ω cm^2

In order to calculate a realistic potential for solar cells from boron-doped Cz silicon, an industrial high-efficiency cell structure featuring fine-line metallization, shallow and well-passivated emitter, and a rear surface structure with dielectric passivation and local laser-fired point contacts was taken into account (see **Table 3**).

Bothe *et al.* [48] have given a fundamental limit of the lifetime in the degraded state as a function of oxygen and boron concentration. It is important to note that this lifetime is valid for an unprocessed wafer. In several publications [48, 49], it was reported that the concentration of the metastable defect is reduced by a factor of 2–3 by high-temperature steps above 700 °C. Since this is the case for our cell process (emitter diffusion, ...), we have assumed the fundamental lifetime limit of Bothe *et al.* multiplied by a factor of 2:

$$\tau_{C_z} = 2 \times 7.675 \times 10^{45} [B_s]^{-0.824} [O_i]^{-1.748} \quad [5]$$

For the calculations presented here, typical oxygen concentrations between 6 and 9 × 10^{17} and 0 cm^{-3} as a reference were chosen. This results in bulk diffusion lengths are shown in **Figure 19**. The quite dramatic difference between the material with no oxygen content and the ones with realistic concentrations is obvious. At low base resistivities, intrinsic recombination channels such as Auger recombination play a dominant role especially for the ideal material. It has to be kept in mind that we have chosen a very high residual lifetime of 1000 µs. This is not always easy to achieve under realistic conditions since the lifetime in p-type silicon is reduced even by low impurity concentrations due to the asymmetric capture cross sections of most metal impurities [123]. However, it is a valuable case study to evaluate the potential of our cell structure under ideal conditions.

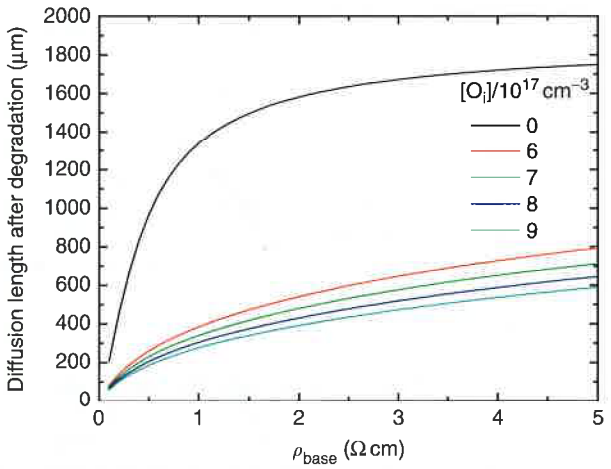

Figure 19 Bulk diffusion length in boron-doped Czochralski (Cz)-grown silicon as a function of base resistivity for different oxygen concentrations.

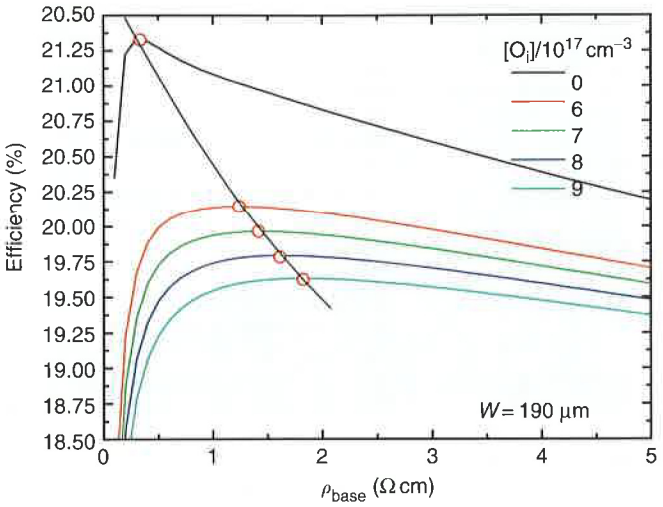

Figure 20 Efficiency as a function of base resistivity for different oxygen concentrations. The maximum efficiencies for each oxygen concentration are denoted by a circle. The pitch of the rear contacts was optimized for each base resistivity. The dots indicate the point of highest efficiency for each individual curve.

For the rear surface structure, we have selected a combination of laser-fired contacts (LFCs) and annealed thermally grown oxide since this results in very high efficiencies and a doping-dependent parameterization of the surface recombination velocity is known [119, 120]. For technical reasons, that is, low deposition temperature, it might be preferable to choose Al_2O_3 as a rear surface passivation layer. However, it will not change the result of our calculation significantly since from a recent publication [124] it is known that using Al_2O_3 nearly identical cell parameters can be achieved as with thermally grown oxide. The pitch of the point contacts is optimized by the spreadsheet-based software PitchMaster [125] as a compromise of recombination losses and base spreading resistance. PitchMaster calculates the cell parameters for the optimum point contact pitch for each individual base doping concentration. The results as a function of base resistivity for a cell thickness W of 190 µm are given in **Figure 20**.

While the cell structure offers an efficiency potential of more than 21%, the best values for oxygen-contaminated materials are in the range between 19.6% and 20.1% for low and high oxygen concentration, respectively. This shows clearly the reduced potential for cells on today's boron-doped Cz-grown silicon and increases the urge for alternatives.

Three options are promising for a reduction of this degradation: (1) the use of thinner wafers to improve the ratio diffusion length/cell thickness [126]; (2) decreasing the boron or oxygen concentration to reduce the light-induced degradation [49, 127]; or (3) the application of the regeneration process as recently demonstrated by Herguth *et al.* [128].

In addition, alternative material types are also of interest. In fact, cells from gallium-doped Cz-silicon show no degradation [129]. The only issue occurring with this material might be the large variation of doping concentration over the ingot due to the low segregation coefficient of gallium. Nevertheless, adapted cell structures show excellent results over a wide doping range [130].

A strong reduction of the oxygen concentration to values below 1 ppma also results in a perfect suppression of light-induced degradation. Magnetic Czochralski silicon (MCz) has shown a very high efficiency potential [129, 131]. Another material, PV-FZ™ [132], with a negligible oxygen concentration was reported to be introduced into the large-scale PV production a few years ago. This material type has shown very high and stable carrier lifetimes for p- and n-doping, but unfortunately the availability of this material type is still not clear at the moment.

Another material type of interest is certainly n-type silicon. n-type Cz-grown material shows no carrier-induced degradation even in the presence of a significant oxygen concentration [116, 133]. Also for mc-Si, excellent minority carrier lifetimes have been measured [134]. This superior material quality is mainly due to the fact that for most relevant defects the ratio of electron to hole capture cross sections is much greater than unity [123] (**Figure 21**).

Therefore, compared to p-type silicon, the minority carrier lifetime for the same defect concentration is much greater in the case of n-type silicon since this parameter is mainly influenced by the hole capture cross section (σ_p). Thus, although the diffusion constant for minority carriers is about a factor of 2.5–3, which reduces the effective diffusion length, this effect is by far over-compensated by the higher lifetime in realistic material.

These superior recombination characteristics also apply for surfaces. The capture cross sections for the silicon interface of common dielectric passivation layers such as SiO_2 or SiN_x are also highly asymmetric, that is, $\sigma_n \gg \sigma_p$ [135–137]. In practice, this means that the n-type surfaces are easier to passivate. In contrast to these physical advantages, a technological drawback is the fact that the classical cell process as described in Section 1.16.2 is not directly compatible with n-type silicon.

In the following two sections, cell structures for p- and n-type silicon, respectively, will be discussed in more detail.

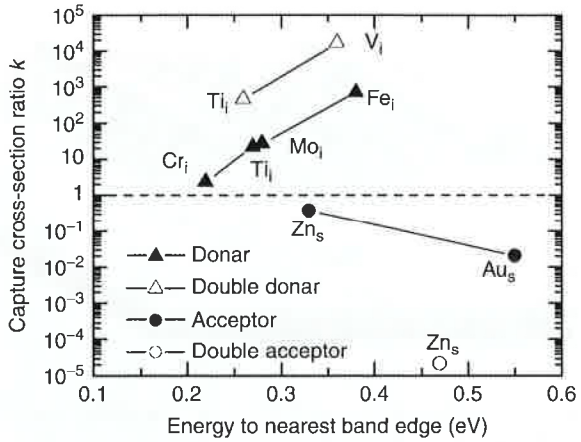

Figure 21 Capture cross sections as a function of energy level for different impurities in crystalline silicon. Reproduced with permission from Macdonald D and Geerligs LJ (2004) *Applied Physics Letters* 85(18): 4061–4063 [123]. Copyright 2004, American Institute of Physics.

1.16.5 High-Efficiency Cell Structures on p-type Silicon

1.16.5.1 Main Approaches for High Efficiencies in p-type Devices

Fortunately, various options exist that allow to surpass the currently industrially achieved solar cell efficiencies. A part of these options can be incorporated into the current solar cell production process without the need to significantly alter the module fabrication, as the concept of having contacts on both sides of the cells will be untouched. The other set of options relate to structural changes of the solar cell. Hereby the first target is the reduction of shading losses by forming back-contacted solar cells. However, up to now, these concepts have not been implemented without a change in the module fabrication process, which is a hurdle for market entry. As this second set of changes also aim at an improved performance of the entire solar cell module, finally an individual gain will be expected at both the cell level and the module level, which should make the development of a suitable module technology very attractive on the midterm.

1.16.5.2 Passivated Emitter and Rear Cell

While solar cell mainstream fabrication was focusing on the Al-BSF solar cell (as described in Section 1.16.2), various research groups fabricated very highly efficient solar cells with contacts on both sides. But a technological gap between the requirements for mass production and the need for clean room environments, photolithography processes, and special cleaning sequences to fabricate the high-efficiency cells did not allow a direct transfer of the developed concepts right away in order to improve and alter the Al-BSF cells. Currently, various technologies have come into the reach of the PV industry, allowing transfer of those concepts that were developed in the early days of PV research and which rose to an extraordinary high level of performance already at that time.

In 1989, Blakers *et al.* presented the PERC (see **Figure 22**) solar cell reaching solar cell efficiencies of 22.8% [11] and even exceeding 23% in a later work [138]. This concept is based on fundamental device structure improvements by introducing a dielectrically passivated rear surface with local point contacts. Due to reduced surface recombination velocity and improved optical performance, cell parameters were improved compared to cells that do not feature dielectrically passivated surfaces. To further

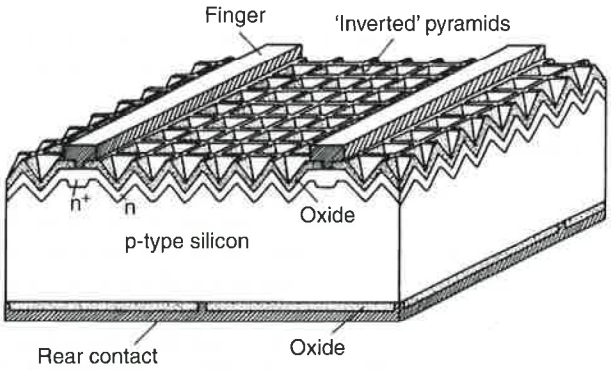

Figure 22 Structure of the PERC (passivated emitter and rear cell) solar cell as proposed in Reference 11. Reprinted with permission from Blakers AW *et al.* (1989) *Applied Physics Letters* 55(13): 1363. Copyright 1989, American Institute of Physics.

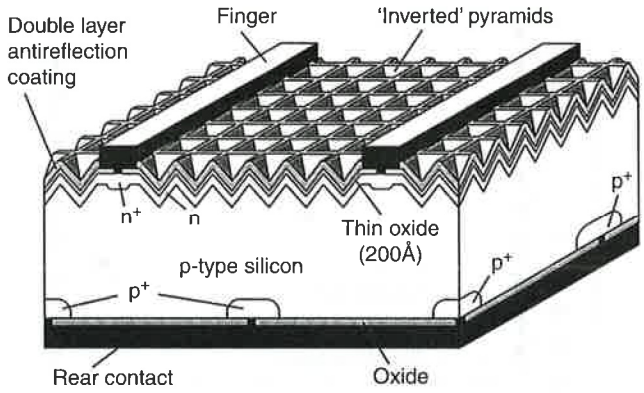

Figure 23 Structure of the PERL (passivated emitter, rear locally diffused cell) solar cell. Reprinted with permission from Zhao *et al.* (1990) *Solar Energy Materials and Solar Cells* 41–42: 87–89. [139]. Copyright 1990 Elsevier.

reduce the recombination of the point contacts and to allow for the use of high-resistivity material, the PERL (see **Figure 23**) solar cell structure was introduced by Zhao *et al.* [140] in 1990. With this concept, cell efficiencies of up to 25% have been achieved [4].

These concepts relate to the passivation and contacting concept used for point contacted back-contact solar cells introduced by Sinton and co-workers [141, 142].

Although these results for PERC and PERL were all achieved on high-quality FZ silicon wafers, excellent results have been achieved on mc-Si substrates [101, 143] and on Cz silicon [144, 145] using such structures. A very substantial reduction of the process complexity was achieved by the so-called RP-PERC (random pyramids, passivated emitter and rear cell) approach, in which amongst other things the inverted pyramid process for front texturing has been replaced by a random pyramid texture (see also Section 1.16.2) saving up to four photolithography steps and achieving excellent efficiencies of up to 21.6% on small-area FZ devices [144]. Further work concentrated on simplification of the formation of the local rear contacts by opening the dielectric passivation using laser ablation processes [146].

Remarkable reduction in the complexity and cost of the process is achieved using the LFC approach in which the point contacts are punched through the passivation layer using a laser while the aluminum layer is already present [147]. Alternatively, the so-called industrial Passivated Emitter and Rear Cell (i-PERC) process [148], in which the dielectric layer is opened before screen-printed aluminum deposition with subsequent firing, can be applied. The i-PERC process was successfully applied by various groups [50, 149]. Detailed analysis of the complex local alloying process was carried out by various researchers [150–152]. It has been reported that during the alloying process considerable amounts of silicon originating from the volume below the local contact are distributed within the aluminum layer which contains liquid phases allowing for fast transport of the silicon in the melt [150]. This silicon depletion can lead to voids depending on the process conditions and contact size and is subject to ongoing investigations [152, 153].

Nekarda *et al.* [154] demonstrated that also the LFC approach is compatible with a screen-printed aluminum layer, which allowed integration of LFC into the already widespread screen-printed aluminum back-contact process which is also compatible with screen-printed front contacts. Recent progress achieved with this type of cells is reported in the literature [96, 104, 155–158] demonstrating efficiencies exceeding 19%. Remarkably high values even on mc-Si substrates have been achieved using LFC technology, leading to large-area multicrystalline solar cells with a maximum efficiency of 19.5% [104]. In this paper also modules have been fabricated from such cells leading to a 17.8% efficient multicrystalline Si-based module, which represents a further world record.

Using high-volume systems the aluminum layers can also be deposited by physical vapor deposition (PVD) mass fabrication [97], and remarkable progress has been reported on using LFC in combination with PVD layers [159].

As these improvements are also accompanied and supported by improved understanding of the underlying physics, the reader is encouraged to look into related publications for deeper understanding of the corresponding structures [53, 120, 121, 125, 160–163].

1.16.5.3 Metal Wrap-Through Solar Cells

Looking at the standard Al-BSF solar cell, the large fraction of shading caused by the busbars becomes immediately apparent. In the current modules, up to three busbars (of approx. 1.5 mm width) are used, which adds up to a total shading loss of approximately 3% of the incoming light (based on a $156 \times 156\,mm^2$ sized solar cell). Further, the interconnection ribbons cannot be made arbitrarily thick, but the mechanical impact on the cells has to be considered, which leads to the use of rather thin ribbons that cause series resistance losses in the module. Based on this challenge, the metal wrap-through (MWT) concept was introduced by Kerschaver *et al.* [164]. In this concept, the busbars of the solar cell are placed on the rear surface. A set of small metallized via holes, which can be drilled by laser processing, connect this busbar through the wafer with the front contact grid (see **Figure 24**).

The size and number of via holes depend strongly on the overall cell design but can be varied with a large degree of freedom. If the current of a large part of the solar cell is supposed to be transported through the hole, then the diameter is usually larger in order

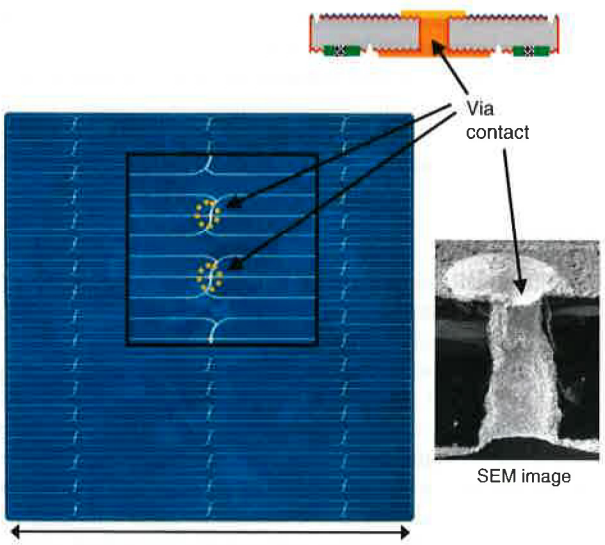

Figure 24 Picture and structure of an MWT (metal wrap-through) solar cell.

to allow a low series resistance contribution of the hole. This has led to the idea of the so-called PUM (pin-up module) [165, 166], which is strongly related to a concept introduced already in 1975 by Hughes Aircraft Company [167, 168].

In concepts similar to Kerschaver's original design suggestions [164], more and smaller holes are applied, which is compatible with the standard front grid in which the fingers are parallel. In both cases, the solar cell features a current collecting grid on the front side, but the interconnection terminals are located on the back surface, which allows new module concepts to be applied. This way the series interconnection can be done by connecting the solar cells to a structured and conducting substrate [169]. It has been demonstrated that this type of interconnection can be carried out by very efficient pick and place automation, leading to very high throughput and very low breakage rates [170, 171]. The fact that no interconnection ribbons are used in this technology allows minimization of the resistive loss that occurs in the standard module fabrication process. Furthermore, the use of conductive adhesives becomes possible, which allows reduction of the mechanical stress within the modules considerably. In total, it has been demonstrated by various workers that the MWT technology allows an efficiency gain of 0.4–0.6% absolute at cell level and an additional gain of 0.3–0.4% at module level, leading to a total gain of approximately 1% absolute for MWT-based modules [172–174]. This has led to excellent module efficiency of up to 16.4% on mc-Si, which represented a world record module at that time [174]. The corresponding proposed MWT solar cell fabrication processes are remarkably close to the standard process mostly used for the fabrication of Al-BSF solar cells. The only amendments to the standard cell process are hole drilling and rear contact isolation, which is applied to ensure a separation of the back minus busbar from the aluminum plus pole. Optionally, a third process is added if the rear minus busbar (which is simultaneously metallizing the vias) is printed with a paste that is different from the paste used for the solder pads of the plus polarity. Choosing different pastes can lead to a slight efficiency advantage, which can overcompensate the cost for the additional process. Various companies and institutes have demonstrated that the fabrication of this cell seems to be feasible [175–178]. Currently, the module production technology and the cost of the related materials seem to be the limiting factors for the introduction of the MWT solar cell, even though very promising technologies are currently evolving such that a near-term large-volume fabrication of MWT modules seems to be possible.

1.16.5.4 MWT-PERC

By combining the advantages of the PERC cells described in Section 1.16.5.2 with the advantages of MWT solar cells described in the previous section, a very attractive concept of an MWT solar cell with passivated surfaces, the so-called MWT-PERC, is obtained. This cell has been demonstrated by various groups [179–181] and it has been shown that the concept – as it is still very close to the standard fabrication process – benefits from most developments that are initially meant to support the standard cell such that the MWT-PERC cell is capable of taking advantage of improvements of the standard process while allowing for significantly higher efficiencies [182]. Most interestingly, a structural advantage of the MWT-PERC solar cell can be worked out by placing the rear minus busbar on top of the rear passivation layer. This way a synergetic effect is achieved as the busbar is not only moved to the back surface but is also eliminated in terms of recombination as it is placed on a passivating layer. Further simplification of the MWT-PERC cells is achieved by the high-performance MWT (HIP-MWT) approach in which the rear minus busbar is not only placed on top of the rear passivation layer, but is also located on top of a p-type doped area while the rear surface emitter is omitted. This approach allows fabrication of HIP-MWT-PERC solar cells by applying simple single-side etching processes, which leads to a remarkably simple process sequence allowing for excellent efficiencies exceeding 20.2% on 125 × 125 mm^2 FZ substrates as recently presented by Thaidigsmann *et al.* [183]. This value represents the highest efficiency achieved with screen-printed contacts and

diffused junctions on p-type substrates, showing the enormous power of the MWT-PERC approach which has only recently entered the R&D centers around the world. Further options for the improvement of MWT solar cells can be found when looking at the metallization of the front surface as it does not have to be compatible with soldering technologies and no busbar needs to be formed. Therefore, it can solely be optimized for excellent contact quality with respect to contact resistance, that is, minimum shading at high aspect ratios. Simplified approaches for seed and plate technology as well as dispensing technology can be applied and further combined with selective emitter concepts.

1.16.5.5 Emitter Wrap-Through Solar Cells

Compared to the MWT solar cells described in the previous sections, the emitter wrap-through (EWT) solar cell concept includes a total ban of the front metallization (first proposed by Gee *et al.* [184]). This is realized by replacing the front contact structure by a set of densely placed vias (approx. one via per mm^2 of cell area) of small diameter (approx. 50 µm). The rear surface of the wafer and the vias feature a further emitter structure which is connected through the vias with the front surface emitter. Only the emitter located on the rear surface is metallized in the EWT concept. The rear emitter is interrupted in a regular and rather dense (pitch is approx. 2 mm) pattern in order to expose the basis of the cell for contact formation. This way an interdigitated metal grid can be formed allowing for efficient current transport (**Figure 25**).

The emitters on the front and rear side are collecting carriers, which makes the EWT cell very attractive for low-lifetime materials. Early EWT solar cells showed rather limited fill factors due to two main challenges with the EWT solar cells. The first challenge was the long exposed pn-junction which was formed as the emitter interruptions are formed to allow the exposure of the basis. As the pitch of this structure is roughly 2 mm, the total length of this type of open pn-junction is about 20 m for a $156 \times 156\ mm^2$ cell. This issue was overcome by introducing passivation layers and suitable technologies to expose the basis without forming a highly recombinative open pn-junction. The second major challenge is the series resistance of the EWT solar cells. First, the current transport through the vias results in additional loss and more severely interdigitated contact grid pattern on the rear surface leads to very long finger structures which essentially extend to the total length of the used wafers. Various groups have addressed these challenges with different technological approaches [185–189]. Using high-performance clean room technologies, it was possible to demonstrate that EWT solar cells are in principle capable of yielding very high efficiencies. Kray *et al.* [190] have achieved remarkably high efficiencies of 22% on very thin substrates using photolithography processes. Mingirulli *et al.* [191] demonstrated 18.8% efficient EWT solar cells with screen-printed fingers (cell size approx. $40 \times 40\ mm^2$) allowing to reach an acceptable series resistance. To reduce the series resistance of the EWT solar cells, Eikelboom *et al.* [192] suggested a busbarless EWT solar cell and a corresponding interconnection method based on conductive adhesives. In a later work, again cell/module concepts have been proposed by Gee and Hacke targeting at reducing the series resistance by distributed terminals [193–195], but during the financial meltdown in 2009 Advent Solar did not get a chance to bring these ideas to market and was finally taken over by the company Applied Materials, at which Gee was able to continue some of the EWT work showing excellent results, with EWT cells of 19% efficiency on large-area Cz substrates featuring distributed screen-printed contact terminals [196]. In parallel to the development of the EWT with screen-printed contacts, Engelhart *et al.* [197] worked on a solar cell that was featuring evaporated contacts which have been structured without photolithography using a PVD metallization process together with very unique contact separation process called RISE (rear interdigitated single evaporation). Furthermore, they have optimized the emitter of the solar cell by exploiting the fact that the front side emitter does not need to be contacted; it thus may have a rather low surface concentration, which allowed together with a very efficient passivation to achieve low sheet resistance emitters (about $40–50\ \Omega\ sq^{-1}$) which still feature very low saturation current densities of about $100\ fA\ cm^{-2}$, which was very important for achieving high open-circuit voltages. This structure allowed to achieve very high conductivities and has led to excellent efficiencies of 21.4% on $91.9\ cm^2$ Cz substrates [198]. Ulzhöfer *et al.* [199, 200] have continued the work on this cell structure, which has considerably increased the understanding of the limiting

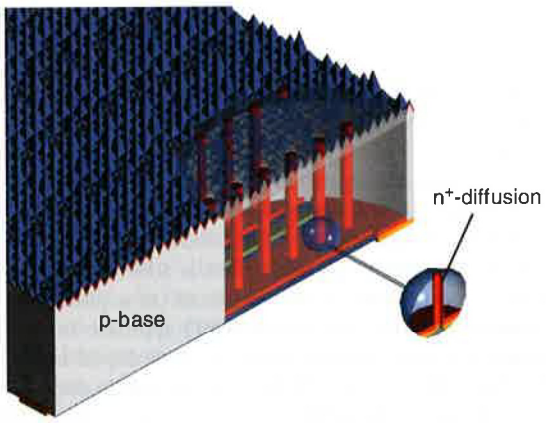

Figure 25 Structure of an EWT (emitter wrap-through) cell.

factors of EWT solar cells. The perspective of EWT solar cells is currently unclear given the fact that only few publications appear per year on this topic; currently, it does not seem to be in the main focus of R&D. Nevertheless, the advantages of the cell concept remain preserved and the concept could be reconsidered if the technological basis for fabrication of such a cell has become more advanced.

1.16.6 High-Efficiency Structures on n-type Silicon

In the previous section, it was shown that improved cell structures with good surface passivation have the potential to reach very high efficiencies. But as was shown in Section 1.16.4.3, the cell performance is also limited by the bulk properties. Therefore, it might be useful to use n-type Cz silicon with its superior physical properties (see Section 1.16.4.3). However, it is not possible to use the well-known and reliable phosphorus diffusion for the emitter formation and alternatives have to be found.

1.16.6.1 Aluminum-Alloyed Back Junction

The easiest way to realize a solar cell on n-type silicon is to utilize the full-area screen-printed Al-alloyed BSF of standard industrial p-type cell structures as the p^+-back junction of n-type cells. As effective passivation of the front surface is an important prerequisite for a high efficiency of back-junction cells, a special metallic ink for aerosol printing of the grid has been developed which also allows weakly doped surfaces to be contacted (**Figure 26**). Even without an additional passivation layer on the rear side, high efficiencies of 19.3% on large cells [201, 202] and 19.8% on small cells [203] were achieved (see **Table 4**).

By the addition of a passivation layer on the rear emitter surface, the emitter dark saturation current (J_{oe}) can be reduced [204] and the internal optical reflectivity increased. In this way, efficiencies exceeding 20% have been demonstrated [203].

By using a structured aluminum-doped emitter on the back surface, it is possible to move the front contacts to the rear surface of the solar cell by forming an interdigitated structure in which plus and minus terminals alternate in a dense pattern. The cell formed this way is a back-contacted back-junction solar cell. Gong *et al.* [205] have presented such a solar cell in which they used screen-printed aluminum paste that was alloyed in a fast firing furnace to form the emitter. In this initial work, the aluminum was printed on a photolithographically structured mask in order to allow the formation of the structured aluminum emitter. After forming the alloy, the aluminum paste residuals as well as the diffusion barrier were etched away. This way in the subsequent process the aluminum emitter could be passivated allowing for low emitter recombination. This process has led to remarkable 19.1% (aperture area 2×2 cm) efficient solar cells fabricated on n-type Cz substrates. Bock *et al.* [206] have applied printed aluminum pastes on unmasked wafers. After firing the paste and etching away the paste residuals and parts of the eutectic layer, the rear surface was structured and a phosphorus diffusion was carried out in order to form an n^{++} region in designated regions of the cell. The cell was passivated on both sides and contacted with a PVD process followed by a contact separation step which allowed to form the interdigitated grid [206]. Within this approach, 19.0% (aperture area 3.97 cm^2) efficient solar cells have been achieved on n-type Cz substrates. Using screen-printed contacts it would be very cost effective if the printed aluminum paste which forms the emitter could also be used as conductor. Furthermore, the minus polarity contact could be formed within the same firing step by a

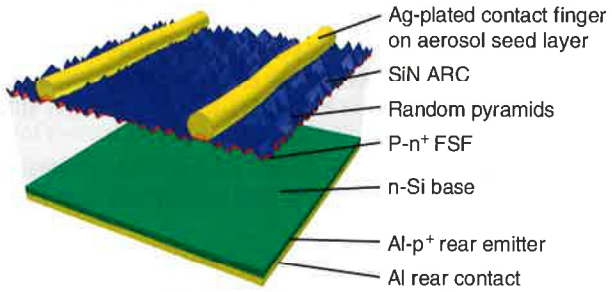

Figure 26 Cell structure with Al-alloyed rear emitter. ARC, antireflection coating; FSF, front surface field.

Table 4 Results of cells with Al-alloyed back junction and no additional rear passivation layer

Process type	*A* (cm^2)	V_{oc} (*mV*)	J_{sc} (*mA* cm^{-2})	*FF* (%)	η (%)
Industrial	12.5 × 12.5	640	37.7	80	19.3[a]
Laboratory	4.0	642	38.7	79.6	19.8[a]

[a] Measurements confirmed by Fraunhofer ISE Callab.

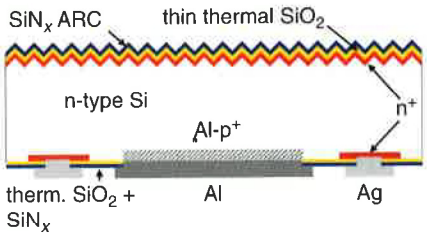

Figure 27 Structure of a back-contacted back-junction solar cell using screen-printed pastes for forming both an aluminum-alloyed emitter and the contact grid [208].

silver-containing paste. This approach is demonstrated by Woehl *et al.* [207]. The corresponding solar cell is shown in **Figure 27**. This approach has resulted in solar cells with an efficiency of 20.0% (aperture area 16.65 cm^2) on n-type FZ silicon substrates [208].

As the various approaches summarized in this section are still in the very early stage of development, there is a lot of potential to increase the achieved efficiency.

1.16.6.2 n-Type Cells with Boron-Diffused Front Emitter

To create a solar cell on n-type silicon and thus utilize the superior characteristics of this material, one can just convert the structure of a standard solar cell resulting in a p^+nn^+ structure (**Figure 28**). The p^+-emitter is created by a boron diffusion, while the n^+-BSF is generated by a phosphorus diffusion. In an industrial process, both profiles are fabricated in a co-diffusion process. Such structures are currently transferred to industry [209, 210]. Significantly higher efficiencies of more than 19% have been reached in lab and pilot line production [211, 212].

The phosphorus BSF is well understood and can be passivated and contacted like the standard emitter of a p-type cell. The contacting, and especially the passivation, of the front boron emitter is more demanding. The standard passivation layer SiN_x [213–215] and the thermally grown SiO_2 layers [213, 216–218] have shown a poor performance. Thus, new layers had to be developed. In most cases, the front surface layer of such cells consists of a thin layer passivating the boron-doped emitter plus a thick layer of PECVD-SiN_x serving as the antireflection coating and hydrogen reservoir. A layer that is easy to realize is created by a wet chemical passivation in a solution of nitric acid [219]. This increases significantly the blue response compared to cells with a pure PECVD-SiN_x layer. To achieve even better surface passivation, it is worth having a closer look at the passivation system. Therefore, lifetime samples with symmetrical boron- and phosphorus-doped emitters were passivated with thermally grown SiO_2. Subsequently, the oxide layers were charged with a corona setup and the carrier lifetime was measured. The measured lifetime can be easily converted to an implied voltage, which indicates the potential of the emitter including passivation (see **Figure 29**).

When no charges are applied, the implied voltage for an oxide-passivated emitter is much better than for the boron-doped emitters. The phosphorus-doped emitter can be improved by adding positive charges resulting in an accumulation of majority carriers. The same field effect passivation can be achieved by adding negative charges on the SiO_2-passivated boron-doped emitter. In fact, the quality of both emitters is identical for a charge resulting in strong accumulation. Therefore, the ideal surface passivation for boron-doped emitters should have a strong negative charge.

A dielectric layer that fulfills this requirement and which can be deposited at rather low temperatures is Al_2O_3. Hoex *et al.* [221] have shown that an Al_2O_3 layer deposited by ALD can reduce the emitter dark saturation current J_{oe} very effectively. Emitter saturation currents down to 10 fA cm^{-2} were measured on Al_2O_3-passivated boron emitters allowing for open-circuit voltages far above 700 mV and perfect blue response.

In order to evaluate the potential of such emitters at cell level, the cell structure shown in **Figure 30** was fabricated by Benick *et al.* [220]. The rear side of the cell shown is passivated with a thermally grown oxide and locally diffused phosphorus BSFs.

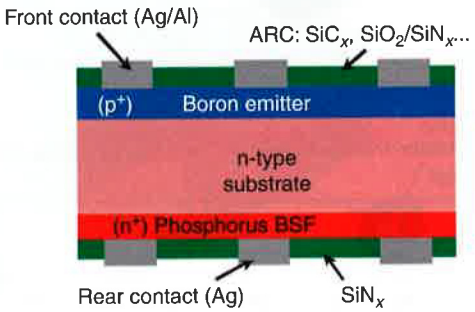

Figure 28 Structure of p^+nn^+ solar cell. BSF, back surface field. Reproduced with permission from Weeber A, Naber R, Guillevin N, *et al.* (2009) Status of n-type solar cells for low-cost industrial production. In: *Proceedings of the 24th Photovoltaic Solar Energy Conference*, pp. 891–895. Hamburg, Germany [209]. Copyright 2009, WIP, Munich.

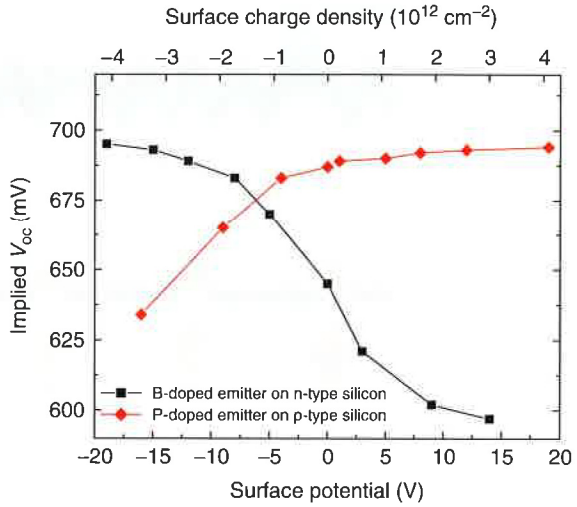

Figure 29 Implied voltages measured on lifetime samples with boron- and phosphorus-doped emitter passivated by a SiO_2 layer as a function of corona charge density. Reproduced from Benick J, Hoex B, van de Sanden MCM, *et al.* (2008) High efficiency n-type Si solar cells on Al_2O_3-passivated boron emitters. *Applied Physics Letters* 92(253504): 253504/253501–253503 [220].

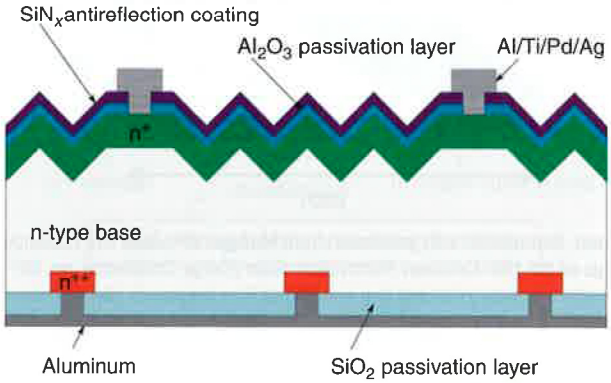

Figure 30 Cell structure with boron-diffused front emitter.

Although this cell still has no selective emitter, which gives room for further improvement, recently an efficiency of 23.9% [222] for a calibrated aperture area (illuminated area includes busbar) measurement has been achieved (see **Table 5**).

In order to transfer this technology from the laboratory to an industrial environment, several processes have to be simplified. The locally diffused P-BSFs of the lab process using masking oxides and photolithography are too complex for industrial application. Therefore, a new process consisting of two steps was developed: (1) PECVD deposition of phosphorus-containing passivation layer system called *PassDop* and (2) simultaneous opening of the layer with a laser and generation of local P-BSFs (see **Figure 31**). Using this new and easy-to-fabricate rear surface process [223], it was possible to achieve a maximum efficiency of 22.4% (see **Table 5**).

1.16.6.3 Back-Contact Solar Cells with Boron-Diffused Back Junction

The A-300 of SunPower [224] (compare **Figure 32**) is a strongly simplified version of the point-contact cell originally developed for concentrator applications at Stanford University [13].

Table 5 Results of cells with boron-diffused front junction ($A = 4$ cm^2)

Rear structure	V_{oc} *(mV)*	J_{sc} *(mA cm^{-2})*	*FF (%)*	η *(%)*
Thermal oxide + locally diffused P-BSF	705	41.1	82.5	23.9[a]
New PassDop layer + laser-fired P-BSF	701	39.8	80.1	22.4[a]
Full-area P-BSF + printed front contacts	654	38.7	80.8	20.5

[a] Measurements confirmed by Fraunhofer ISE Callab.
P-SF, phosphorus back surface field.

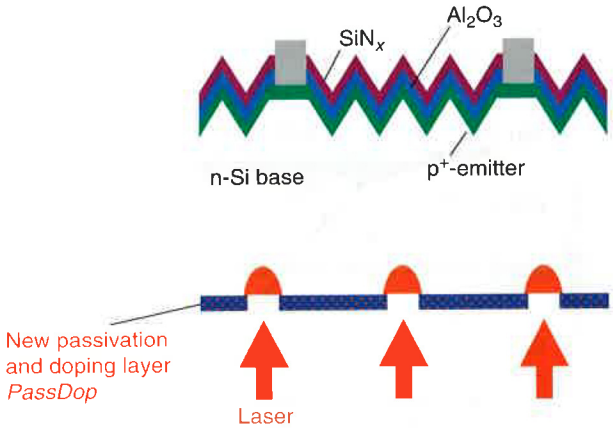

Figure 31 Laser process to create contact openings and local P-BSF (phosphorus back surface field) using the *PassDop* layer. After this process step, an Al layer is evaporated on the rear surface [201].

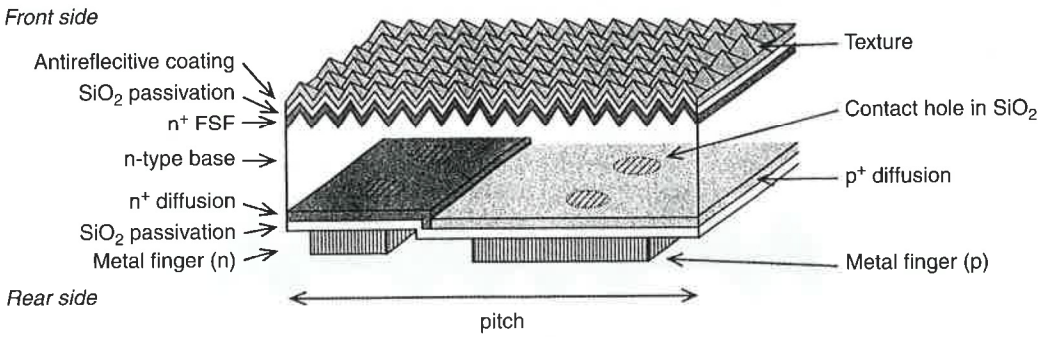

Figure 32 Point-contact cell of SunPower. Reproduced with permission from Mulligan WP, Rose DH, Cudzinovic MJ, *et al.* (2004) Manufacture of solar cells with 21% efficiency. In: *Proceedings of the 19th European Photovoltaic Solar Energy Conference*, pp. 387–390. Paris, France [1]. Copyright 2004, WIP, Munich.

The main feature of this 22% efficient cell in mass production [225] is the absence of any metal contacts on the front side since both electrodes are placed on the rear surface as an interdigitated grid. Thus, nearly all carriers have to diffuse from the front surface where they are photogenerated to the collecting pn-junction at the rear surface. Therefore, the bulk diffusion length has to be high (see previous section) and especially the surface recombination velocity at the front has to be very low. This task is managed by an excellently passivating SiO_2 layer on a lowly doped n^+ front surface field. Although back-contact cells are obviously extremely attractive in terms of efficiency and aesthetics, they also pose very high demands on material quality and process technology. Especially the fabrication of the rear surface structure, that is, the separation of p- and n-diffused regions or p- and n-electrodes, is an issue. One interesting opportunity for this task is the use of laser technologies [226].

Another important design aspect of interdigitated rear contact solar cells is the so-called 'electrical shading' effect [225, 227–229]. Although rear contact solar cells have no metal contacts on the front side and thus optical shading is avoided, regions with lower collection efficiency can occur. Since the width of the BSF regions in industrial back-junction cells is in the region of several times the cell thickness, minority carriers that are generated in this region have to travel considerably longer than carriers that are generated directly above the collecting emitter (see **Figure 33**). Even in high-lifetime material, the collection efficiency for these carriers is reduced, leading to a lower short-circuit current as can be seen on the right side of **Figure 33**. Therefore, the BSF region should be reduced to a minimum. SunPower has successfully reduced or even eliminated the electrical shading and increased efficiency by more than 1% in production [225].

However, when reducing the BSF region, one has to consider that the metallization for the p-contact should have approximately the same width as the emitter contacts. Thus the n-contact will overlap the emitter region in the finished cell and measures have to be taken to avoid a shunt. This can be achieved by the so-called 'buried emitter' concept, where the emitter profile is overcompensated by BSF at the surface [230–233] leading to improved cell performance [234]. The other possibility is to cover the rear surface with a passivating and insulating layer which avoids shunts (see **Figure 34**) and allows for a decoupling of the emitter/BSF and grid geometry. Such layers are available and resulted in cells with excellent performance and without electrical shading [227].

The most recent generation of A300 cells have additionally used passivated contacts to reduce the impact of metal–semiconductor interface recombination. The record efficiency of these cells is 24.2% with a remarkable open-circuit voltage of 721 mV [235].

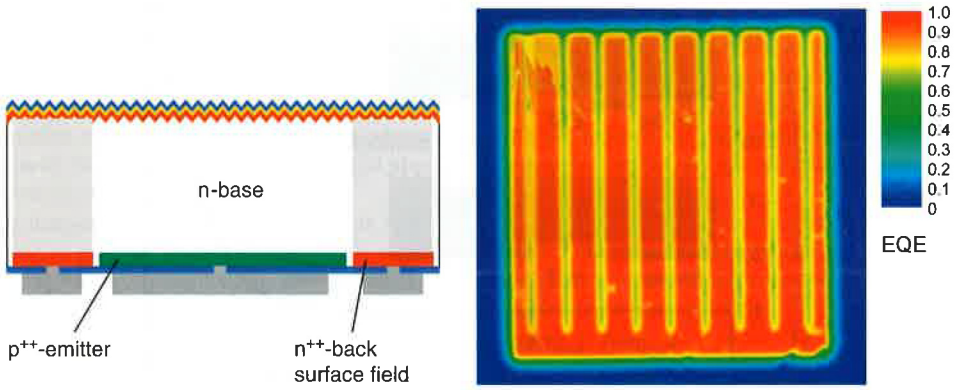

Figure 33 Back-junction solar cell and electrical shading effect. Minority carriers that are generated in the gray regions above the n-BSFs (back surface fields) have to travel laterally to the collecting p-emitter. Since the distances are much larger compared to the cell thickness, carrier collection in this region is strongly reduced (see light beam-induced current map on the right side) [229]. EQE, External quantum efficiency.

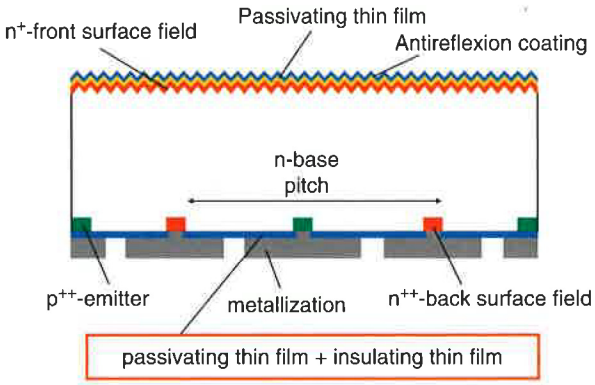

Figure 34 Interdigitated back-junction solar cell with decoupled emitter/BSF and grid geometry using a passivating and insulating film [227].

1.16.6.4 Heterojunction Solar Cells

The p^+-emitter on the n-substrate for the HIT cell of Sanyo [236, 237] is not based on boron diffusion but is formed by the deposition of a p-doped a-Si layer resulting in a heterojunction (see **Figure 35**). Also, the rear surface is passivated by an a-Si layer in order to obtain the full potential of the monocrystalline n-type silicon. The HIT cells by Sanyo prove the excellent surface passivation quality of solar cells with heterojunctions resulting in voltages of 743 mV on 98 µm thick n-type wafers [239]. Efficiencies well above 22% can be achieved using this cell structure.

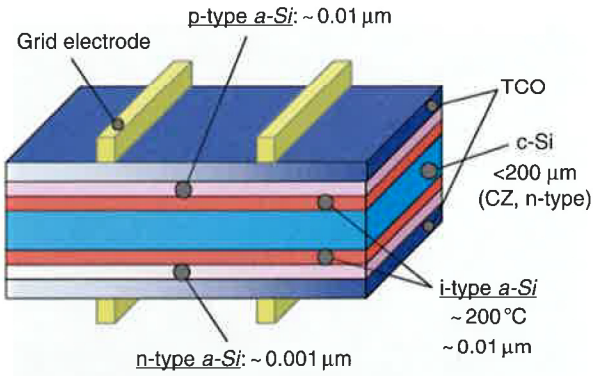

Figure 35 Front structure of the HIT (heterojunction with intrinsic thin-layer) cell. Reproduced from Taira S, Yoshimine Y, Baba T, *et al.* (2007) Our approaches for achieving hit solar cells with more than 23% efficiency. In: *Proceedings of the 22nd European Photovoltaic Solar Energy Conference*, pp. 932–935. Milan, Italy [238]. Copyright 2007, WIP, Munich. TCO, Transparent conducting oxide.

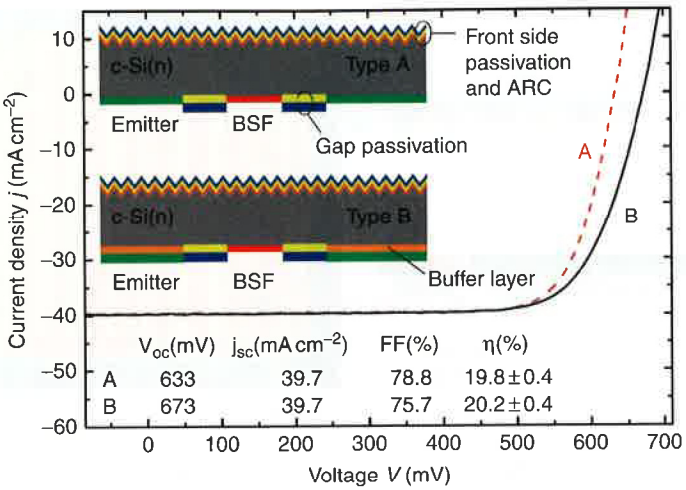

Figure 36 Results on interdigitated heterojunction back-contact cells. BSF, back surface field; ARC, antireflection coating. Reprinted with permission from Mingirulli N *et al.* (2011) *Physica Status Solidi RRL* 5(49): 159–161 [253]. Copyright 2011, Wiley VCH, Weinheim, Germany.

Up to now, the HIT cell has only been produced by Sanyo, but this situation will change since important patents are running out. Therefore, several institutes and also the equipment manufacturers have intensified their research activities to develop an HIT-like cell structure [240–248].

The major advantage of the HIT cell structure is its perfect surface passivation, which allows for very high open-circuit voltages. In contrast, the achieved currents are only moderate. This is due to the parasitic absorption of photons in the amorphous emitter on the front side. The diffusion length is quite small so that IQE for short-wavelength photons is relatively low. Therefore, a cell structure with front heteroemitter is always a compromise between high-voltage, good transport properties and blue response. A possibility to avoid this parasitic effect is to use heterojunctions in an interdigitated back-junction cell design. Several groups have been working in this field [249–252]. The best efficiency reported so far is 20.2% [253], but of course the potential of this structure is much higher since it combines in an ideal way the advantages of a back-contact solar cell (high current) with those of a standard heterojunction cell (high voltage) (**Figure 36**).

1.16.6.5 Alternative Emitters

1.16.6.5.1 Polysilicon emitters

Instead of using a-Si, one can also deposit doped polysilicon [254–256]. This has the advantage that the absorption in polysilicon is lower and the temperature stability is higher. To obtain best results, it is advantageous to use a thin intermediate dielectric layer to passivate the interface and to block diffusion out of the polysilicon emitter resulting in a very abrupt junction (**Figure 37**). This concept was revisited using modern microelectronic equipment and a thin rapid thermal oxide (RTO) as an interfacial layer [257]. Open-circuit voltages of up to 678 mV have been reached with this promising approach.

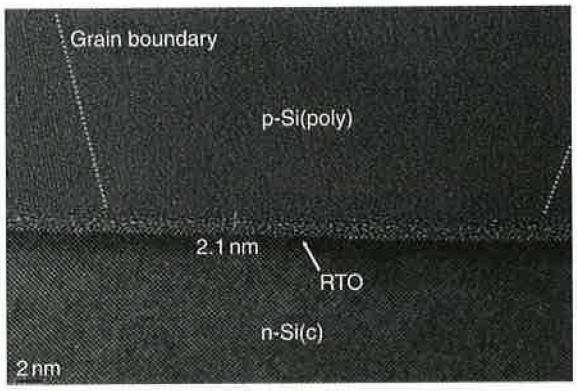

Figure 37 Cross section through a polysilicon emitter. RTO, rapid thermal oxide. Reprinted with permission from Borden P, *et al.* (2008) *Proceedings of the 23rd Photovoltaic Solar Energy Conference*, pp. 1152. [257]. Copyright 2008, WIP, Munich.

1.16.6.5.2 Implanted emitters

Another technology from microelectronic industry to generate doped layers is ion implantation. Ion implantation allows to generate exactly defined doping profiles and to achieve very uniform doping. After the ion implantation, the wafers have to be annealed to remove the damage introduced by the implantation process. This is extremely critical for solar cells in order to obtain low emitter saturation currents, J_{oe}. Recently, it was shown that with an appropriate high-temperature anneal process very low saturation currents of 20 and 24 fA cm^{-2} for boron and phosphorus emitters, respectively, can be achieved [222]. This would allow in both cases open-circuit voltages above 700 mV.

An interesting feature of ion implantation is the *in situ* masking of implantation allowing locally defined doping profiles. This feature was utilized to generate monocrystalline cells with ion-implanted selective emitters. Efficiencies of greater than 19% have been achieved [258]. Local doping is even more interesting for interdigitated back-junction solar cells with their complex doping pattern on the rear. Using this technique, efficiencies of up to 20% have been reported [259].

1.16.7 Conclusion

This chapter on the current status and new activities of crystalline silicon PV could only give a small insight into the enormous spectrum of research and technology activities in this field and is thus condemned to incompleteness. On the other hand, this is also a very good sign for the sustainability of crystalline silicon PV. The strong research activities show that crystalline silicon PV, which is often regarded as the 'old technology' of PV, is alive and kicking and will remain so in the coming decades. To ensure such a bright future, a strong cooperation between research and industry is crucial.

References

[1] Mulligan WP, Rose DH, Cudzinovic MJ, *et al.* (2004) Manufacture of solar cells with 21% efficiency. In: *Proceedings of the 19th European Photovoltaic Solar Energy Conference*, pp. 387–390. Paris, France. Munich, Germany: WIP Renewable Energies.

[2] van Sark WGJHM, Alsema EA, Junginger HM, *et al.* (2008) Accuracy of progress ratios determined from experience curves: The case of photovoltaic technology development. *Progress in Photovoltaics* 16: 441–453.

[3] Ohl RS (1941) Light Sensitive Electric Device. US Patent 240,252.

[4] Green MA (2009) The path to 25% silicon solar cell efficiency: History of silicon cell evolution. *Progress in Photovoltaics* 17(3): 183–189.

[5] Chapin DM, Fuller CS, and Pearson GL (1954) A new silicon p-n junction photocell for converting solar radiation into electrical power. *Journal of Applied Physics* 25: 676–677.

[6] Perlin J (1999) *From Space to Earth*. Ann Arbor, MI: Aatec Publications.

[7] Wolf M (1963) The effects of a drift field on solar cells. In: *Proceedings of the 3rd IEEE Photovoltaic Specialists Conference*, p. B12. Washington, DC, USA. Piscataway, NJ, USA: IEEE.

[8] Hess WN (1964) The effects of high altitude explosions. In: LeGalley D and Rosen A (eds.) *Space Physics*, pp. 573–610. New York: Wiley.

[9] Mandelkorn J, McAfee C, Kesperis J, *et al.* (1962) Fabrication and characteristics of phosphorous-diffused silicon solar cells. *Journal of the Electrochemical Society* 109(4): 313–318.

[10] Blakers AW and Green MA (1986) 20% efficiency silicon solar cells. *Applied Physics Letters* 48(3): 215–217.

[11] Blakers AW, Wang A, Milne AM, *et al.* (1989) 22.8% efficient silicon solar cell. *Applied Physics Letters* 55(13): 1363–1365.

[12] Zhao J, Wang A, Altermatt PP, *et al.* (1994) 24% efficient silicon solar cells. In: *Proceedings of the 1st World Conference on Photovoltaic Energy Conversion*, pp. 1477–1480. Waikoloa, HI, USA. Piscataway, NJ, USA: IEEE.

[13] Sinton RA, Kwark Y, Gan JY, and Swanson RM (1986) 27.5-percent silicon concentrator solar cells. *IEEE Electron Device Letters* 7(10): 567–569.

[14] Swanson RM (1986) Point-contact solar cells: Modeling and experiment. *Solar Cells* 17(1): 85–118.

[15] Zhao J, Wang A, and Green MA (1999) 24.5% efficiency silicon PERT cells on MCZ substrates and 24.7% efficiency PERL cells on FZ substrates. *Progress in Photovoltaics: Research and Applications* 7(6): 471–474.

[16] Swanson RM (2005) Approaching the 29% limit efficiency of silicon solar cells. In: *Proceedings of the 31st IEEE Photovoltaic Specialists Conference*, pp. 889–894. Orlando, FL, USA. Piscataway, NJ, USA: IEEE.

[17] Schultz O, Glunz SW, and Willeke G (2004) Multicrystalline silicon solar cells exceeding 20% efficiency. *Progress in Photovoltaics: Research and Applications* 12(7): 553–558.

[18] Green M, Emery K, Hishikawa Y, and Warta W (2010) Solar cell efficiency tables (version 35). *Progress in Photovoltaics: Research and Applications* 18: 144–150.

[19] Shockley W and Queisser HJ (1961) Detailed balance limit of efficiency of p-n junction solar cells. *Journal of Applied Physics* 32(3): 510–519.

[20] Kerr MJ, Cuevas A, and Campbell P (2003) Limiting efficiency of crystalline silicon solar cells due to Coulomb-enhanced Auger recombination. *Progress in Photovoltaics: Research and Applications* 11(2): 97–104.

[21] Tajima M, Ikebe M, Ohshita Y, and Ogura A (2010) Photoluminescence analysis of iron contamination effect in multicrystalline silicon wafers for solar cells. *Journal of Electronic Materials* 39(6): 747–750.

[22] Bustarret E, Bensouda M, Habrard MC, and Bruyere JC (1988) Configurational statistics in a-$Si_xN_yH_z$ alloys: A quantitative bonding analysis. *Physical Review B* 38(12): 8171.

[23] Hezel R and Jaeger K (1989) Low-temperature surface passivation of silicon for solar cells. *Journal of the Electrochemical Society* 136(2): 518–523.

[24] Szlufcik J, De Clercq K, De Schepper P, *et al.* (1994) Improvement in multicrystalline silicon solar cells after thermal treatment of PECVD silicon nitride Ar coating. In: *Proceedings of the 12th European Photovoltaic Solar Energy Conference*, pp. 1018–1021. Amsterdam, The Netherlands. Munich, Germany: WIP Renewable Energies.

[25] Ralph EL (1975) Recent advancements in low cost solar cell processing. In: *Proceedings of the 11th IEEE Photovoltaic Specialists Conference*, pp. 315–316. Scottsdale, AZ, USA. Piscataway, NJ, USA: IEEE.

[26] Frisson L, Honoré M, Mertens R, *et al.* (1980) Silicon solar cells with screen printed diffusion and metallization. In: *Proceedings of the 14th IEEE Photovoltaic Specialists Conference*, pp. 941–942. San Diego, CA, USA. Piscataway, NJ, USA: IEEE.

[27] Mardesich N, Pepe A, Bunyan S, *et al.* (1980) A low-cost photovoltaic cell process based on thick film techniques. In: *Proceedings of the 14th IEEE Photovoltaic Specialists Conference*, pp. 943–947. San Diego, CA, USA. Piscataway, NJ, USA: IEEE.

[28] Kontermann S, Hörteis M, Kasemann M, *et al.* (2009) Physical understanding of the behavior of silver thick-film contacts on n-type silicon under annealing conditions. *Solar Energy Materials and Solar Cells* 2009(93): 1630–1635.

[29] Schubert G (2006) Thick Film Metallisation of Crystalline Silicon Solar Cells. Dissertation, Universität Konstanz.

[30] Ballif C, Huljic DM, Willeke G, and Hessler-Wyser A (2003) Silver thick-film contacts on highly doped n-type silicon emitters: Structural and electronic properties of the interface. *Applied Physics Letters* 82(12): 1878–1880.

[31] Schubert G, Horzel J, Kopecek R, *et al.* (2005) Silver thick film contact formation on lowly doped phosphorous emitters. In: *Proceedings of the 20th European Photovoltaic Solar Energy Conference*, pp. 934–937. Barcelona, Spain. Munich, Germany: WIP Renewable Energies.

[32] Li ZGL and Cheng LK (2009) Electron microscopy study of front-side Ag contact in crystalline Si solar cells. *Journal of Applied Physics* 105(6): 066102.

[33] Rauer M, Woehl R, Rühle K, *et al.* (2011) Aluminum alloying in local contact areas on dielectrically passivated rear surfaces of silicon solar cells. *IEEE Electron Device Letters* 32(7): 916–918.

[34] Lölgen P, Leguijt C, Eikelboom JA, *et al.* (1993) Aluminium back-surface field doping profiles with surface recombination velocities below 200 cm/s. In: *Proceedings of the 23rd IEEE Photovoltaic Specialists Conference*, pp. 1490, 1236–1442. Louisville, KY, USA.

[35] Huster F and Schubert G (2005) ECV doping profile measurements of aluminium alloyed back surface fields. In: *Proceedings of the 20th European Photovoltaic Solar Energy Conference*, pp. 1462–1465. Barcelona, Spain. Munich, Germany: WIP Renewable Energies.

[36] Krause J, Woehl R, and Biro D (2010) Analysis of local Al-p^+-layers for solar cells processed by small screen-printed structures. In: *Proceedings of the 25th European Photovoltaic Solar Energy Conference and Exhibition*, pp. 1899–1904. Valencia, Spain. Munich, Germany: WIP Renewable Energies.

[37] Bentzen A (2006) Phosphorus Diffusion and Gettering in Silicon Solar Cells. Dissertation, University of Oslo.

[38] Voyer C, Biro D, Wagner K, *et al.* (2006) Fabrication of textured solar cells using sprayed phosphoric acid as the dopant source for the in-line emitter diffusion. In: *21st European Photovoltaic Solar Energy Conference*, pp. 1157–1160. Dresden, Germany. Munich, Germany: WIP Renewable Energies.

[39] Aichberger SV (2003) Deeper than blue: Market survey on deposition systems for silicon nitride. *PHOTON International* (March).

[40] Holmann M (2008) Rear Surface Conditioning and Passivation for Locally Contacted Crystalline Silicon Solar Cells. Dissertation, Universität Konstanz.

[41] Wolke W, Jäckle A, Preu R, *et al.* (2004) SiN:H anti-reflection coatings for c-Si solar cells by large scale inline sputtering. In: *Proceedings of the 19th European Photovoltaic Solar Energy Conference*, pp. 419–422. Paris, France. Munich, Germany: WIP Renewable Energies.

[42] Huster F (2005) Investigation of the alloying process of screen printed aluminium pastes for the BSF formation on silicon solar cells. In: *Proceedings of the 20th European Photovoltaic Solar Energy Conference*, pp. 1466–1469. Barcelona, Spain. Munich, Germany: WIP Renewable Energies.

[43] Huster F (2005) Aluminium-back surface field: Bow investigation and elimination. In: *Proceedings of the 20th European Photovoltaic Solar Energy Conference*, pp. 635–638. Barcelona, Spain. Munich, Germany: WIP Renewable Energies.

[44] Krieg A (2007) Inbetriebnahme und Weiterentwicklung eines automatisierten IV-Kennlinienmessplatzes und Entwicklung eines Verfahrens zur Materialverfolgung in der Solarzellenproduktion. Masterarbeit, Fachhochschule für Technik und Wirtschaft Berlin.

[45] International Electrotechnical Commission (2008) International Standard, IEC 60904-3, Edition 2. Photovoltaic devices – Part 3: Measurement principles for terrestrial photovoltaic (PV) solar devices with reference spectral irradiance data. ISBN 2-8318-9705-X.

[46] Basore PA and Clugston DA (1996) PC1D version 4 for windows: From analysis to design. In: *Proceedings of the 25th IEEE Photovoltaic Specialists Conference*, pp. 377–381. Washington, DC, USA.

[47] Thaidigsmann B, Wolf A, and Biro D (2009) Accurate determination of the IQE of screen printed silicon solar cells by accounting for the finite reflectance of metal contacts. In: *Proceedings of the 24th European Photovoltaic Solar Energy Conference*, pp. 2056–2059. Hamburg, Germany.

[48] Bothe K, Sinton R, and Schmidt J (2005) Fundamental boron–oxygen-related carrier lifetime limit in mono- and multicrystalline silicon. *Progress in Photovoltaics: Research and Applications* 13: 287–296.

[49] Glunz SW, Rein S, Lee JY, and Warta W (2001) Minority carrier lifetime degradation in boron-doped Czochralski silicon. *Journal of Applied Physics* 90(5): 2397–2404.

[50] Gatz S, Hannebauer H, Hesse R, *et al.* (2011) 19.4%-efficient large-area fully screen-printed silicon solar cells. *Physica Status Solidi Rapid Research Letters* 5(4): 147–149.

[51] Hermle M (2008) Analyse Neuartiger Silizium- und III-V-Solarzellen Mittels Simulation und Experiment. Dissertation, Universität Konstanz.

[52] Hermle M, Schneiderlöchner E, Grupp G, and Glunz SW (2005) Comprehensive comparison of different rear side contacting methods for high-efficiency solar cells. In: *Proceedings of the 20th European Photovoltaic Solar Energy Conference*, pp. 810–813. Barcelona, Spain.

[53] Kray D, Hermle M, and Glunz SW (2008) Theory and experiment on the back side reflectance of silicon wafer solar cells. *Progress in Photovoltaics: Research and Applications* 16: 1–15.

[54] Zhao J, Wang A, Altermatt PP, *et al.* (1994) 24% efficient PERL silicon solar cell: Recent improvements in high efficiency silicon cell research. In: *Proceedings of the 1st World Conference on Photovoltaic Energy Conversion*, pp. 87–99. Waikoloa, HI, USA.

[55] Knobloch J, Aberle A, Warta W, and Voss B (1990) Starting points for raising the efficiency of practical silicon solar cells. In: *Proceedings of the 5th International Photovoltaic Science and Engineering Conference*. Kyoto, Japan. Tokyo, Japan: ICS.

[56] Schneiderlöchner E, Preu R, Lüdemann R, and Glunz SW (2002) Laser-fired rear contacts for crystalline silicon solar cells. *Progress in Photovoltaics: Research and Applications* 10: 29–34.

[57] Aberle AG (1999) *Crystalline Silicon Solar Cells: Advanced Surface Passivation and Analysis of Crystalline Silicon Solar Cells*. Sydney, NSW, Australia: Centre for Photovoltaic Engineering.

[58] Goetzberger A, Voß B, and Knobloch J (1997) *Sonnenenergie: Photovoltaik, Physik und Technologie der Solarzelle*. Stuttgart, Germany: Teubner.

[59] Deal BE and Grove AS (1965) General relationship for the thermal oxidation of silicon. *Journal of Applied Physics* 36(12): 3770–3778.

[60] Han C-J and Helms CR (1987) Parallel oxidation mechanism for Si oxidation in dry O_2. *Journal of the Electrochemical Society: Solid-State Science and Technology* 134(5): 1297–1302.

[61] Biro D, Mack S, Wolf A, *et al.* (2009) Thermal oxidation as a key technology for high efficiency screen printed industrial silicon solar cells. In: *Proceedings of the 34th IEEE Photovoltaic Specialists Conference*, pp. 1594–1599. Philadelphia, PA, USA. Piscataway, NJ, USA: IEEE.

[62] Schmidt J, Lauinger T, Aberle AG, and Hezel R (1996) Record low surface recombination velocities on low-resistivity silicon solar cell substrates. In: *Proceedings of the 25th IFFF Photovoltaic Specialists Conference*, pp. 413–416. Washington, DC, USA. Piscalaway, NJ, USA: IEEE.

[63] Mueller T, Schwertheim S, Scherff M, and Fahrner WR (2008) High quality passivation for heterojunction solar cells by hydrogenated amorphous silicon suboxide films. *Applied Physics Letters* 92(033504): 033504/033501–033503.

[64] Vetter M, Martín I, Ferre R, *et al.* (2007) Crystalline silicon surface passivation by amorphous silicon carbide films. *Solar Energy Materials and Solar Cells* 91: 174–179.

[65] Wolke W, Catoir J, Emanuel G, *et al.* (2005) Surface passivation for solar cells by large scale inline sputtering of silicon nitride. In: *Proceedings of the 20th European Photovoltaic Solar Energy Conference*, pp. 733–736. Barcelona, Spain. Munich, Germany: WIP Renewable Energies.

[66] Dauwe S, Mittelstädt L, Metz A, and Hezel R (2002) Experimental evidence of parasitic shunting in silicon nitride rear surface passivated solar cells. *Progress in Photovoltaics: Research and Applications* 10(4): 271–278.

[67] Hoex B, Heil SBS, Langereis E, *et al.* (2006) Ultralow surface recombination of c-Si substrates passivated by plasma-assisted atomic layer deposited Al_2O_3. *Applied Physics Letters* 89(042112): 042112/042111–042113.

[68] Saint-Cast P, Kania D, Hofmann M, *et al.* (2009) Very low surface recombination velocity on p-type c-Si by high-rate plasma-deposited aluminum oxide. *Applied Physics Letters* 95: 151–502.

[69] Schmidt J, Veith B, and Brendel R (2009) Effective surface passivation of crystalline silicon using ultrathin Al_2O_3 films and Al_2O_3/SiN_x stacks. *Physica Status Solidi Rapid Research Letters* 3(9): 287–289.

[70] Dauwe S, Schmidt J, and Hezel R (2002) Very low surface recombination velocities on p- und n-type silicon wafers passivated with hydrogenated amorphous silicon films. In: *Proceedings of the 29th IEEE Photovoltaic Specialists Conference*, pp. 1246–1249. New Orleans, LA, USA. Piscataway, NJ, USA: IEEE.

[71] Hofmann M, Saint-Cast P, Bareis D, *et al.* (2009) Towards a-Si:H rear passivated industrial-type silicon solar cells. In: *Proceedings of the 24th European Photovoltaic Solar Energy Conference*, pp. 1539–1543. Hamburg, Germany. Munich, Germany: WIP Renewable Energies.

[72] Hoornstra J and Heurtault B (2009) Stencil print applications and progress for crystalline silicon solar cells. In: *Proceedings of the 24th European Photovoltaic Solar Energy Conference*, pp. 1–4. Hamburg, Germany. Munich, Germany: WIP Renewable Energies.

[73] Chen X, Church K, Yang H, *et al.* (2011) Improved front side metallization for silicon solar cells by direct printing. In: *IEEE Photovoltaic Specialists Conference*. Seattle, WA, USA. Piscataway, NJ, USA: IEEE.

[74] Pospischil M, Zengerle K, Specht J, *et al.* (2011) Investigations of thick-film-paste rheology for dispensing applications. In: *Proceedings of the 1st SiliconPV. Freiburg, Germany*. Freiburg, Germany: PSE.

[75] Specht J, Zengerle K, Pospischil M, *et al.* (2010) High aspect ratio front contacts by single step dispensing of metal pastes. In: *Proceedings of the 25th European Photovoltaic Solar Energy Conference and Exhibition*, pp. 1867–1870. Valencia, Spain. Munich, Germany: WIP Renewable Energies.

[76] Glunz SW, Aleman M, Bartsch J, *et al.* (2008) Progress in advanced metallization technology at Fraunhofer ISE. In: *Proceedings of the 33rd IEEE Photovoltaic Specialists Conference*, pp. 1–4. San Diego, CA, USA. Piscataway, NJ, USA: IEEE.

[77] Galiazzo M, Furin V, Tonini D, *et al.* (2010) Double printing of front contact Ag in c-Si solar cells. In: *25th European Photovoltaic Solar Energy Conference and Exhibition*, pp. 2338–2340. Valencia, Spain. Munich, Germany: WIP Renewable Energies.

[78] Raabe B, Huster F, McCann M, and Fath P (2005) High aspect ratio screen printed fingers. In: *20th European Photovoltaic Solar Energy Conference*, pp. 931–933. Barcelona, Spain. Munich, Germany: WIP Renewable Energies.

[79] Mette A, Richter PL, Hörteis M, and Glunz SW (2007) Metal aerosol jet printing for solar cell metallization. *Progress in Photovoltaics: Research and Applications* 115: 621–627.

[80] Hörteis M and Glunz SW (2008) Fine line printed silicon solar cells exceeding 20% efficiency. *Progress in Photovoltaics: Research and Applications* 16(7): 555–560.

[81] Ebong A, Rounsaville B, Cooper I, *et al.* (2010) High-efficiency silicon solar cells with ink jetted seed and plated grid on high sheet resistance emitter. In: *IEEE Photovoltaic Specialists Conference*, pp. 1364–1367. Honolulu, HI, USA.

[82] Durkee LF (1979) Method of Plating by Means of Light. US Patent 4,144,139, 13 March 1979.

[83] Grenon LA (1981) Electroplating Method. US Patent 4,251,327, 17 February 1981.

[84] Mette A, Schetter C, Wissen D, *et al.* (2006) Increasing the efficiency of screen-printed silicon solar cells by light-induced silver plating. In: *Proceedings of the 4th World Conference on Photovoltaic Energy Conversion*, pp. 1056–1059. Waikoloa, HI, USA. Piscataway, NJ, USA: IEEE.

[85] Green MA (2011) Ag requirements for silicon wafer-based solar cells. *Progress in Photovoltaics* 19(8): 911–916. doi: 10.1002/pip.1125.

[86] Bartsch JM, Mondon A, Schetter C, *et al.* (2010) Copper as conducting layer in advanced front side metallization processes for crystalline silicon solar cells, exceeding 20% efficiency on printed seed layers. In: *Proceedings of the 35th IEEE Photovoltaic Specialists Conference*. Honolulu, HI, USA. Piscataway, NJ, USA: IEEE.

[87] Braun S, Emre E, Raabe B, and Hahn G (2010) Electroless nickel and copper metallization: Contact formation on crystalline silicon and background plating behavior on PECVD SiN_x:H layers. In: *25th European Photovoltaic Solar Energy Conference and Exhibition*. Valencia, Spain. Munich, Germany: WIP Renewable Energies.

[88] Hernández JL, Tous L, Allebe C, *et al.* (2010) Application of CMOS metal barriers to copper plated silicon solar cells. In: *25th European Photovoltaic Solar Energy Conference and Exhibition*, pp. 1479–1483. Valencia, Spain. Munich, Germany: WIP Renewable Energies.

[89] Posthuma NE, Hernandez JL, Lazov V, *et al.* (2009) Investigation of copper plated contacts for silicon solar cells. In: *24th European Photovoltaic Solar Energy Conference*, pp. 997–1001.Hamburg, Germany, 21–25 September. Munich, Germany: WIP Renewable Energies.

[90] Bartsch J, Mondon A, Bayer K, *et al.* (2010) Quick determination of copper-metallization long-term impact on silicon solar cells. *Journal of the Electrochemical Society* 157(10): H942–H946.

[91] Aleman M, Bay N, Barucha D, *et al.* (2009) Advances in electroless nickel plating for the metallization of silicon solar cells using different structuring techniques for the arc. In: *Proceedings of the 24th European Photovoltaic Solar Energy Conference*, pp. 1414–1418. Hamburg, Germany. Munich, Germany: WIP Renewable Energies.

[92] Knorz A, Aleman M, Grohe A, *et al.* (2009) Laser ablation of antireflection coatings for plated contacts yielding solar cell efficiencies above 20%. In: *Proceedings of the 24th European Photovoltaic Solar Energy Conference*, pp. 1002–1005. Hamburg, Germany. Munich, Germany: WIP Renewable Energies.

[93] Bruton TM, Mason NB, Roberts S, *et al.* (2003) Towards 20% efficient silicon solar cells manufactured at 60 MWp per annum. In: *Proceedings of the 3rd World Conference on Photovoltaic Energy Conversion*, pp. 899–902. Osaka, Japan. Piscataway, NJ, USA: IEEE.

[94] Shi Z, Wenham S, and Ji J (2009) Mass production of the innovative PLUTO solar cell technology. In: *Proceedings of the 34th IEEE Photovoltaic Specialists Conference*, pp. 1922–1926. Philadelphia, PA, USA. Piscataway, NJ, USA: IEEE.

[95] Rohatgi A, Narasimha S, Ebong AU, and Doshi P (1999) Understanding and implementation of rapid thermal technologies for high-efficiency silicon solar cells. *IEEE Transactions on Electron Devices* 46(10): 1970–1977.

[96] Nekarda J-F, Hörteis M, Lottspeich F, *et al.* (2010) Comparison of the three different metallization concepts for LFC cells. In: *Proceedings of the 25th European Photovoltaic Solar Energy Conference and Exhibition*, pp. 2245–2249. Valencia, Spain.

[97] Nekarda J, Reinwand D, Grohe A, *et al.* (2009) Industrial PVD metallization for high efficiency crystalline silicon solar cells. In: *Proceedings of the 34th IEEE Photovoltaic Specialists Conference*, pp. 1–5. Philadelphia, PA, USA. Piscataway, NJ, USA: IEEE.

[98] Istratov AA, Buonassisi T, McDonald RJ, *et al.* (2003) Metal content of multicrystalline silicon for solar cells and its impact on minority carrier diffusion length. *Journal of Applied Physics* 94(10): 6552–6559.

[99] Buonassisi T, Istratov AA, Pickett MD, *et al.* (2006) Chemical natures and distributions of metal impurities in multicrystalline silicon materials. *Progress in Photovoltaics: Research and Applications* 14(6): 513–531.

[100] Bentzen A, Holt A, Kopecek R, *et al.* (2006) Gettering of transition metal impurities during phosphorus emitter diffusion in multicrystalline silicon solar cell processing. *Journal of Applied Physics* 99: 093509.

[101] Schultz O, Glunz SW, Riepe S, and Willeke GP (2006) High-efficiency solar cells on phosphorus gettered multicrystalline silicon substrates. *Progress in Photovoltaics: Research and Applications* 14: 711–719.

[102] Macdonald D and Cuevas A (2000) The trade-off between phosphorus gettering and thermal degradation in multicrystalline silicon. In: *Proceedings of the 16th European Photovoltaic Solar Energy Conference*, pp. 1707–1710. Glasgow, UK. Munich, Germany: WIP Renewable Energies.

[103] Hahn G, Käs M, and Herzog B (2010) Hydrogenation in crystalline silicon materials for photovoltaic application. *Solid State Phenomena* 156–158: 343–349.

[104] Engelhart P, Zimmermann G, Klenke C, *et al.* (2011) R&D pilot-line production of multi-crystalline Si solar cells with top efficiencies exceeding 19%. In: *IEEE Photovoltaic Specialists Conference*. Seattle, WA, USA. Piscataway, NJ, USA: IEEE.

[105] Breitenstein O, Bauer J, Wagner J-M, *et al.* (2009) Physical mechanisms of breakdown in multicrystalline silicon solar cells. In: *Proceedings of the 34th IEEE Photovoltaic Specialists Conference*. Philadelphia, PA, USA. Piscataway, NJ, USA: IEEE.

[106] Kwapil W, Kasemann M, Gundel P, *et al.* (2009) Diode breakdown related to recombination active defects in block-cast multicrystalline silicon solar cells. *Journal of Applied Physics* 106: 063530.

[107] Cuevas A (2008) The paradox of compensated silicon. In: *Conference on Optoelectronics and Microelectronic Materials and Devices*, pp. 238–241. Sydney, NSW, Australia. Piscataway, NJ, USA: IEEE.

[108] Macdonald D, Rougieux F, Cuevas A, *et al.* (2009) Light-induced boron–oxygen defect generation in compensated p-type Czochralski silicon. *Journal of Applied Physics* 105: 093704.

[109] Peter K, Kopecek R, Pernau T, *et al.* (2005) Analysis of multicrystalline solar cells from solar grade silicon feedstock. In: *Proceedings of the 31st IEEE Photovoltaic Specialists Conference*, pp. 927–930. Orlando, FL, USA. Piscataway, NJ, USA: IEEE.

[110] Petter K, Ludwig Y, Bakowskie R, *et al.* (2010) Latest results on production of solar cells from UMG-Si feedstock. In: *Silicon for the Chemical and Solar Industry X*. Ålesund – Geiranger, Norway. Trondheim, Norway: NTNU.

[111] Haunschild J, Glatthaar M, Riepe S, and Rein S (2010) Quality control using luminescence imaging in production of mc-solar cells from UMG feedstock. In: *Proceedings of the 35th IEEE Photovoltaic Specialists Conference*. Honolulu, HI, USA.

[112] Kwapil W, Wagner M, Schubert MC, and Warta W (2010) High net doping concentration responsible for critical diode breakdown behavior of upgraded metallurgical grade multicrystallilne silicon solar cells. *Journal of Applied Physics* 108: 023708.

[113] Kray D, Kampwerth H, Schneiderlöchner E, *et al.* (2004) Comprehensive experimental study on the performance of very thin laser-fired high-efficiency solar cells. In: *Proceedings of the 19th European Photovoltaic Solar Energy Conference*, pp. 608–611. Paris, France. Munich, Germany: WIP Renewable Energies.

[114] Fischer H and Pschunder W (1973) Investigation of photon and thermal induced changes in silicon solar cells. In: *Proceedings of the 10th IEEE Photovoltaic Specialists Conference*, pp. 404–411. Palo Alto, CA, USA. Piscataway, NJ, USA: IEEE.

[115] Knobloch J, Glunz SW, Henninger V, *et al.* (1995) 21% efficient solar cells processed from Czochralski grown silicon. In: *Proceedings of the 13th European Photovoltaic Solar Energy Conference*, pp. 9–12. Nice, France. Munich, Germany: WIP Renewable Energies.

[116] Schmidt J, Aberle AG, and Hezel R (1997) Investigation of carrier lifetime instabilities in Cz-grown silicon. In: *Proceedings of the 26th IEEE Photovoltaic Specialists Conference*, pp. 13–18. Anaheim, CA, USA.

[117] Glunz SW, Rein S, Warta W, *et al.* (1998) On the degradation of Cz-silicon solar cells. In: *Proceedings of the 2nd World Conference on Photovoltaic Energy Conversion*, pp. 1343–1346. Vienna, Austria. Piscataway, NJ, USA: IEEE.

[118] Kerr MJ and Cuevas A (2002) General parameterization of Auger recombination in crystalline silicon. *Journal of Applied Physics* 91(4): 2473–2480.

[119] Schultz O, Mette A, Hermle M, and Glunz SW (2008) Thermal oxidation for crystalline silicon solar cells exceeding 19% efficiency applying industrially feasible process technology. *Progress in Photovoltaics: Research and Applications* 16: 317–324.

[120] Kray D and Glunz SW (2006) Investigation of laser-fired rear-side recombination properties using an analytical model. *Progress in Photovoltaics: Research and Applications* 14: 195–201.

[121] Fischer B (2003) Loss Analysis of Crystalline Silicon Solar Cells Using Photoconductance and Quantum Efficiency Measurements. Dissertation, Universität Konstanz.

[122] Cox RH and Strack H (1967) Ohmic contacts for GaAs devices. *Solid State Electronics* 10: 1213–1218.

[123] Macdonald D and Geerligs LJ (2004) Recombination activity of interstitial iron and other transition metal point defects in p- and n-type crystalline silicon. *Applied Physics Letters* 85(18): 4061–4063.

[124] Saint-Cast P, Benick J, Kania D, *et al.* (2010) High-efficiency c-Si solar cells passivated with ALD and PECVD aluminum oxide. *IEEE Electron Device Letters* 31(7): 695–697.

[125] Wolf A, Biro D, Nekarda J-F, *et al.* (2010) Comprehensive analytical model for locally contacted rear surface passivated solar cells. *Journal of Applied Physics* 108(124510): 1–13.

[126] Münzer KA, Holdermann KT, Schlosser RE, and Sterk S (1998) Improvements and benefits of thin crystalline silicon solar cells. In: *Proceedings of the 2nd World Conference on Photovoltaic Energy Conversion*, pp. 1214–1219. Vienna, Austria.

[127] Rein S, Warta W, and Glunz SW (2000) Investigation of carrier lifetime in p-type Cz-silicon: Specific limitations and realistic prediction of cell performance. In: *Proceedings of the 28th IEEE Photovoltaic Specialists Conference*, pp. 57–60. Anchorage, AK, USA. Piscataway, NJ, USA: IEEE.

[128] Herguth A, Schubert G, Kaes M, and Hahn G (2006) A new approach to prevent the negative impact of the metastable defect in boron doped cz silicon solar cells. In: *Proceedings of the 4th World Conference on Photovoltaic Energy Conversion*, pp. 940–943. Waikoloa, HI, USA. Piscataway, NJ, USA: IEEE.

[129] Glunz SW, Rein S, Knobloch J, *et al.* (1999) Comparison of boron- and gallium-doped p-type Czochralski silicon for photovoltaic application. *Progress in Photovoltaics: Research and Applications* 7(6): 463–469.

[130] Glunz SW, Rein S, and Knobloch J (2000) Stable Czochralski silicon solar cells using gallium-doped base material. In: *Proceedings of the 16th European Photovoltaic Solar Energy Conference*, pp. 1070–1075. Glasgow, UK. Munich, Germany: WIP Renewable Energies.

[131] Zhao J, Wang A, and Green MA (2001) 24.5% efficiency PERT silicon solar cells on SEH MCZ substrates and cell performance on other SEH CZ and FZ substrates. *Solar Energy Materials and Solar Cells* 66: 27–36.

[132] Vedde J, Clausen T, and Jensen L (2003) Float-zone silicon for high volume production of solar cells. In: *Proceedings of the 3rd World Conference on Photovoltaic Energy Conversion*, pp. 943–946. Osaka, Japan.

[133] Yoshida T and Kitagawara Y (1996) Bulk lifetime decreasing phenomena induced by light-illumination in high-purity p-type CZ-Si crystals. In: *Proceedings of the 4th International Symposium on High Purity Silicon IV*, pp. 450–454. San Antonio, TX, USA. Pennington, NJ, USA: ECS.

[134] Cuevas A, Kerr MJ, Samundsett C, *et al.* (2002) Millisecond minority carrier lifetimes in n-type multicrystalline silicon. *Applied Physics Letters* 81(26): 4952–4954.

[135] Aberle AG, Glunz S, and Warta W (1992) Impact of illumination level and oxide parameters on Shockley–Read–Hall recombination at the Si–SiO_2 interface. *Journal of Applied Physics* 71(9): 4422–4431.

[136] Eades WD and Swanson RM (1984) Determination of the capture cross section and degeneracy factor of Si–SiO_2 interface states. *Applied Physics Letters* 44(10): 988–990.

[137] Schmidt J, Schuurmans FM, Sinke WC, *et al.* (1997) Observation of multiple defect states at silicon–silicon nitride interfaces fabricated by low-frequency plasma-enhanced chemical vapor deposition. *Applied Physics Letters* 71(2): 252–254.

[138] Green MA, Blakers AW, Zhao J, *et al.* (1990) Characterization of 23-percent efficient silicon solar cells. *IEEE Transactions on Electron Devices* 37(2): 331–336.

[139] Zhao J, Wang A, Altermatt PP, *et al.* (1996) 24% efficient PERL silicon solar cell: Recent improvements in high efficiency silicon cell research. *Solar Energy Materials and Solar Cells* 41/42: 87–99.

[140] Zhao J, Wang A, and Green MA (1990) 24% efficient PERL structure silicon solar cells. In: *Proceedings of the 21st IEEE Photovoltaic Specialists Conference*, pp. 333–335. Kissimmee, FL, USA.

[141] Sinton RA, Kwark Y, Gruenbaum P, and Swanson RM (1985) Silicon point contact concentrator solar cells. In: *Proceedings of the 18th IEEE Photovoltaic Specialists Conference*, pp. 61–65. Las Vegas, NV, USA. Piscataway, NJ, USA: IEEE.

[142] King RR, Sinton RA, and Swanson RM (1988) Front and back surface fields for point-contact solar cells. In: *Proceedings of the 20th IEEE Photovoltaic Specialists Conference*, pp. 538–544. Las Vegas, NV, USA. Piscataway, NJ, USA: IEEE.

[143] Zhao J, Wang A, and Green MA (1998) 19.8% efficient multicrystalline silicon solar cells with 'honeycomb' textured front surface. In: *Proceedings of the 2nd World Conference on Photovoltaic Energy Conversion*, pp. 1681–1684. Vienna, Austria. Piscataway, NJ, USA: IEEE.

[144] Glunz SW, Knobloch J, Biro D, and Wettling W (1997) Optimized high-efficiency silicon solar cells with $J_{sc} = 42$ mA/cm^2 and ⊠ = 23.3%. In: *Proceedings of the 14th European Photovoltaic Solar Energy Conference*, pp. 392–395. Barcelona, Spain. Munich, Germany: WIP Renewable Energies.

[145] Glunz SW, Köster B, Leimenstoll T, *et al.* (2000) 100 cm^2 solar cells on Czochralski silicon with an efficiency of 20.2%. *Progress in Photovoltaics: Research and Applications* 8(2): 237–240.

[146] Glunz SW, Preu R, Schaefer S, *et al.* (2000) New simplified methods for patterning the rear contact of RP-PERC high-efficiency solar cells. In: *Proceedings of the 28th IEEE Photovoltaic Specialists Conference*, pp. 168–171. Anchorage, AK, USA. Piscataway, NJ, USA: IEEE.

[147] Preu R, Schneiderlöchner E, Grohe A, *et al.* (2002) Laser-fired contacts – Transfer of a simple high efficiency process scheme to industrial production. In: *Proceedings of the 29th IEEE Photovoltaic Specialists Conference*, pp. 130–133. New Orleans, LA, USA.

[148] Agostinelli G, Choulat P, Dekkers HFW, *et al.* (2005) Advanced dry processes for crystalline silicon solar cells. In: *Proceedings of the 31st IEEE Photovoltaic Specialists Conference*, pp. 1149–1152. Orlando, FL, USA. Piscataway, NJ, USA: IEEE.

[149] Münzer KA, Schöne J, Teppe AMH, *et al.* (2011) Physical properties of industrial 19% rear side passivated Al-LBSFR- solar cells. In: *Proceedings of the 1st SiliconPV*, pp. 415–420. Freiburg, Germany: PSE.

[150] Uruena A, John J, Beaucarne G, *et al.* (2009) Local Al-alloyed contacts for next generation Si solar cells. In: *Proceedings of the 24th European Photovoltaic Solar Energy Conference*, pp. 1–4. Hamburg, Germany. Munich, Germany: WIP Renewable Energies.

[151] Urrejola E, Peter K, Glatz-Reichenbach J, *et al.* (2010) Influence of the Al–Si alloy formation in narrow dielectric barrier openings on the specific contact resistance. In: *Proceedings of the 25th European Photovoltaic Solar Energy Conference and Exhibition*, pp. 2176–2178. Valencia, Spain. Munich, Germany: WIP Renewable Energies.

[152] Urrejola E, Peter K, Plagwitz H, and Schubert C (2011) Silicon diffusion in aluminum for rear passivated solar cells. *Applied Physics Letters* 98(153508): 1–3.

[153] Urrejola E, Peter K, Plagwitz H, and Schubert G (2010) Al–Si alloy formation in narrow p-type Si contact areas for rear passivated solar cells. *Journal of Applied Physics* 107(124516): 1–5.

[154] Nekarda J, Stumpp S, Gautero L, *et al.* (2009) LFC on screen printed aluminium rear side metallization. In: *Proceedings of the 24th European Photovoltaic Solar Energy Conference*, pp. 1411–1415. Hamburg, Germany. Munich, Germany: WIP Renewable Energies.

[155] Böscke T, Hellriegel R, Wütherich T, *et al.* (2011) Fully screen-printed PERC cells with laser-fired-contacts – An industrial cell concept with 19.5% efficiency. In: *37th IEEE PVSC*. Seattle, WA, USA (in press). Piscataway, NJ, USA: IEEE.

[156] Hofmann M, Saint-Cast P, Suwito D, *et al.* (2009) Overview on crystalline silicon solar cells using PECVD rear passivation and laser-fired contacts. In: *Proceedings of the 24th European Photovoltaic Solar Energy Conference*, pp. 1517–1522. Hamburg, Germany. Munich, Germany: WIP Renewable Energies.

[157] Mack S, Jäger U, Kästner G, *et al.* (2010) Towards 19% efficient industrial PERC devices using simultaneous front emitter and rear surface passivation by thermal oxidation. In: *Proceedings of the 35th IEEE Photovoltaic Specialists Conference*, pp. 34–38. Honolulu, HI, USA. Piscataway, NJ, USA: IEEE.

[158] Mack S, Jäger U, Wolf A, *et al.* (2010) Simultaneous front emitter and rear surface passivation by thermal oxidation – An industrially feasible approach to a 19% efficient PERC device. In: *Proceedings of the 25th European Photovoltaic Solar Energy Conference and Exhibition*, pp. 2218–2222. Valencia, Spain. Munich, Germany: WIP Renewable Energies.

[159] Wolf A, Wotke EA, Mack S, *et al.* (2010) Pilot processing of 18.6% efficient rear surface passivated silicon solar cells with screen printed front contacts. In: *Proceedings of the 25th European Photovoltaic Solar Energy Conference and Exhibition*, pp. 1391–1395. Valencia, Spain. Munich, Germany: WIP Renewable Energies.

[160] Catchpole KR and Blakers AW (2000) Modelling of the PERC structure with stripe and dot back contacts. In: *Proceedings of the 16th European Photovoltaic Solar Energy Conference*, pp. 1719–1722. Glasgow, UK. Munich, Germany: WIP Renewable Energies.

[161] Catchpole KR and Blakers AW (2002) Modelling the PERC structure for industrial quality silicon. *Solar Energy Materials and Solar Cells* 73(2): 189–202.

[162] Schöfthaler M, Rau U, Füssel W, and Werner JH (1993) Optimization of the back contact geometry for high efficiency solar cells. In: *Proceedings of the 23rd IEEE Photovoltaic Specialists Conference*, pp. 315–320. Louisville, KY, USA. Piscataway, NJ, USA: IEEE.

[163] Plagwitz H and Brendel R (2006) Analytical model for the diode saturation current of point-contacted solar cells. *Progress in Photovoltaics: Research and Applications* 14: 1–12.

[164] van Kerschaver E, Einhaus R, Szlufcik J, *et al.* (1998) A novel silicon solar cell structure with both external polarity contacts on the back surface. In: *Proceedings of the 2nd World Conference on Photovoltaic Energy Conversion*, pp. 1479–1482. Vienna, Austria. Piscataway, NJ, USA: IEEE.

[165] Burgers AR, Bultman JH, Tip AC, and Sinke WC (2001) Metallisation patterns for interconnection through holes. *Solar Energy Materials and Solar Cells* 65(1–4): 347–353.

[166] Bultman JH, Weeber AW, Brieko MW, *et al.* (2000) Pin up module: A design for higher efficiency, easy module manufacturing and attractive appearance. In: *Proceedings of the 16th European Photovoltaic Solar Energy Conference*, p. 1210. Glasgow, UK. Munich, Germany: WIP Renewable Energies.

[167] DeJong PN (1975) Solar Cell Contact Design. US Patent 3,903,428, 2 September 1975.

[168] Pack GJ (1975) Solar Cell Connections. US Patent 3,903,427, 2 September 1975.

[169] Gee JM (1997) Simplified module assembly using back-contact crystalline-silicon solar cells. In: *Proceedings of the 26th IEEE Photovoltaic Specialists Conference*, pp. 1085–1088. Anaheim, CA, USA.

[170] Späth M, De Jong PC, Bennett IJ, *et al.* (2008) A novel module assembly line using back contact solar cells. In: *Proceedings of the 16th IEEE Photovoltaic Specialists Conference*, pp. 1–6. San Diego, CA, USA. Piscataway, NJ, USA: IEEE.

[171] Späth M, de Jong PC, Bennett IJ, *et al.* (2008) First experiments on module assembly line using back-contact solar cells. In: *Proceedings of the 23rd European Photovoltaic Solar Energy Conference*. pp. 2917–2921. Valencia, Spain. Munich, Germany: WIP Renewable Energies.

[172] van Kerschaver E, De Wolf S, Allebé C, and Szlufcik J (2001) High performance modules based on back contacted solar cells. In: *Proceedings of the 17th European Photovoltaic Solar Energy Conference*, pp. 417–420. Munich, Germany: WIP Renewable Energies.

[173] Clement F, Lutsch M, Kubera T, *et al.* (2007) Industrially feasible multi crystalline metal wrap through (MWT) silicon solar cells exceeding 16% efficiency. In: *Technical Digest of the 17th International Photovoltaic Solar Energy Conference*, pp. 406–407. Fukuoka, Japan.

[174] Bennett IJ, Tjengdrawira A, Mewe A, *et al.* (2009) World record module efficiency for large and thin mc-Si MWT cells. In: *Proceedings of the 24th European Photovoltaic Solar Energy Conference*, pp. 3258–3261. Hamburg, Germany.

[175] Dross F, Allebé C, Ma Y, *et al.* (2007) High-efficiency (average 16.0%) industrial-type rear-contacts multicrystalline silicon solar cells. In: *Technical Digest of the 17th International Photovoltaic Solar Energy Conference*, pp. 410–411. Fukuoka, Japan. Tokyo, Japan: ICS.

[176] Lahmer D, Lossen J, Meyer K, *et al.* (2009) Pilot-line processing of Cz-Si MWT solar cells with an efficiency gain of 0.3%. In: *Proceedings of the 24th European Photovoltaic Solar Energy Conference*, pp. 2168–2171. Hamburg, Germany. Munich, Germany: WIP Renewable Energies.

[177] Späth M, De Jong PC, Lust S, and Clasen H (2006) Solder version of 8 inch back-contacted solar cells. In: *Proceedings of the 15th International Photovoltaic Science & Engineering Conference*, pp. 1003–1004. Shanghai, China. Tokyo, Japan: ICS.

[178] van den Donker MN, Wijnen PAM, Krantz S, *et al.* (2008) The Starfire project: Towards in-line mass production of thin high efficiency backcontacted multicrystalline silicon solar cells. In: *Proceedings of the 23rd European Photovoltaic Solar Energy Conference*, pp. 1–3. Valencia, Spain. Munich, Germany: WIP Renewable Energies.

[179] Dross F, van Kerschaver E, Allebé C, *et al.* (2006) Impact of rear-surface passivation on MWT performances. In: *Proceedings of the 4th World Conference on Photovoltaic Energy Conversion*, pp. 1291–1294. Waikoloa, HI, USA. Piscataway, NJ, USA: IEEE.

[180] Romijn I, Lamers M, Stassen A, *et al.* (2007) Aspire: A new industrial MWT cell technology enabling high efficiencies on thin and large mc-Si wafers. In: *Proceedings of the 22nd European Photovoltaic Solar Energy Conference*, pp. 1043–1049. Milan, Italy. Munich, Germany: WIP Renewable Energies.

[181] Thaidigsmann B, Wolf A, Clement F, *et al.* (2010) Combining the advantages of wrap through metallization and rear surface passivation into industrial MWT-PERC devices. In: *Proceedings of the 25th European Photovoltaic Solar Energy Conference and Exhibition*, pp. 2227–2230. Valencia, Spain. Munich, Germany: WIP Renewable Energies.

[182] Biro D, Thaidigsmann B, Clement F, *et al.* (2011) MWT meets PERC: Towards 20% efficient industrial silicon solar cells. In: *IEEE Photovoltaic Specialists Conference*. Seattle, WA, USA. Piscataway, NJ, USA: IEEE.

[183] Thaidigsmann B, Lohmüller E, Jäger U, *et al.* (2011) Large-area p-type HIP-MWT silicon solar cells with screen printed contacts exceeding 20% efficiency. *Physica Status Solidi Rapid Research Letters* 5(8): 286–288.

[184] Gee JM, Schubert WK, and Basore PA (1993) Emitter wrap-through solar cell. In: *Proceedings of the 23rd IEEE Photovoltaic Specialists Conference*, pp. 265–270. Louisville, KY, USA.

[185] Kress A, Fath P, Willeke G, and Bucher E (1998) Low-cost back contact silicon solar cells applying the emitter-wrap-through (EWT) concept. In: *Proceedings of the 2nd World Conference on Photovoltaic Energy Conversion*, pp. 1547–1550. Vienna, Austria. Piscataway, NJ, USA: IEEE.

[186] Haverkamp H, Scholz S, and Hahn G (2008) Screen printed EWT cells: Limitations and alternative approaches to the manufacturing process. In: *Proceedings of the 23rd European Photovoltaic Solar Energy Conference*, pp. 1945–1948. Valencia, Spain. Munich, Germany: WIP Renewable Energies.

[187] Faika K, Wagner M, Fath P, and Bucher E (2000) Simplification of EWT (emitter wrap-through) solar cell fabrication using Al–P-codiffusion. In: *Proceedings of the 28th IEEE Photovoltaic Specialists Conference*, pp. 260–263. Anchorage, AK, USA. Piscataway, NJ, USA: IEEE.

[188] Schönecker A, de Moor HHC, Burgers AR, *et al.* (1997) An industrial multi-crystalline EWT solar cell with screen printed metallization. In: *Proceedings of the 14th European Photovoltaic Solar Energy Conference*, pp. 796–799. Barcelona, Spain. Munich, Germany: WIP Renewable Energies.

[189] Fallisch A, Stüwe D, Neubauer R, *et al.* (2010) Inkjet structured EWT silicon solar cells with evaporated aluminum metallization and laser-fired contacts. In: *Proceedings of the 35th IEEE Photovoltaic Specialists Conference*, pp. 3125–3130. Honolulu, HI, USA. Piscataway, NJ, USA: IEEE.

[190] Kray D, Dicker J, Osswald D, *et al.* (2003) Progress in high-efficiency emitter-wrap-through cells on medium quality substrates. In: *Proceedings of the 3rd World Conference on Photovoltaic Energy Conversion*, pp. 1340–1343. Osaka, Japan. Piscataway, NJ, USA: IEEE.

[191] Mingirulli N, Stüwe D, Specht J, *et al.* (2009) 18.8% EWT-cells with screen-printed metallization and single step side selective emitter formation. In: *Proceedings of the 24th European Photovoltaic Solar Energy Conference*, pp. 1979–1984. Hamburg, Germany. Munich, Germany: WIP Renewable Energies.

[192] Eikelboom DWK, Burgers AR, Goris MJAA, *et al.* (2001) Conductive adhesives for interconnection of busbarless emitter wrap-through solar cells on a structured metal foil. In: *Proceedings of the 17th European Photovoltaic Solar Energy Conference*, pp. 1547–1550. Munich, Germany: WIP Renewable Energies.

[193] Gee JM, Meakin D, Southimath S, *et al.* (2009) Development of commercial-scale photovoltaic modules using monolithic module assembly. In: *34th IEEE Photovoltaic Specialists Conference*, pp. 2133–2137. Philadelphia, PA, USA. Piscataway, NJ, USA: IEEE.

[194] Hacke P, Gee J, Kumar P, *et al.* (2009) Optimized emitter wrap-through cells for monolithic module assembly. In: *34th IEEE Photovoltaic Specialists Conference*. Philadelphia, PA. Piscataway, NJ, USA: IEEE.

[195] Haller I (1990) Ion–molecule reactions in the silane–ammonia system. *Journal of Physical Chemistry* 1990(94): 4135–4137.

[196] Gee JM, Kumar P, Howarth J, *et al.* (2010) Development of industrial high-efficiency back-contact Czochralski-silicon solar cells. In: *25th European Photovoltaic Solar Energy Conference and Exhibition*, pp. 1342–1345. Valencia, Spain. Munich, Germany: WIP Renewable Energies.

[197] Engelhart P, Teppe A, Merkle A, *et al.* (2005) The RISE-EWT (rear interdigitated single evaporation – emitter wrap through) solar cell – A new approach towards simple high efficiency silicon solar cells. In: *Laseranwendungen in der Photovoltaik*. Dieburg, Germany: Coherent Lambda Physik GmbH.

[198] Engelhart P (2007) Lasermaterialbearbeitung als Schlüsseltechnologie zum Herstellen rückseitenkontaktierter Siliciumsolarzellen. PhD Thesis, Universität Hannover.

[199] Ulzhöfer C, Hermann S, Harder N-P, *et al.* (2008) The origin of reduced fill factors of emitter-wrap-through-solar cells. *Physica Status Solidi Rapid Research Letters* 2(6): 251–253.

[200] Ulzhöfer C, Altermatt PP, Harder NP, and Brendel R (2010) Loss analysis of emitter-wrap-through silicon solar cells by means of experiment and three-dimensional device modeling. *Journal of Applied Physics* 107(10): 104–509.

[201] Glunz SW, Benick J, Biro D, *et al.* (2010) n-type silicon – Enabling efficiencies >20% in industrial production. In: *Proceedings of the 35th IEEE Photovoltaic Specialists Conference*, pp. 50–56. Honolulu, HI, USA.

[202] Schmiga C, Rauer M, Rüdiger M, *et al.* (2010) Aluminium-doped p^+ silicon for rear emitters and back surface fields: Results and potentials of industrial n- and p-type solar cells. In: *Proceedings of the 25th European Photovoltaic Solar Energy Conference and Exhibition*, pp. 1163–1168. Valencia, Spain. Munich, Germany: WIP Renewable Energies.

[203] Schmiga C, Hörteis M, Rauer M, *et al.* (2009) Large-area n-type silicon solar cells with printed contacts and aluminium-alloyed rear emitter. In: *Proceedings of the 24th European Photovoltaic Solar Energy Conference*, pp. 1167–1170. Hamburg, Germany. Munich, Germany: WIP Renewable Energies.

[204] Rauer M, Schmiga C, Hermle M, and Glunz SW (2009) Passivation of screen-printed aluminium-alloyed emitters for back junction n-type silicon solar cells. In: *Proceedings of the 24th European Photovoltaic Solar Energy Conference*, pp. 1059–1062. Hamburg, Germany.

[205] Gong C, Van Kerschaver E, Robbelein J, *et al.* (2010) Screen-printed aluminium-alloyed p^+ emitter on high-efficiency n-type interdigitated back-contact silicon solar cells. *IEEE Electron Device Letters* 31(6): 576–578.

[206] Bock R, Mau S, Schmidt J, and Brendel R (2010) Back-junction back-contact n-type silicon solar cells with screen-printed aluminium-alloyed emitter. *Applied Physics Letters* 96(263507): 1–3.

[207] Woehl R, Krause J, Granek F, and Biro D (2011) 19.7% efficient all-screen-printed back-contact back-junction silicon solar cell with aluminum-alloyed emitter. *IEEE Electron Device Letters* 32(3): 345–347.

[208] Woehl R, Keding R, Rüdiger M, *et al.* (2011) 20% efficient screen-printed and aluminium-alloyed back-contact back-junction cells and interconnection scheme of point-shaped metallized cells. In: *IEEE Photovoltaic Specialists Conference*. Seattle, WA, USA. Piscataway, NJ, USA: IEEE.

[209] Weeber A, Naber R, Guillevin N, *et al.* (2009) Status of n-type solar cells for low-cost industrial production. In: *Proceedings of the 24th Photovoltaic Solar Energy Conference*, pp. 891–895. Hamburg, Germany.

[210] Mihailetchi VD, Jourdan J, Edler A, *et al.* (2010) Screen-printed n-type silicon solar cells for industrial application. In: *Proceedings of the 25th European Photovoltaic Solar Energy Conference*, pp. 1446–1448. Valencia, Spain.

[211] Guillevin N, Heurtault BJB, Geerligs LJ, and Weeber AW (2011) Development towards 20% efficient Si MWT solar cells for low-cost industrial production. In: *Proceedings of the 1st SiliconPV*, pp. 9–16. Freiburg, Germany: PSE.

[212] Richter A, Henneck S, Benick J, *et al.* (2010) Firing stable Al_2O_3/SiN_x layer stack passivation for the front side boron emitter of n-type silicon solar cells. In: *Proceedings of the 25th European Photovoltaic Solar Energy Conference and Exhibition*, pp. 1453–1459. Valencia, Spain. Munich, Germany: WIP Renewable Energies.

[213] Altermatt PP, Plagwitz H, Bock R, *et al.* (2006) The surface recombination velocity at boron-doped emitters: Comparison between various passivation techniques. In: *Proceedings of the 21st European Photovoltaic Solar Energy Conference*, pp. 647–650. Dresden, Germany. Munich, Germany: WIP Renewable Energies.

[214] Kerr MJ (2002) Surface, Emitter and Bulk Recombination in Silicon and Development of Silicon Nitride Passivated Solar Cells. Dissertation, Australian National University.

[215] Libal J, Petres R, Buck T, *et al.* (2005) N-type multicrystalline silicon solar cells: BBr_3-diffusion and passivation of P^+-diffused silicon surfaces. In: *Proceedings of the 20th European Photovoltaic Solar Energy Conference*, pp. 793–796. Barcelona, Spain.

[216] King RR and Swanson RM (1991) Studies of diffused boron emitters: Saturation current, bandgap narrowing, and surface recombination velocity. *IEEE Transactions on Electron Devices* 38(6): 1399–1409.

[217] Cuevas A, Stuckings M, Lau J, and Petravic M (1997) The recombination velocity of boron diffused silicon surfaces. In: *Proceedings of the 14th European Photovoltaic Solar Energy Conference*, pp. 2416–2419. Barcelona, Spain. Munich, Germany: WIP Renewable Energies.

[218] Zhao J, Schmidt J, Wang A, *et al.* (2003) Performance instability in n-type PERT silicon solar cells. In: *Proceedings of the 3rd World Conference on Photovoltaic Energy Conversion*, pp. 923–926. Osaka, Japan. Piscataway, NJ, USA: IEEE.

[219] Mihailetchi VD, Komatsu Y, and Geerligs LJ (2008) Nitric acid pretreatment for the passivation of boron emitters for n-type base silicon solar cells. *Applied Physics Letters* 92 (063510): 1–3.

[220] Benick J, Hoex B, van de Sanden MCM, *et al.* (2008) High efficiency n-type Si solar cells on Al_2O_3-passivated boron emitters. *Applied Physics Letters* 92(253504): 253504/253501–253503.

[221] Hoex B, Schmidt J, Bock R, *et al.* (2007) Excellent passivation of highly doped p-type Si surfaces by the negative-charge-dielectric Al_2O_3. *Applied Physics Letters* 91(112107): 112107/112101–112103.

[222] Benick J, Richter A, Li T-A, *et al.* (2010) Effect of a post-deposition anneal on Al_2O_3/Si interface properties. In: *Proceedings of the 35th IEEE Photovoltaic Specialists Conference*, pp. 891–896. Honolulu, HI, USA. Piscataway, NJ, USA: IEEE.

[223] Suwito D, Jäger U, Benick J, *et al.* (2010) Industrially feasible rear passivation and contacting scheme for high efficiency n-type solar cells yielding a V_{oc} of 700 mV. *IEEE Transactions on Electron Devices* 57(8): 2032–2036.

[224] McIntosh KR, Cudzinovic MJ, Smith DD, *et al.* (2003) The choice of silicon wafer for the production of low-cost rear-contact solar cells. In: *Proceedings of the 3rd World Conference on Photovoltaic Energy Conversion*, pp. 971–974. Osaka, Japan.

[225] De Ceuster D, Cousins P, Rose D, *et al.* (2007) High volume production of >22% efficiency silicon solar cells. In: *Proceedings of the 22nd European Photovoltaic Solar Energy Conference*, pp. 816–819. Milan, Italy. Munich, Germany: WIP Renewable Energies.

[226] Huljic D, Zerres T, Mohr A, *et al.* (2006) Development of a 21% back-contact monocrystalline silicon solar cell for large-scale production. In: *21st European Photovoltaic Solar Energy Conference*, pp. 765–768. Dresden, Germany. Munich, Germany: WIP Renewable Energies.
[227] Reichel C, Reusch M, Granek F, *et al.* (2010) Decoupling charge carrier collection and metallization geometry of back-contacted back-junction silicon solar cells by using insulating thin films. In: *Proceedings of the 35th IEEE Photovoltaic Specialists Conference*, pp. 1034–1038. Honolulu, HI, USA. Piscataway, NJ, USA: IEEE.
[228] Hermle M, Granek F, Schultz-Wittmann O, and Glunz SW (2008) Shading effects in back-junction back-contacted silicon solar cells. In: *Proceedings of the 33rd IEEE Photovoltaic Specialists Conference*, pp. 1–4. San Diego, CA, USA. Piscataway, NJ, USA: IEEE.
[229] Reichel C, Granek F, Hermle M, and Glunz SW (2010) Enhanced current collection in backcontacted back-junction Si solar cells by overcompensating a boron emitter with a phosphorus base-type doping. *Physica Status Solidi A* 207(8): 1978–1981.
[230] Moehlecke A, Del Cañizo C, Zanesco I, and Luque A (1998) Floating junction passivation of p^+ emitters. In: *Proceedings of the 2nd World Conference and Exhibition on Photovoltaic Solar Energy Conversion*, pp. 1551–1554. Vienna, Austria.
[231] Harder N-P, Mertens V, and Brendel R (2008) Buried emitter solar cell structures: Decoupling of metallisation geometry and carrier collection geometry of back contacted solar cells. *Physica Status Solidi Rapid Research Letters* 2(4): 148–150.
[232] Benick J, Schultz-Wittmann O, Schön J, and Glunz SW (2008) Surface passivation schemes for high-efficiency n-type Si solar cells. *Physica Status Solidi Rapid Research Letters* 2(4): 145–147.
[233] Granek F, Hermle M, Reichel C, *et al.* (2008) High-efficiency back-contact back-junction silicon solar cell research at Fraunhofer ISE. In: *Proceedings of the 23rd European Photovoltaic Solar Energy Conference*, pp. 991–995. Valencia, Spain.
[234] Mertens V, Bordihn S, Larionova Y, *et al.* (2009) The buried emitter solar cell concept: Interdigitated back-junction structure with virtually 100% emitter coverage of the cell area. In: *Proceedings of the 24th European Photovoltaic Solar Energy Conference*, pp. 934–936. Hamburg, Germany.
[235] Cousins PJ, Smith DD, Luan H-C, *et al.* (2010) Generation 3: Improved performance at lower cost. In: *Proceedings of the 35th IEEE Photovoltaic Specialists Conference*, pp. 275–278. Honolulu, HI, USA. Piscataway, NJ, USA: IEEE.
[236] Kawamoto K, Nakai T, Baba T, *et al.* (2001) A high-efficiency HIT™ solar cell (21.0% ~ 100 cm^2) with excellent interface properties. In: *Technical Digest of the International PVSEC-12*, pp. 289–290. Jeju, Korea. Tokya, Japan: ICS.
[237] Fujishima D, Inoue H, Tsunomura Y, *et al.* (2010) High-performance HIT solar cells for thinner silicon wafers. In: *Proceedings of the 35th IEEE Photovoltaic Specialists Conference*, pp. 3137–3140. Honolulu, HI, USA. Piscataway, NJ, USA: IEEE.
[238] Taira S, Yoshimine Y, Baba T, *et al.* (2007) Our approaches for achieving hit solar cells with more than 23% efficiency. In: *Proceedings of the 22nd European Photovoltaic Solar Energy Conference*, pp. 932–935. Milan, Italy. Munich, Germany: WIP Renewable Energies.
[239] Taguchi M, Tsunomura Y, Inoue H, *et al.* (2009) High-efficiency HIT solar cell on thin (< 100 μm) silicon wafer. In: *Proceedings of the 24th European Photovoltaic Solar Energy Conference*, pp. 1690–1693. Hamburg, Germany. Munich, Germany: WIP Renewable Energies.
[240] van Sark WGJHM, Korte L, and Roca F (2011) *Physics and Technology of Amorphous–Crystalline Heterostructure Silicon Solar Cells*. Heidelberg, Germany: Springer.
[241] Bätzner DL, Andrault Y, Andreetta L, *et al.* (2011) Properties of high efficiency silicon heterojunction cells. In: *Proceedings of the 1st SiliconPV*. Freiburg, Germany: PSE.
[242] Korte L, Conrad E, Angermann H, *et al.* (2009) Advances in a-Si:H/c-Si heterojunction solar cell fabrication and characterization. *Solar Energy Materials and Solar Cells* 93(6–7): 905–910.
[243] Schulze TF, Korte L, Conrad E, *et al.* (2010) Electrical transport mechanisms in a-Si:H/c-Si heterojunction solar cells. *Journal of Applied Physics* 107: 023711.
[244] Ballif C, Olibet S, De Wolf S, *et al.* (2009) High efficiency heterojunction solar cells: Fundamental and practical aspects. In: *Proceedings of the 18th International Photovoltaic Science and Engineering Conference*. Kolkata, India. Tokyo, Japan: ICS.
[245] Pysch D, Meinhardt C, Ritzau K.-U, *et al.* (2010) Comparison of intrinsic amorphous silicon buffer layers for silicon heterojunction. In: *Proceedings of the 35th IEEE Photovoltaic Specialists Conference*, pp. 3570–3576. Honolulu, HI, USA. Piscataway, NJ, USA: IEEE.
[246] Mueller T, Schwertheim S, Mueller N, *et al.* (2010) High efficiency silicon heterojunction solar cell using novel structure. In: *Proceedings of the 35th IEEE Photovoltaic Specialists Conference*, pp. 683–688. Honolulu, HI, USA. Piscataway, NJ, USA: IEEE.
[247] Rahmouni M, Datta A, Chatterjee P, *et al.* (2010) Carrier transport and sensitivity issues in heterojunction with intrinsic thin layer solar cells on N-type crystalline silicon: A computer simulation study. *Journal of Applied Physics* 107: 054521.
[248] Branz HM, Teplin CW, Young DL, *et al.* (2008) Recent advances in hot-wire CVD R&D at NREL: From 18% silicon heterojunction cells to silicon epitaxy at glass-compatible temperatures. *Thin Solid Films* 516(5): 743–746.
[249] Desrues T, De Vecchi S, Souche F, *et al.* (2011) Development of interdigitated back contact silicon heterojunction (IBC Si-HJ) solar cells. In: *Proceedings of the 1st SiliconPV*, pp. 294–300. Freiburg, Germany: PSE.
[250] Lu M, Bowden S, Das U, and Birkmire R (2007) Interdigitated back contact silicon heterojunction solar cell and the effect of front surface passivation. *Applied Physics Letters* 91(063507): 1–3.
[251] Tucci M, Serenelli L, Salza E, *et al.* (2007) Novel scheme of amorphous/crystalline silicon heterojunction solar cell. In: *Proceedings of the 22nd European Photovoltaic Solar Energy Conference*, pp. 1600–1603. Milan, Italy. Munich, Germany: WIP Renewable Energies.
[252] Stangl R, Bivour M, Conrad E, *et al.* (2007) Recash – A novel high efficiency buried grid rear contact amorphous/crystalline silicon heterojunction solar cell concept. In: *Proceedings of the 22nd European Photovoltaic Solar Energy Conference*, pp. 870–874. Milan, Italy. Munich, Germany: WIP Renewable Energies.
[253] Mingirulli N, Haschke J, Gogolin R, *et al.* (2011) Efficient interdigitated back-contacted silicon heterojunction solar cells. *Physica Status Solidi Rapid Research Letters* 5(4): 159–161.
[254] Yablonovitch E, Gmitter T, Swanson RM, and Kwark YH (1985) A 720 mV open circuit voltage SiO_x:c-Si:SiO_x double heterostructure solar cell. *Applied Physics Letters* 47(11): 1211–1213.
[255] Tarr NG (1985) A polysilicon emitter solar cell. *IEEE Electron Device Letters* 6(12): 655–658.
[256] Green MA (1995) *Silicon Solar Cells: Advanced Principles and Practice*. Sydney, NSW, Australia: Centre for Photovoltaic Devices and Systems UNSW.
[257] Borden P, Xu L, McDougall B, *et al.* (2008) Polysilicon tunnel junctions as alternates to diffused junctions. In: *Proceedings of the 23rd European Photovoltaic Solar Energy Conference*, pp. 1149–1152. Valencia, Spain. Munich, Germany: WIP Renewable Energies.
[258] Rohatgi A and Meier D (2010) Developing novel low-cost, high-throughput processing techniques for 20%-efficient monocrystalline silicon solar cells. *Photovoltaics International* 10: 87–94.
[259] Bateman N, Sullivan P, Reichel C, *et al.* (2011) High quality ion implanted boron emitters in an interdigitated back contact solar cell with 20% efficiency. In: *Proceedings of the 1st SiliconPV*, pp. 509–514. Freiburg, Germany: PSE.